THESIS

AMPLIFICATION OF SUPERCRITICAL SURFACE

WAVES IN STEEP OPEN CHANNELS NEAR LAS

VEGAS, NEVADA

Submitted by

Noah Isaac Friesen

Department of Civil and Environmental Engineering

In partial fulfillment of the requirements

For the Degree of Master of Science

Colorado State University

Fort Collins, Colorado

Summer 2007

COLORADO STATE UNIVERSITY

April 25, 2007

WE HEREBY RECOMMEND THAT THE THESIS PREPARED UNDER OUR SUPERVISION BY NOAH ISAAC FRIESEN ENTITLED AMPLIFICATION OF SUPERCRITICAL SURFACE WAVES IN STEEP OPEN CHANNELS NEAR LAS VEGAS, NEVADA BE ACCEPTED AS FULFILLING IN PART REQUIREMENTS FOR THE DEGREE OF MASTER OF SCIENCE.

Committee on Graduate Work

_____
Chih Ted Yang

_____
Richard Eykholt

_____
Advisor – Pierre Julien

_____
Department Head – Luis Garcia

ABSTRACT OF THESIS

AMPLIFICATION OF SUPERCRITICAL SURFACE WAVES IN STEEP OPEN

CHANNELS NEAR LAS VEGAS, NEVADA

Supercritical surface waves occur in steep open channels. The celerity and amplification of these waves can be calculated using the dynamic wave approximation of the Saint-Venant equation. The method developed by Tsai and Yen was used in this thesis. Given the assumption of a small perturbation on a uniform base flow, the method shows that the amplification characteristics over a single wavelength depend on the Froude number and wavelength. All flood waves amplify when Froude numbers are greater than 1.5 and attenuate when Froude numbers are less than 1.5.

For practical applications, a new parameter is defined to compare the amplification of surface waves of varying wavelength over a fixed channel length. This factor represents the amplification of a given wave over a fixed channel length rather than over a single wavelength. Analysis showed that short waves will amplify more than long waves over the same channel length, and that the

highest amplification occurs when the waves are short and the Froude number is 3.44.

A 5 km long flood drainage channel located in Las Vegas, Nevada, was selected for practical applications. At this study site, waves with lengths between 10 m and 5 km were analyzed. For the waves examined, dimensionless celerity was between 1.36 and 1.66, and the relative amplification factor was less than 0.55. The normalized-length amplification was shown to increase up to 0.5 as wavelength decreased, which equates to an amplitude increase of 66%. Over a 543 m length of channel, waves can grow from 0.5 m to 0.8 m at the maximum discharge of 100 m^3/s. Three practical ways to reduce wave amplification in the channel include: (1) increasing the roughness; (2) decreasing the slope; and (3) reducing the available development length.

Noah Friesen
Department of Civil and Environmental Engineering
Colorado State University
Fort Collins, CO 80523
Summer 2007

AKNOWLEDGEMENTS

I would like to thank Dr. Jennifer Duan and the Desert Research Institute for providing the opportunity to work on this subject along with much guidance and help. I would also like to thank Dr. Pierre Julien for being my advisor and providing useful ideas on what direction to take my research. I extend thanks to Dr. Chih Ted Yang for being on my committee and providing a different outlook on hydraulics problems. I also am thankful to Dr. Richard Eykholt for participating on my committee.

Additionally, I would like to thank my family and especially my parents for being constantly supportive. I would also like to thank Lori, for being a friend when I was new to Las Vegas. Finally, I would like to thank the members of the SCA, who graciously beat the stress out of me when I needed it.

TABLE OF CONTENTS

TABLE OF FIGURES

LIST OF SYMBOLS

A	Dummy variable used in Equations (2.61) and (2.62)
a	Cross-sectional area
a_c	Acceleration
a_n	Normal cross-sectional area
B	Dummy variable used in Equations (2.61) and (2.62)
c	Dimensional wave celerity
c^*	Dimensionless wave celerity
d_s	Representative grain size
F_n	Froude number of uniform flow
Fr	Froude number of any flow
g	Acceleration due to gravity
i	Square root of negative one
j	Indicator of primary or secondary wave
L_0	Normalized length
n	Manning's roughness coefficient
P	Wetted perimeter
q	Unit discharge
q^*	Dimensionless unit discharge
R	Hydraulic radius
R_n	Hydraulic radius of normal flow
S_0	Channel bed slope
S_f	Friction slope
T	Wave period
t	Time
t^*	Dimensionless time
u	Velocity of flow
u_b^*	Dimensionless base velocity
u_n	Normal flow velocity
u^*	Dimensionless velocity
$u`^*$	Velocity perturbation
$\hat{u}$	Amplitude of velocity perturbation
W	Channel width
x	Distance along the channel
x^*	Dimensionless location in the channel
y	Water depth
y_b	Base flow depth
y_b^*	Dimensionless base flow depth
y_n	Normal flow depth
y^*	Dimensionless depth
$y`^*$	Depth perturbation
$\hat{y}$	Amplitude of depth perturbation
α	Friction equation coefficient
β^*	Complex propagation number

β_r^*	Real part of β^*
β_c^*	Imaginary part of β^*
δ^*	Dimensionless logarithmic amplitude decrement
$\delta`$	Dimensionless fixed-length amplitude decrement
θ	Dummy variable used in Equations (2.61) and (2.62)
θ^*	Phase variable for small perturbation
λ	Wavelength of perturbation
π	Pi
σ^*	Wave number
τ	Wave Period
τ^*	Dimensionless wave period
φ	Unit conversion constant used in Manning's equation

Chapter 1: Introduction

Steep storm drainage channels such as those found in Las Vegas, Nevada will convey supercritical flow. These channels are necessary for draining the Las Vegas Valley during intense storms. Figure 1.1 is an example of the extreme flooding that can occur.

Figure 1.1 - Runoff flowing through a drainage channel during the 1999 flood (from Las Vegas Sun)

It is obvious from this photograph that storm drainage is a major issue in Las Vegas. Floodwaters can cause extensive damage if the drainage channels are not sufficient to hold the flood. However, these channels are costly to build and thus it is desirable to keep the size and depth of the channels as small as possible within the constraint that the channels must be able to pass the design flood. Minimizing the amount of freeboard that is added to the depth to allow for unforeseen circumstances is one good way to reduce the cost of channel construction. To minimize this freeboard, the behavior of the water within the channel must be well understood. Waves that form within the channel will increase the depth, requiring more freeboard. Currently, waves in supercritical flow have not been studied extensively. Because of this, design guidelines for the construction of steep channels are often overly conservative and lack a good theoretical basis. The design of channels in the Las Vegas Valley is regulated by the Clark County Regional Flood Control District (CCRFCD). The design manual currently in use (CCRFCD 1999) contains a simple method for computing the expected height of roll waves based on Froude number and width-depth ratio. This criterion is based on limited theoretical studies, and would benefit from increased study.

There are four key objectives in this study, and they are:

1. The main objective of this thesis is to increase understanding of supercritical wave behavior. An analytical method for the analysis of small perturbations was developed by Tsai and Yen (2004). This method allows for the calculation of dimensionless celerity and attenuation for waves based on the wavelength and Froude number. Tsai and Yen only applied their method to subcritical flow. The method itself is applicable to all flow regimes, and so this thesis will extend the application to supercritical flow. The method as used by Tsai and Yen finds the attenuation over a single wavelength.

2. Secondly, this thesis will examine the method developed by Tsai and Yen to see if there are any areas of potential improvement. Ultimately, the goal with any engineering study is to apply the results to real world systems. Particular focus will therefore be given to enhancements that enable a better or easier application to practical results. Wave amplitude change over a fixed channel length rather than over a single wavelength would be useful to know, and a parameter will be defined to represent this amplitude change.

3. Third, the method previously introduced will be applied to an existing flood drainage channel in Las Vegas. Specifically, the channel known as F-1

channel in Las Vegas will be analyzed. Waves will be theoretically imposed on flow within this channel and the propagation speed and amplification of those waves will be calculated and analyzed. A wide variety of wavelengths and discharges will be studied to ensure that the results are as complete as possible given the limitations of the method.

4. The final objective of this thesis is to use the results generated in the previous objective to suggest possible methods for reducing or eliminating wave amplification in the F-1 channel. Different approaches will be examined and recommendations given.

The remainder of this thesis will be organized in several different chapters. The second chapter will look at previous studies that have been done in the area of supercritical wave formation and propagation.

Chapter 2: Literature Review

2.1 Previous Studies

The flow through steep channels during a storm event is inherently non-uniform and unsteady. Due to small perturbations in both flow velocity and depth, waves can develop within the flow. Although supercritical wave behavior has not been studied in great detail, there has been a variety of relevant work done over the years.

The Saint-Venant equations express the ideas of conservation of mass and momentum in differential form. The Saint-Venant equations do not have a known exact analytical solution. Because of this, there has been much work done over the years to develop approximations and numerical solutions to these equations.

Ponce and Simons (1977) published a seminal paper on wave dynamics in open channels. They utilized the theory of linear stability to analyze the celerity and attenuation of small shallow water waves. Relationships were developed that provided a first-order approximation that depended on the Froude number and the dimensionless wave number. Ponce and Simons gave a mostly qualitative analysis on the propagation of waves over a large range of Froude numbers.

They also examined the applicability of different wave approximations. They identified three main wave bands corresponding to different wave numbers. Small wave numbers fell into the kinematic wave band, with constant celerity and no attenuation or amplification. Large wave numbers caused waves to behave as gravity waves, with a (different) constant celerity and again no attenuation. In the middle they identified the dynamic wave band, where the full Saint-Venant equations were required to adequately describe the propagation mechanics.

A number of studies since then have also looked at the applicability and usefulness of different approximations to the Saint-Venant equations. Ferrick (1985) studied the different approximations of the Saint-Venant equations with the goal of providing quantitative criteria for the determination of when each wave approximation is appropriate. The criteria developed were based on the balance between friction and inertia forces in the wave. One important aspect of this analysis was that several case studies were used to verify and complete the criteria.

Later, Ferrick and Goodman (1998) compared linear solutions of the dynamic wave and diffusion wave approximation to a non-linear diffusion wave. All of the case studies used in this analysis were subcritical, with the highest Froude number being 0.96. As in the previous study by Ferrick (1985), the instability

point was found to occur at a Froude number equal to 2. The authors found that the linear and non-linear models have good agreement at low Froude numbers, but start to diverge as the Froude number increases towards the instability point. Ferrick (2005) again looked at comparisons between linear and non-linear waves. In that study, it was stated that wave development distances for the monoclinal wave are short for steep and shallow flow. The monoclinal wave that was examined was a rapid transition from a low steady flow to a higher steady flow.

Moussa and Bocquillon (1996) also created a set of criteria for use in determining when each wave approximation is appropriate. The parameters used in this study to define each approximation's applicable range were the Froude number and the period of the input hydrograph. As with Ferrick (1985), the criteria focused on the balance between friction and inertia terms in the Saint-Venant equations. Moussa and Bocquillon also went on to focus on the diffusive wave and examined different numerical solutions to that approximation. The authors also stated that wave approximations will not typically be valid when the depth and velocity change rapidly.

Mishra and Seth (1996) looked at the use of hysteresis to aid in the understanding of wave propagation in natural channels. This study used the

7

hysteresis that is present in a rating curve during a flood event to quantify which wave approximations (such as the gravity wave or kinematic wave) are appropriate in different situations. It was found that the degree of the hysteresis effect in the rating curve is a good indicator of the energy loss within the flood wave. Relationships were also postulated between the hysteresis and the celerity, attenuation, and wave number of the studied waves. Perumal, Shrestha, and Chaube (2004) also examined the hysteresis present in flood rating curves. The applicability of the Jones formula was examined for the conversion of stage to discharge.

Chung and Kang (2006) developed another criterion to classify wave types in natural channels. They decoupled the Saint-Venant equations using Laplacian frequency domains. The wave classification system developed is based on normalized specific energy, and incorporates the system developed by Ferrick and colleagues. This study also looked briefly at supercritical flow, from a numerical modeling standpoint.

In addition to analytical studies looking at the viability of different wave approximations, other analytical and theoretical work has been done involving supercritical flow or waves. Lyn and Altinakar (2002) produced an analytical solution of the coupled Saint-Venant and Exner equations. They observed that in

a mobile-bed system, strict definitions of supercritical and subcritical flow are not valid. In near-critical flow, bed waves and surface waves will interact strongly.

Ponce, Taher-shamsi, and Shetty (2003) used the method of Ponce and Simons (1977) to look at the propagation of dam break waves. The authors found that at a certain distance downstream of the dam, the attenuation of the wave will cause the peak discharge to be independent of the discharge through the dam break. Singh, Li, and Wang (1998) also looked at the attenuation of dam break waves. They used a second-order approximation of the Saint-Venant equations in that study. Further investigation into the theory of dam break waves was done by Wu, Huang, and Zheng (1999). They found that the wave properties will be defined solely by the ratio of initial upstream and downstream depths.

Venutelli (2004) performed a direct integration of a particular case of the gradually-varied flow equation and applied it to steep channels. Mizamura, Yamasaka, and Adachi (2003) performed analytical and experimental studies on flow through side outlets in steep channels. Criteria were developed to aid in calculating discharge through these outlets. Mizamura (2005) later refined the criteria. Graber (2006) performed a theoretical analysis of supercritical expansions and unstable water surface formation.

Mizamura (1995) performed both analytical and experimental studies on flow over wavy beds and with wavy side walls. Supercritical and subcritical flow were both looked at. Analytical results were not in agreement with experiments for supercritical flow with wavy walls. Molls and Zhao (2000) developed two numerical models to examine the waves generated in supercritical flow due to a wavy boundary. They compared the numerical results to experimental results from Mizamura (1995) with mixed effectiveness.

Menendez (1993) examined open channel waves from the perspective of looking at the form that a perturbation will have after a long time. It was found that any perturbation in a space-limited channel will, after enough time has past, be in the form of a bell, a step, or a sinusoid. This study considered only linear effects, but stated that linear solutions to the wave equations give good results due to the fact that large waves exhibit similar behavior, in a qualitative sense, as small waves. Froude numbers up to 2 were examined using a formulation based on the Chezy equation of resistance to flow. The use of this equation places the threshold for stability at 2, rather than 1.5 as is the case for the Manning equation for resistance, as will be shown later in the present study. Unstable waves at Froude numbers above 2 were not examined in any detail.

Tsai and Yen (2001) performed a detailed analytical study on the propagation of waves in shallow open channel flow. The downstream boundary condition in the channel was accounted for and its effects on wave propagation were examined. Laplace transforms were used as an alternative method of analyzing wave behavior. However, this study was limited to strictly subcritical flow. Tsai and Yen (2004) examined wave propagation in gradually-varied flow, such as an M1 or S1 profile. Steep channels were looked at, but the flow within these channels was limited to subcritcal, convectively decelerating flow in an S1 profile. Tsai (2003) used the methods of Tsai and Yen to examine the applicability of different wave approximations to different situations. Chung, Aldama, and Smith (1993) also looked at the effects of backwater on wave propagation. The diffusive wave approximation was used, which limits the results to subcritical flow only.

Onizuka and Odai (1998) used a method of approximating the Saint-Venant equations that allowed them to analytically inspect translatory waves in subcritical flow. Later, the authors made a more detailed study of the approximation, which is called the Burgers equation model (Odai, Kubo, Onizuka & Osato 2006). The results were still only valid for subcritical flow. Ponce, Rao, and Mansury (1999) analytically examined the attenuation of small waves formed by the opening of canal gates. A simple criterion was developed to aid canal operators with timing the opening of gates.

Recently, Ridolfi, Porporato, and Revelli (2006) derived the Green's function of the linear form of the Saint-Venant equations and used it to consider the behavior of waves in both subcritical and supercritical flow. The authors found that waves propagating in open channels will be composed of three distinct sub-waves; one downstream front, one upstream front, and one exponential wave. The Green's function derivation allowed the authors to examine the cause of the instability at a Froude number equal to 2. The study states that when the Froude number is greater than or equal to 2, the body of a wave will have a celerity greater than the front of the wave. This causes the wave damping that occurs at lower Froude numbers to disappear, and the wave amplifies. If a sufficient amount of time is allowed for the wave to grow, a roll wave will form at which point the wave is breaking and can no longer amplify.

A range of experimental studies have also been performed on supercritical flow. Chamani and Beirami (2002) looked into supercritical flow over drops. Empirical relationships were created to predict the energy loss when supercritical flow goes over a drop. In a similar vein, Lin, Huang, Suen, and Hsieh (2002) measured the velocity distribution of subcritical and supercritical flow over a drop.

Julien and Hartley (1986) studied the formation of roll waves in laminar sheet flow. The conditions in this study were subcritical, with very shallow flow. Because the flow was laminar, this study revealed that the flow can become unstable and produce amplifying waves at a theoretical Froude number of 0.5. Roll waves were actually observed in subcritical sheet flow at Froude numbers as low as 0.74. This study also examined the length that was necessary for the formation of these roll waves. The relationship found for the formation length of roll waves involved the momentum correction factor as a key parameter.

Einhellig and Pugh (2001) examined a physical model of a side weir designed for use in a steep channel. Ghodsian (2003) also looked at discharge over side weirs in supercritical channels. Equations were developed empirically for the calculation of discharge over these weirs.

Supercritical flow can also occur in closed-conduit systems. Supercritical flow through storm sewers has been the subject of numerous experiments by Hager and colleagues. Oliveto, Biggiero and Hager (1997) experimentally studied supercritical flow in sewers with bottom outlets. Design guidelines were presented. Reinauer and Hager (1998) experimented on supercritical flow in a converging open channel. Design guidelines were empirically created for these convergences. Giudice, Gisonni, and Hager (2000) performed experiments in

bend manholes for supercritical flow. Giudice and Hager (2001) later performed additional experiments on supercritical flow through manholes. Gargano and Hager (2002) looked at supercritical sewer flow, and recommended revising design standards for this case based on their experimental results. Finally, Martino, Gisonni, and Hager (2002) performed experiments on supercritical flow through sewers with the goal of examining sharp drop-offs and cross-section changes.

One development that may aid the experimental study of wave dynamics was made by Miyamoto and Kanda (2002). They presented a novel method of measuring both the elevation and velocity of rapidly varying water surfaces including supercritical waves.

The third main area of research in recent years has been numerical modeling. There is an almost infinite array of model types available. Different numerical schemes, grids and underlying equations make it possible to model almost any problem numerically.

Hicks, Steffler, and Yasmin (1997) looked at the viability of 1-D models for dam-break wave propagation. Mixed results were obtained when including supercritical flow. Unami, Kawachi, Babar, and Itagaki (1999) created a 2-D

numerical model to study supercritical flow down spillways. Mingham and Causon (1998) created a numerical model to look at bore wave propagation. The model is applicable to both subcritical and supercritical flow. These two researchers then teamed up with Ingram (Causon, Mingham, and Ingram 1999) and used a 2-D finite volume numerical model to study supercritical flow and wave heights and locations. Kruger and Rutschmann (2001) expanded this study with the use of more detailed shallow water equations.

Kruger and Rutschmann (2006) later created a very detailed numerical model for supercritical flow. This model is based on the Navier-Stokes equations and addresses flow separation and wave breaking at high Froude numbers. It was observed that wave heights will increase with Froude number.

Schwanenberg and Harms (2004) created a numerical model for trans-critical flow. They compared the model with actual dam-break measurements, with good results. Ying, Khan, and Wang (2004) developed a numerical model based on the Saint-Venant equations that is applicable to supercritical and transcritical flow. Valiani and Caleffi (2005) examined the applicability of numerical models to supercritical flow in sharp bends.

Zoppou and Roberts (2003) compared a wide variety of numerical models and looked at the accuracy of a modeled dam break, with and without supercritical flow.

Burg, Huddleston, and Berger (2001) used optimization to solve for channel geometry given a desired water surface profile. They applied this technique to supercritical flow in channel transitions.

2.2 Theory

One issue that needs to be accounted for in the design of steep open channels is the depth of flow within the channel. For steady and uniform flow, this depth would simply be a function of the channel properties such as geometry and roughness, along with the flow rate. However, steady uniform flow is not always present in real channels. There are many reasons that this ideal situation may not occur. The flow in a channel can be unsteady due to increases or decreases in the intensity of rainfall, as well as surges in flow caused by dam breaks, along with many other possibilities. With this unsteady flow, the depth in the channel is also a function of time. The unsteady flow fluctuations will cause the depth and velocity of the flow to vary in time rather than being constant. Another possible reason that steady uniform flow may not be present is when the flow is gradually varied in space. Gradually varied flow is when the parameters of the

flow change along the main direction of flow. This type of flow can be either steady or unsteady. Unsteady, gradually varied flow is the most general case, where the flow parameters can vary in both space and time.

The Saint-Venant equations can be used to describe the general unsteady, gradually varied case. These equations use the principles of both conservation of mass, and conservation of momentum. As noted by Lai, Baltzer, and Schaffranek (2003) care must be taken to ensure that the final equations used are consistent with the initial conservation assumptions. Using these equations, backwater profiles can be developed that give the depth and velocity of flow along the entire relevant reach and for the relevant stretch of time. When the flow is varied in either space or time, waves can form in the channel. The Saint-Venant equations can also be used to describe these waves. If the full Saint-Venant equations are used to describe a wave with no terms left out, the resulting model is called the dynamic wave model. By neglecting certain terms within the Saint-Venant equations other simplified wave models can be developed, such as the kinematic wave, diffusive wave and gravity wave (Julien 2002). Yen and Tsai (2001) made a case for referring to the diffusive wave approximation as the non-inertia wave. These simplified models have the advantage of being easier to use, and can give good results when used in the proper situations.

One-dimensional unsteady supercritical flow in open channels is governed by the Saint-Venant equations (Graf 1998). These equations can be stated as follows (Tsai 2005):

$$\frac{\partial y}{\partial t} + u \frac{\partial y}{\partial x} + y \frac{\partial u}{\partial x} = 0 \tag{2.1}$$

$$\frac{\partial u}{\partial t} + u \frac{\partial u}{\partial x} + g \frac{\partial y}{\partial x} + g \left(S_f - S_0 \right) = 0 \tag{2.2}$$

Where:

y = flow depth

t = time

u = flow velocity

x = spatial distance along the channel

g = gravitational acceleration

S_f = friction slope of the flowing water

S_0 = bed slope of the channel

The first of these equations is a statement of the principle of conservation of mass. The second equation is a version of the conservation of momentum principle. Because these equations contain derivatives in both space and time, they are valid for the general case of unsteady, gradually-varied flow. This statement of the Saint-Venant equations assumes that the channel is very wide

compared to its depth, and so the flow depth is essentially equal to the hydraulic radius. A visual depiction of the flow parameters contained in Equations (2.1) and (2.2) is shown below in Figure 2.1.
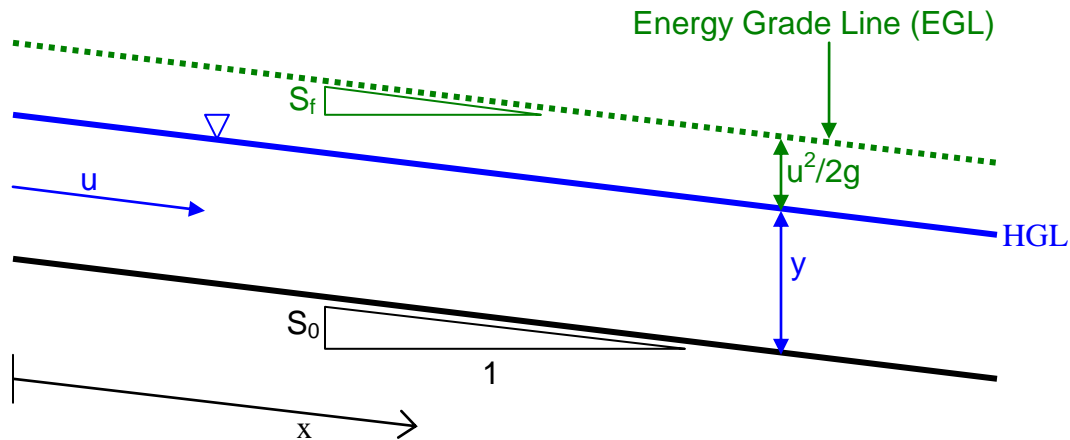
Figure 2.1 - Flow parameters

The friction slope term, S_f, in Equation (2.2) is representative of the rate of energy dissipation within the flowing water. The friction slope is most often defined using semi-empirical resistance equations such as the Chezy equation or Manning's equation. For this study, the Manning equation will be used. The Manning equation is similar in form to the Chezy equation, but contains an additional term of $y^{1/6}$. This has the result that the resistance coefficient used in Manning's equation can be reasonably approximated as being constant with depth, while the Chezy coefficient is not constant with depth (Tsai and Yen 2001). The Manning equation can be written as:

19

$$S_f = \frac{u^2 n^2}{\phi^2 R^{4/3}}$$ (2.3)

Where:

n = roughness coefficient for Manning's equation

ϕ = constant depending on the units used

R = hydraulic radius

This shows that the friction slope will increase proportional to the square of the velocity, and will decrease when the depth is increased. To be in the supercritical regime, flow will typically have a high velocity and small depth, which results in a high value for the friction slope. Manning's equation is strictly valid only for steady uniform flow. However, it is quite commonly used for unsteady and non-uniform flow conditions. Also, when looking at unsteady flow, care must be taken to ensure proper use of the energy and momentum equations (Field, Lambert, & Williams 1998).

The definition of supercritical flow can be stated as flow with a Froude number greater than one. The Froude number can be found using:

$$Fr = \frac{u}{\sqrt{gy}}$$ (2.4)

Where:

Fr = Froude number

The Froude number is a ratio of the inertial forces to the gravitational forces in flowing water. Along with the friction slope, the Froude number is one of the defining characteristics of a backwater profile. Backwater profiles can be categorized into different groups based on the parameters of the channel and of the flow within that channel. For a given flow rate, the bed slope in a channel can be defined as either "steep" or "mild" depending on the relative magnitudes of the normal depth and critical depths (Mays 2005). The normal depth can be found using Equation (2.3) and setting the friction slope equal to the bed slope. This signifies a situation where the flow in the channel is controlled by the channel, and the flow is uniform. The critical depth can be found by setting the Froude number equal to one, and solving for depth. If the normal depth is higher than the critical depth, the channel is mild. If the normal depth is below the critical depth, the channel is steep at that flow rate. A steep channel corresponds to the uniform flow condition in that channel being supercritical. Depending on where the actual flow depth lies, the flow in a steep channel can be further subdivided into three zones. If the flow depth is greater than critical depth, the flow is subcritical and is within zone 1. If the flow is less than critical depth, but still greater than normal depth, the flow is supercritical and within zone 2. Zone 3 is when the flow depth is less than normal depth, and is also supercritical. Flow

that approaches critical depth is often unstable. If the channel and flow parameters are constant, the flow will asymptotically approach normal depth.

It should be stressed that the derivations in the rest of this chapter are based on the work of Tsai and Yen. Because the results were published in a peer-reviewed journal, the author has taken as a given that the derivation is correct both theoretically and mathematically. Following the derivation of Tsai (2005), the Saint-Venant equations can be non-dimensionalized. The dimensionless parameters used are as follows:

$$x^* = \frac{x}{L_0} \tag{2.5}$$

$$t^* = \frac{u_n t}{L_0} \tag{2.6}$$

$$u^* = \frac{u}{u_n} \tag{2.7}$$

$$y^* = \frac{y}{y_n} \tag{2.8}$$

Where:

x^* = dimensionless distance along the channel

t^* = dimensionless time

u^* = dimensionless flow velocity, expressed as a ratio to the normal flow velocity

y^* = dimensionless ratio of the flow depth to the normal depth

$$L_0 = y_n/S_0$$

y_n = normal flow depth calculated using a resistance equation

u_n = flow velocity associated with the normal flow depth

The parameter L_0 can be thought of as the longitudinal distance along the channel necessary for the bed to drop in elevation an amount equal to the normal depth. Visually, this is shown in Figure 2.2.
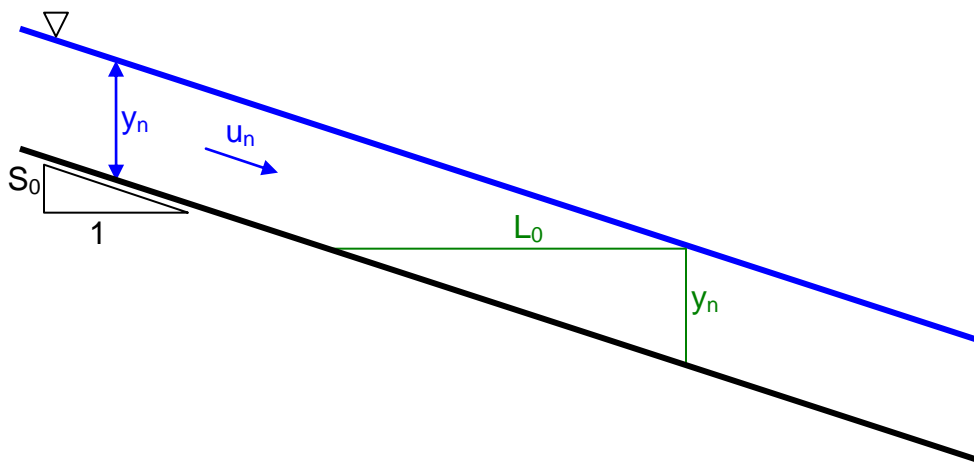
Figure 2.2 - Normalized length

These four dimensionless parameters can be inserted into Equations (2.1) and (2.2). The depth and velocity will be equal to the normal depth and velocity when the friction slope is equal to the channel slope.

$$S_0 = \frac{u_n^2 n^2}{\phi^2 R_n^{4/3}} \qquad (2.9)$$

Where:

R_n = hydraulic radius at normal flow conditions

With this, the ratio between the friction slope and the bed slope can be expressed as

$$\frac{S_f}{S_0} = \left(\frac{u}{u_n}\right)^2 \left(\frac{R}{R_n}\right)^{-\alpha} \qquad \textbf{(2.10)}$$

Where:

α = a constant that will vary based on which resistance equation is used.

With Manning's equation, α will have a value of 4/3, while if the Chezy or Darcy-Weisbach resistance equations are used, α will have a value of unity. If, as in the statement of the Saint-Venant equations used in this study, the channel is assumed to be wide relative to its depth, the hydraulic radius R will be equal to the depth y. Noting that the ratios in Equation (2.10) are the same as in Equations (2.7) and (2.8), Equation (2.10) can be rewritten as

$$\frac{S_f}{S_0} = \frac{u^{*2}}{y^{*\alpha}} \qquad \textbf{(2.11)}$$

With these equations defined, the Saint-Venant equations can then be non-dimensionalized. The dimensionless ratios in Equations (2.5) - (2.8) can be rearranged to give

$$x = \frac{x^* y_n}{S_0} \tag{2.12}$$

$$t = \frac{t^* y_n}{u_n S_0} \tag{2.13}$$

$$u = u^* u_n \tag{2.14}$$

$$y = y^* y_n \tag{2.15}$$

These equations can then be substituted into Equation (2.1).

$$\frac{\partial \left(y^* y_n \right)}{\partial \left(\dfrac{t^* y_n}{u_n S_0} \right)} + u^* u_n \frac{\partial \left(y^* y_n \right)}{\partial \left(\dfrac{x^* y_n}{S_0} \right)} + y^* y_n \frac{\partial \left(u^* u_n \right)}{\partial \left(\dfrac{x^* y_n}{S_0} \right)} = 0 \tag{2.16}$$

The normal flow case will be constant with time as long as the geometry of the channel does not change. Pulling all of the constant terms outside of the derivatives and canceling gives

$$\frac{\partial y^*}{\partial t^*} + u^* \frac{\partial y^*}{\partial x^*} + y^* \frac{\partial u^*}{\partial x^*} = 0 \tag{2.17}$$

This is in the same form as Equation (2.1) with all of the variables replaced with their dimensionless equivalents. Similarly, Equation (2.2) can be rearranged noting that

$$S_f - S_0 = S_0\left(\frac{S_f}{S_0} - 1\right) = S_0\left(\frac{u^{*2}}{y^{*\alpha}} - 1\right) \tag{2.18}$$

And so

$$\frac{\partial\left(u^*u_n\right)}{\partial\left(\frac{t^*y_n}{u_nS_0}\right)} + u^*u_n\frac{\partial\left(u^*u_n\right)}{\partial\left(\frac{x^*y_n}{S_0}\right)} + g\frac{\partial\left(y^*y_n\right)}{\partial\left(\frac{x^*y_n}{S_0}\right)} + gS_0\left(\frac{u^{*2}}{y^{*\alpha}} - 1\right) = 0 \tag{2.19}$$

Again, the constant terms can be taken out of the derivatives and terms can be cancelled. Additionally, the entire equation can be divided by gS_0 to give

$$\frac{u_n^2}{gy_n}\left(\frac{\partial u^*}{\partial t^*} + u^*\frac{\partial u^*}{\partial x^*}\right) + \frac{\partial y^*}{\partial x^*} + \left(\frac{u^{*2}}{y^{*\alpha}} - 1\right) = 0 \tag{2.20}$$

The first term in Equation (2.20) is the same as Fn^2, where Fn is the Froude number at normal conditions; $Fn = u_n / \sqrt{gy_n}$.

The equation that describes the change in depth with space for a gradually-varied flow profile is

$$\frac{dy}{dx} = \frac{S_0 - S_f}{1 - Fr^2} \tag{2.21}$$

As previously explained, the relative magnitudes of the terms in Equation (2.21) determine the type of water surface profile that will be present. If the base flow in

a channel is defined as y_b, a dimensionless base flow can be defined as y_b^* in a similar manner as the earlier dimensionless parameters. Once again the dimensionless parameters can be inserted into Equation (2.21) and terms cancelled. The resulting equation is

$$\frac{dy_b^*}{dx^*} = \frac{1 - S_f/S_0}{1 - Fr^2}$$ (2.22)

Using the method of Tsai (2005) which is based on the work of Ponce and Simons (1977), a linear stability analysis can be done on the dimensionless Saint-Venant equations to find the celerity and attenuation/amplification factor of a wave. This linear analysis assumes that the wave is of infinitesimal amplitude, although some studies (Menendez, 1993) have indicated that waves of reasonable dimensions will be quantitatively similar to infinitesimal waves. A perturbation that is imposed mathematically on the steady base flow can be depicted as

$$y^* = y_b^* + y^{`*}$$ (2.23)

$$u^* = u_b^* + u^{`*}$$ (2.24)

Where:

$y^{`*}$ = depth perturbation

$u^{`*}$ = velocity perturbation

A visual depiction of this perturbation can be seen in Figure 2.3. The vertical scale in Figure 2.3 is exaggerated to show detail.
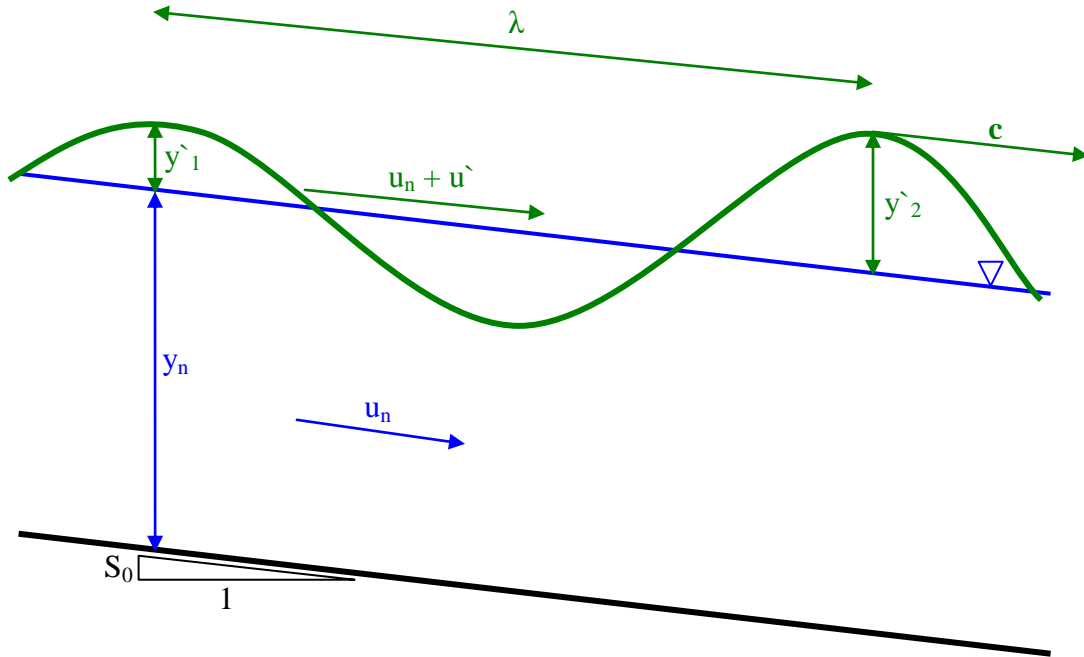
Figure 2.3 – Small wave perturbation on base flow

The first term in Equations (2.23) and (2.24) is a first order term, while the second term is assumed to be a lower order of magnitude than the first term. The perturbations can be expressed as a sinusoid using the relationship of Euler

$$y^{\grave{}*} = \hat{y}e^{i\theta*} \tag{2.25}$$

$$u^{\grave{}*} = \hat{u}e^{i\theta*} \tag{2.26}$$

Where:

$\hat{y}$ = amplitude of the depth perturbation

$\hat{u}$ = amplitude of the velocity perturbation

i = the square root of -1

θ^{*} = a phase variable

These definitions can be used with Equation (2.17) to give

$$\frac{\partial \left(y_b^{*} + y^{`*} \right)}{\partial t^{*}} + \left( u_b^{*} + u^{`*} \right) \frac{\partial \left(y_b^{*} + y^{`*} \right)}{dx^{*}} + \left( y_b^{*} + y^{`*} \right) \frac{\partial \left(u_b^{*} + u^{`*} \right)}{\partial x^{*}} = 0 \qquad \textbf{(2.27)}$$

Separating the derivatives and rearranging gives

$$\frac{\partial y^{`*}}{\partial t^{*}} + u_b^{*} \frac{\partial y_b^{*}}{\partial x^{*}} + u_b^{*} \frac{\partial y^{`*}}{\partial x^{*}} + y_b^{*} \frac{\partial u_b^{*}}{\partial x^{*}} + y_b^{*} \frac{\partial u^{`*}}{\partial x^{*}}$$
$$+ u^{`*} \left( \frac{\partial y_b^{*}}{\partial x^{*}} + \frac{\partial y^{`*}}{\partial x^{*}} \right) + y^{`*} \left( \frac{\partial u_b^{*}}{\partial x^{*}} + \frac{\partial u^{`*}}{\partial x^{*}} \right) = 0 \qquad \textbf{(2.28)}$$

With the definition of $u^{`*}$ and $y^{`*}$ in Equations (2.25) and (2.26), the derivatives of those terms can be found as

$$\frac{\partial y^{`*}}{\partial t^{*}} = \hat{y}ie^{i\theta*} \frac{\partial \theta^{*}}{\partial t^{*}} = iy^{`*} \frac{\partial \theta^{*}}{\partial t^{*}} \qquad \textbf{(2.29)}$$

$$\frac{\partial y^{`*}}{\partial x^{*}} = \hat{y}ie^{i\theta*} \frac{\partial \theta^{*}}{\partial x^{*}} = iy^{`*} \frac{\partial \theta^{*}}{\partial x^{*}} \qquad \textbf{(2.30)}$$

$$\frac{\partial u^{`*}}{\partial t^{*}} = \hat{u}ie^{i\theta*} \frac{\partial \theta^{*}}{\partial t^{*}} = iu^{`*} \frac{\partial \theta^{*}}{\partial t^{*}} \qquad \textbf{(2.31)}$$

$$\frac{\partial u^{`*}}{\partial x^{*}} = \hat{u}ie^{i\theta*} \frac{\partial \theta^{*}}{\partial x^{*}} = iu^{`*} \frac{\partial \theta^{*}}{\partial x^{*}} \qquad \textbf{(2.32)}$$

Thus the exponential terms will disappear from Equation (2.28) giving

$$iy^{`*}\frac{\partial\theta^{*}}{\partial t^{*}} + u_{b}^{*}\frac{\partial y_{b}^{*}}{\partial x^{*}} + u_{b}^{*}iy^{`*}\frac{\partial\theta^{*}}{\partial x^{*}} + y_{b}^{*}\frac{\partial u_{b}^{*}}{\partial x^{*}} + y_{b}^{*}iu^{`*}\frac{\partial\theta^{*}}{\partial x^{*}}$$
$$+ u^{`*}\frac{\partial y_{b}^{*}}{\partial x^{*}} + u^{`*}iy^{`*}\frac{\partial\theta^{*}}{\partial x^{*}} + y^{`*}\frac{\partial u_{b}^{*}}{\partial x^{*}} + y^{`*}iu^{`*}\frac{\partial\theta^{*}}{\partial x^{*}} = 0$$

(2.33)

Because the perturbations $y^{`*}$ and $u^{`*}$ are assumed to be of small magnitude, the product of two of these variables will be equivalent to a higher order term that can be neglected. Canceling terms where possible and combining gives

$$u^{`*}\left[\frac{\partial y_{b}^{*}}{\partial x^{*}} + y_{b}^{*}i\frac{\partial\theta^{*}}{\partial x^{*}}\right] + y^{`*}\left[i\frac{\partial\theta^{*}}{\partial t^{*}} + u_{b}^{*}i\frac{\partial\theta^{*}}{\partial x^{*}} + \frac{\partial u_{b}^{*}}{\partial x^{*}}\right]$$
$$+ u_{b}^{*}\frac{\partial y_{b}^{*}}{\partial x^{*}} + y_{b}^{*}\frac{\partial u_{b}^{*}}{\partial x^{*}} = 0$$

(2.34)

The unit discharge for flow in a channel can be described as

$$q = uy$$

(2.35)

Where:

q = the discharge per unit width in the channel

Therefore the dimensionless unit discharge can be seen to be

$$q^{*} = u^{*}y^{*}$$

(2.36)

Where:

q^{*} = the dimensionless unit discharge

For steady flow conditions, the value of q^{*} will be equal to unity. This means that

$$u^* y^* = u_b{}^* y_b{}^* = 1 \qquad (2.37)$$

Using this relationship, base flow parameters can be expressed as either depth or velocity. Taking derivatives with respect to space gives

$$\frac{\partial u_b{}^*}{\partial x^*} = -y_b{}^{*-2} \frac{\partial y_b{}^*}{\partial x^*} \qquad (2.38)$$

$$\frac{\partial y_b{}^*}{\partial x^*} = -u_b{}^{*-2} \frac{\partial u_b{}^*}{\partial x^*} \qquad (2.39)$$

The final two terms in Equation (2.34) can then be stated as

$$
\begin{aligned}
u_b{}^* \frac{\partial y_b{}^*}{\partial x^*} + y_b{}^* \frac{\partial u_b{}^*}{\partial x^*} &= u_b{}^* \frac{\partial y_b{}^*}{\partial x^*} - y_b{}^{*-1} \frac{\partial y_b{}^*}{\partial x^*} \\
&= y_b{}^{*-1} \frac{\partial y_b{}^*}{\partial x^*} - y_b{}^{*-1} \frac{\partial y_b{}^*}{\partial x^*}
\end{aligned}
\qquad (2.40)
$$

These terms are then equal to zero, and the final equation for conservation of mass with an infinitesimal linear perturbation is

$$u^{`*} \left[ \frac{\partial y_b{}^*}{\partial x^*} + y_b{}^* i \frac{\partial \theta^*}{\partial x^*} \right] + y^{`*} \left[i \frac{\partial \theta^*}{\partial t^*} + u_b{}^* i \frac{\partial \theta^*}{\partial x^*} + \frac{\partial u_b{}^*}{\partial x^*} \right] = 0 \qquad (2.41)$$

It is interesting to note that the depth of the perturbation is multiplied by a time derivative, but the velocity of the perturbation is not.

Plugging Equations (2.25) and (2.26) into Equation (2.20) gives

$$Fn^2\left[\frac{\partial\left(u_b^* + u^{`*}\right)}{\partial t^*} + \left(u_b^* + u^{`*}\right)\frac{\partial\left(u_b^* + u^{`*}\right)}{\partial x^*}\right]$$
$$+\frac{\partial\left(y_b^* + y^{`*}\right)}{\partial x^*} + \frac{\left(u_b^* + u^{`*}\right)^2}{\left(y_b^* + y^{`*}\right)^\alpha} - 1 = 0$$

(2.42)

Utilizing Equations (2.29) - (2.32) as well as rearranging and canceling terms gives

$$Fn^2\left(iu^{`*}\frac{\partial\theta^*}{\partial t^*} + iu_b^* u^{`*}\frac{\partial\theta^*}{\partial x^*} + u^{`*}\frac{\partial u_b^*}{\partial x^*}\right) + \frac{u_b^{*2} + 2u_b^* u^{`*}}{\left(y_b^* + y^{`*}\right)^\alpha}$$
$$+ Fn^2\left(\frac{\partial u_b^*}{\partial t^*} + u_b^*\frac{\partial u_b^*}{\partial x^*}\right) + iy^{`*}\frac{\partial\theta^*}{\partial x^*} + \frac{\partial y_b^*}{\partial x^*} - 1 = 0$$

(2.43)

A Taylor Series expansion of the term $\left(y_b^* + y^{`*}\right)^\alpha$ around the value y_b^* gives

$$\left(y_b^* + y^{`*}\right)^\alpha = y_b^{*\alpha} + \alpha y_b^{*\alpha-1} y^{`*} + \frac{\alpha\left(\alpha - 1\right)}{2}y_b^{*\alpha-2} y^{*2}$$

(2.44)

The last term in this equation can be neglected because it is of a lower order of magnitude. Using this in Equation (2.43) with further rearranging gives

$$u^{`*}\left[Fn^2\left(i\frac{\partial\theta^*}{\partial t^*} + iu_b^*\frac{\partial\theta^*}{\partial x^*} + \frac{\partial u_b^*}{\partial x^*}\right)\right] + y^{`*}\left[i\frac{\partial\theta^*}{\partial x^*}\right] + Fn^2 u_b^*\frac{\partial u_b^*}{\partial x^*}$$
$$+\frac{\partial y_b^*}{\partial x^*} - 1 + \left(u_b^{*2} + 2u_b^* u^{`*}\right)\left(y_b^{*-\alpha} - \alpha y_b^{*-\alpha-1} y^{`*}\right) = 0$$

(2.45)

This can once again be simplified using Equation (2.37) to

$$u^{`*}\left[Fn^2\left(i\frac{\partial\theta^*}{\partial t^*}+iu_b^*\frac{\partial\theta^*}{\partial x^*}+\frac{\partial u_b^*}{\partial x^*}\right)+2y_b^{*-1-\alpha}\right]$$

$$+y^{`*}\left[i\frac{\partial\theta^*}{\partial x^*}-\alpha y_b^{*-3-\alpha}\right]+Fn^2u_b^*\frac{\partial u_b^*}{\partial x^*}+\frac{\partial y_b^*}{\partial x^*}-1+y_b^{*-\alpha-2}=0$$

(2.46)

Because the terms of interest are the ones that are multiplied by the perturbation quantities $u^{`*}$ and $y^{`*}$, the other terms can be neglected in this analysis, leaving the following as the perturbed version of the conservation of momentum equation

$$u^{`*}\left[Fn^2\left(i\frac{\partial\theta^*}{\partial t^*}+iu_b^*\frac{\partial\theta^*}{\partial x^*}+\frac{\partial u_b^*}{\partial x^*}\right)+2y_b^{*-1-\alpha}\right]$$

$$+y^{`*}\left[i\frac{\partial\theta^*}{\partial x^*}-\alpha y_b^{*-3-\alpha}\right]=0$$

(2.47)

This along with Equation (2.41) gives a coefficient matrix multiplied by a column vector with $u^{`*}$ and $y^{`*}$ in it. As stated by Tsai (2005) as well as Ponce and Simons (1977), the determinate of this matrix must be equal to zero for the solution to be non-trivial. Taking the determinate equal to zero gives

$$\left[\frac{\partial y_b^*}{\partial x^*}+y_b^*i\frac{\partial\theta^*}{\partial x^*}\right]\left[i\frac{\partial\theta^*}{\partial x^*}-\alpha y_b^{*-3-\alpha}\right]-\left[i\frac{\partial\theta^*}{\partial t^*}+u_b^*i\frac{\partial\theta^*}{\partial x^*}+\frac{\partial u_b^*}{\partial x^*}\right]$$

$$*\left[Fn^2\left(i\frac{\partial\theta^*}{\partial t^*}+iu_b^*\frac{\partial\theta^*}{\partial x^*}+\frac{\partial u_b^*}{\partial x^*}\right)+2y_b^{*-1-\alpha}\right]=0$$

(2.48)

At this point, several additional quantities can be defined. The phase variable, θ^*, has both a time and space derivative. These are represented by

$$\frac{\partial \theta^*}{\partial t^*} = -\beta^* \tag{2.49}$$

$$\frac{\partial \theta^*}{\partial x^*} = \sigma^* \tag{2.50}$$

Where:

$\beta^* = \beta_r^* + \beta_c^* = $ a complex propagation number

$\sigma^* = $ dimensionless wave number

The dimensionless wave number is a way of quantifying the wave frequency in a dimensionless manner, and is defined as

$$\sigma^* = \frac{2\pi L_0}{\lambda} \tag{2.51}$$

Where:

$\lambda = $ the wavelength of the small perturbation

The celerity of a wave is defined as its propagation speed and is given mathematically as

$$c = \frac{\lambda}{T} \tag{2.52}$$

Where:

$c = $ wave celerity

$T = $ wave period

A dimensionless celerity can be then defined as the ratio of celerity to normal flow velocity

$$c^* = \frac{c}{u_n}$$ (2.53)

Where:

c^* = dimensionless celerity

According to Ponce and Simons (1977), the real component of the complex propagation number β^* can be expressed as

$$\beta_r^* = \frac{2\pi L_0}{T u_n}$$ (2.54)

Combining this with the definition of the wave number in Equation (2.51), the dimensionless celerity can be expressed as

$$c^* = \frac{\beta_r^*}{\sigma^*}$$ (2.55)

Wave attenuation and amplification can be described by an exponential terms like so

$$y = y_0 e^{\beta_c^* t^*}$$ (2.56)

Equation(2.56) can be rearranged such that

$$\beta_c^* t^* = \ln\left(\frac{y}{y_0}\right) \tag{2.57}$$

The product of the imaginary component of the propagation number and dimensionless time can be defined as the logarithmic attenuation factor, δ^*.

Again following Ponce and Simons (1977), this attenuation factor can be restated as

$$\delta^* = \beta_c^* t^* = 2\pi \frac{\beta_c^*}{\left|\beta_r^*\right|} \tag{2.58}$$

With the definitions of dimensionless celerity and attenuation factor, these two parameters can be solved for using Equation (2.48). The complex propagation number β^* can be found by solving Equation (2.48), realizing that it is a quadratic equation with a complex square root. According to Tsai (2003), the complex propagation number for the full dynamic wave is

$$\beta_c^* = y_b^{*-2} \frac{dy_b^*}{dx^*} - \frac{1}{Fn^2} y_b^{*-1-\alpha} + \frac{1}{Fn^2}(A^2 + B^2)^{1/4} \cos\frac{\theta + 2(j-1)\pi}{2} \tag{2.59}$$

$$\beta_r^* = \sigma^* y_b^{*-1} + \frac{1}{F_n^2}(A^2 + B^2)^{1/4} \sin\frac{\theta + 2(j-1)\pi}{2} \tag{2.60}$$

Where:

$$A = y_b^{*-2-2\alpha} + F_n^2\left[-\sigma^{*2}y_b^* - \alpha y_b^{*-3-\alpha}\left(\frac{dy_b^*}{dx^*}\right)\right]$$

$$B = F_n^2 \left[\sigma^* \left(\frac{dy_b^*}{dx^*} \right) - \alpha \sigma^* y_b^{*-2-\alpha} \right]$$

$$\theta = \cos^{-1} \left[\frac{A}{\left(A^2 + B^2 \right)^{1/2}} \right]$$

This then leads to the definition of the dimensionless celerity and attenuation factor as

$$c^* = y_b^{*-1} + \frac{1}{\sigma^* F_n^2} (A^2 + B^2)^{1/4} \sin \frac{\theta + 2(j-1)\pi}{2}$$

(2.61)

$$\delta^* = 2\pi \frac{F_n^2 y_b^{*-2} \dfrac{dy_b^*}{dx^*} - y_b^{*-1-\alpha} + (A^2 + B^2)^{1/4} \cos \dfrac{\theta + 2(j-1)\pi}{2}}{\left| (A^2 + B^2)^{1/4} \sin \dfrac{\theta + 2(j-1)\pi}{2} + \sigma^* F_n^2 y_b^{*-1} \right|}$$

(2.62)

The two equations can be used to find the celerity and attenuation factor of any small wave in gradually varied flow. Tsai and Yen have used these equations to examine the propagation of waves in subcritical flow. A sample of the results found by them is shown in Figure 2.4 (Tsai 2005). These results will be expanded in the following chapters to include supercritical flow, as well as be applied to a specific drainage channel in Las Vegas, Nevada.
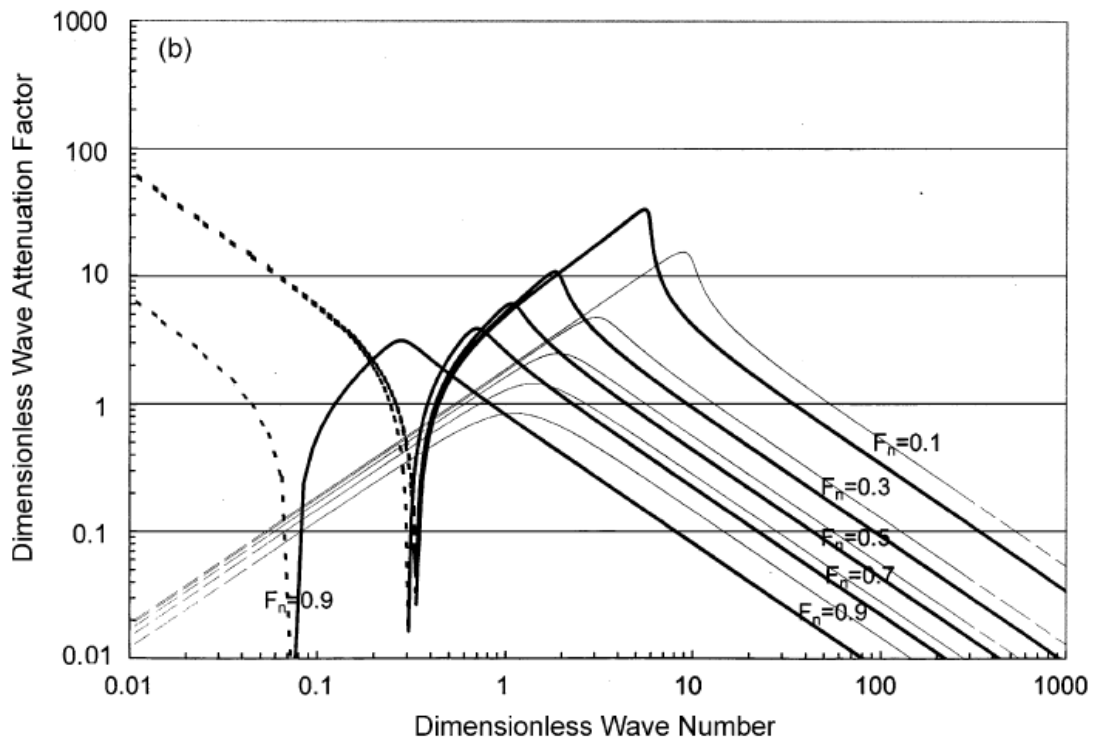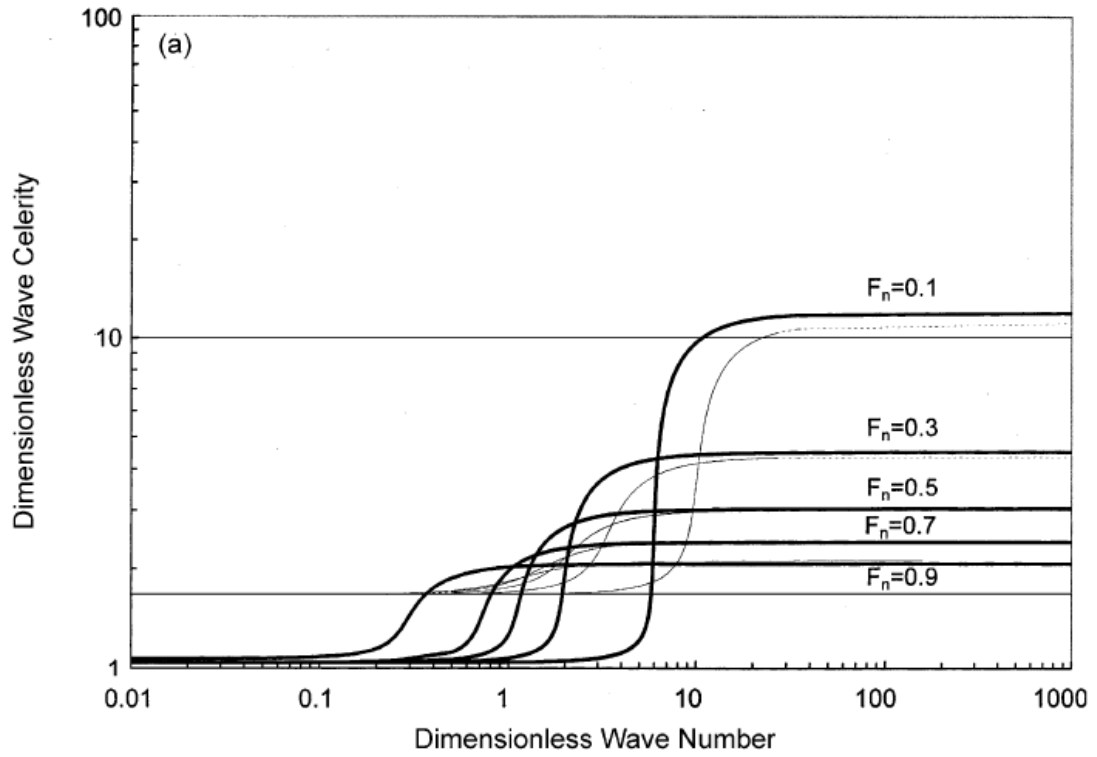
Figure 2.4 - Celerity and attenuation from Tsai (2005)

Chapter 3: Theoretical Results and Analysis

The celerity and attenuation of waves was examined for a variety of flow conditions and situations. The main zone of interest for this study is when the Froude number of the flow is between approximately 2 and 4, as these values are commonly found in Las Vegas storm drainage canals (Duan and Chen 2003). However, Froude numbers outside of this range will also be subject to a theoretical investigation based on Equations (2.61) and   (2.62).   The dimensionless celerity and attenuation factor will be calculated for a wide range of Froude numbers and the results examined.

3.1 Celerity and attenuation factor versus wave number

For a given Froude number, the wave number can be varied along a range. Ponce and Simons (1977) stated that the secondary wave will attenuate along the entire wave number spectrum for all Froude numbers. Since the case of wave attenuation is not of chief interest in this study, only the primary wave will be investigated. The base flow in the Las Vegas storm drainage canals can be assumed to be steady and uniform, with the wave perturbation imposed on it. Manning's equation is the most widely used equation for frictional resistance in

open channels, and will be used in this study. The method used to calculate both

dimensionless celerity and amplification factor is detailed below.

1) The first step is to select a Froude number. In this calculation example,

   Fn = 2.66 will be used.

2) Next, a wave number must be selected. A wave number of 1 will be used

   for this computation.

3) The value of alpha is determined by the resistance equation used.

   Manning's equation is being used in this study, and therefore α = 4/3.

4) Because of the assumption of uniform base flow, yb* is equal to unity, due

   to the fact that the base flow depth is equal to normal depth. Also,

   because the base flow is assumed constant with distance, the parameter

   $dy_b^* / dx^* = 0$.

5) As stated above, the primary wave will be the focus of this study, and so j

   = 1.

6) With these values, the dummy variables A, B, and θ can be found like so

$$A = 1^{-2-2(4/3)} + 2.66^2\left[-\left(2 \cdot 1\right) - \left(\frac{4}{3}\right)1^{-3-(4/3)} \cdot 0\right]$$
$$= 1 + 7.08\left(-1\right)$$
$$= -6.08$$

$$B = 2.66^2\left[1 \cdot 0 - \left(\frac{4}{3}\right)1 \cdot 1^{-2-(4/3)}\right]$$
$$= 7.08 \cdot \left(-1.33\right)$$
$$= -9.43$$

$$\theta = \cos^{-1}\left\{\frac{-6.08}{\left[\left(-6.08\right)^2 + \left(-9.43\right)^2\right]^{1/2}}\right\}$$
$$= \cos^{-1}\left(\frac{-6.08}{11.22}\right)$$
$$= \cos^{-1}\left(-0.541\right)$$
$$= 2.14$$

7) With the three numbers found in step 6, the dimensionless celerity can be

calculated using Equation (2.61)

$$c^* = 1^{-1} + \frac{1}{1 \cdot 2.66^2}\left[\left(-6.08\right)^2 + \left(-9.43\right)^2\right]^{1/4}\sin\left[\frac{2.14 + 2\left(-1\right)\pi}{2}\right]$$
$$= 1 + 0.141\left(25.9\right)^{0.25}\sin\left(.07\right)$$
$$= 1 + 0.472 \cdot 0.877$$
$$= 1.416$$

8) Then, using Equation (2.62), the attenuation factor can be found

$$\delta^* = 2\pi\left\{\frac{2.66^2\cdot 1^{-2}\cdot 0 - 1^{-1-4/3}+\left[\left(-6.08\right)^2+\left(9.43\right)^2\right]^{1/4}\cos\left[\frac{2.14+2\left(-1\right)\pi}{2}\right]}{\left|\left[\left(-6.08\right)^2+\left(9.43\right)^2\right]^{1/4}\sin\left[\frac{2.14+2\left(-1\right)\pi}{2}\right]+1\cdot 2.66^2\cdot 1^{-1}\right|}\right\}$$

$$= 2\pi\left[\frac{-1+\left(25.9\right)^{0.25}\cos\left(.07\right)}{\left|\left(25.9\right)^{0.25}\sin\left(.07\right)+7.08\right|}\right]$$

$$= 2\pi\left(\frac{0.614}{10.02}\right)$$

$$= 0.379$$

9) At this point, a new wave number can be chosen, and steps 6-8 can be repeated until a line for the chosen Froude number is found.

10) Once the line for the chosen Froude number is completed, a new Froude number can be chosen, and a line plotted for that.

A plot of dimensionless celerity versus wave number is shown in Figure 3.1. This is similar to a plot created by Ponce and Simons (1977) with the difference that Manning's equation was used here while Ponce and Simons used the Chezy equation.
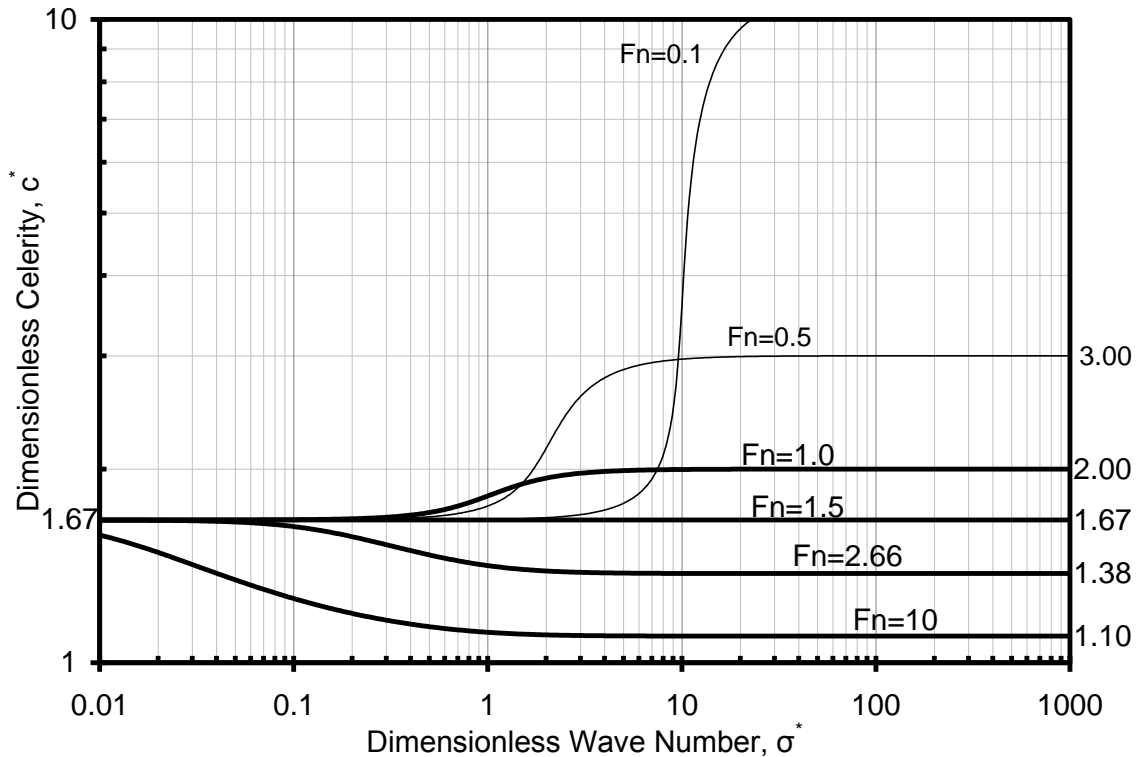
Figure 3.1 - Dimensionless celerity vs. wave number

It can be seen in Figure 3.1 that the dimensionless celerity of any wave will

approach 1.667 or 5/3 when the wave number is small. Using the definition of

wave number in Equation (2.51) it can be seen that the wave number is

inversely proportional to the wavelength of the disturbance. Therefore a small

wave number indicates a perturbation of large wavelength. Waves of this type

will travel with a constant celerity irrespective of Froude number. This conclusion

confirms the common result found in Graf (1998) as well as many other sources.

An increasing wave number corresponds to waves of decreasing length. As the

wave number increases, the dimensionless celerity of propagation for the wave

will deviate from the constant value found for very long waves. Wave traveling in

flow with high Froude numbers will deviate very quickly from this constant value. Figure 3.1 shows that waves with a Froude number of 10 will have dimensionless celerities different than 5/3 at wave numbers less than 0.01. The smaller the Froude number, the shorter waves must get before the dimensionless celerity will deviate from 5/3. Flow with a Froude number of 0.1 will not deviate until the wave number is greater than 1.0.

Regardless of Froude number, all of the lines in Figure 3.1 have one trend in common. After starting at a constant dimensionless celerity of 5/3 for low wave numbers, all of the Froude number lines will deviate from that value for a while and then become constant again for high wave numbers. The Froude number controls the degree as well as the sharpness of this deviation. A Froude number of 0.1 will deviate quite far from 5/3 at higher wave numbers, and will change from 5/3 to its upper constant value of 11 over a relatively short range of wave numbers. This creates a very steep slope in the line for Fr = 0.1 in Figure 3.1. As the Froude number increases, the slope around the inflection point of each line will become milder. Also, the constant dimensionless celerity that is achieved at high wave numbers (short wavelengths) will decrease as Froude number increases. As the Froude number of the flow increases, the base velocity is increasing. Because the dimensionless celerity is the ratio of celerity to base flow velocity, if the dimensionless celerity and base flow velocity are both

high, the dimensional celerity must be extremely high to overcome the influence of the high base flow velocity. This would result in wave speeds that are unreasonably fast, and so as the base flow velocity increases, the maximum dimensionless wave celerity will decrease. As the Froude number gets very high, the dimensionless celerity will approach unity, and waves will propagate at the same speed as the base flow.

A Froude number of 1.5 is the threshold value for determining if the dimensionless celerity will increase or decrease as the wave number increases. Froude numbers below this threshold will increase, while flow with Froude numbers above 1.5 will have a decreasing dimensionless celerity. Flow with a Froude number of exactly 1.5 will have a constant dimensionless celerity of 5/3 regardless of wave number and hence wavelength. This threshold of 1.5 is dependant on the assumptions made in the derivation above. The threshold will change if different assumptions are made. For example, if the Chezy or Darcy-Weisbach equations are used instead of the Manning equation for frictional resistance, the threshold value will be a Froude number of 2. Figure 3.1 indicates that waves traveling in flow with high Froude numbers will have a celerity slower than that of a kinematic wave, while waves with a low Froude number will travel faster than a kinematic wave, at higher wave numbers.

The dimensionless attenuation factor can also be calculated for a variety of Froude numbers and wave numbers. By plotting the same range of Froude numbers as are in Figure 3.1, Figure 3.2 and Figure 3.3 can be produced. These plots have the same range of wave numbers as Figure 3.1. Negative values for the dimensionless attenuation factor, δ^*, indicate that the wave will attenuate as it propagates. Positive values indicate that waves will amplify. Once again, a Froude number of 1.5 is seen to be the threshold value. Froude numbers below the threshold will have waves that attenuate for all wave numbers. Above the threshold, all waves will amplify. Waves that exist in flow with a Froude number of exactly 1.5 will travel downstream with no amplitude change. It is still possible and likely that the shape of a wave will change even if the amplitude does not.
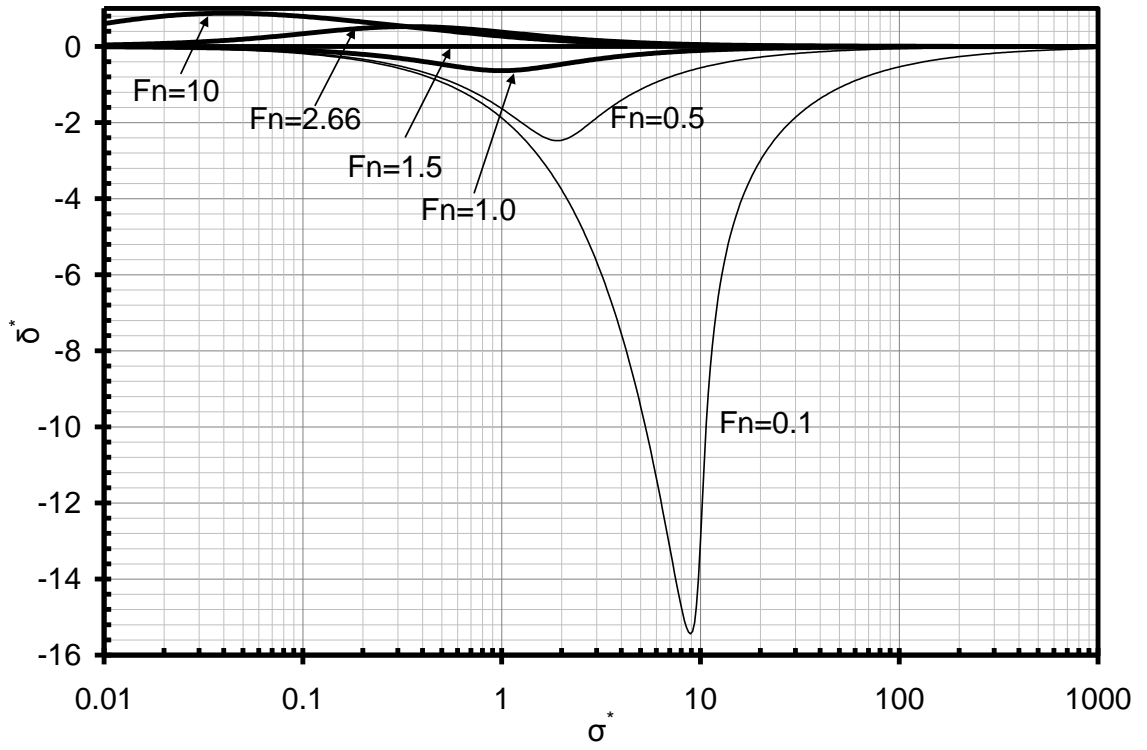
Figure 3.2 - Dimensionless attenuation factor versus wave number
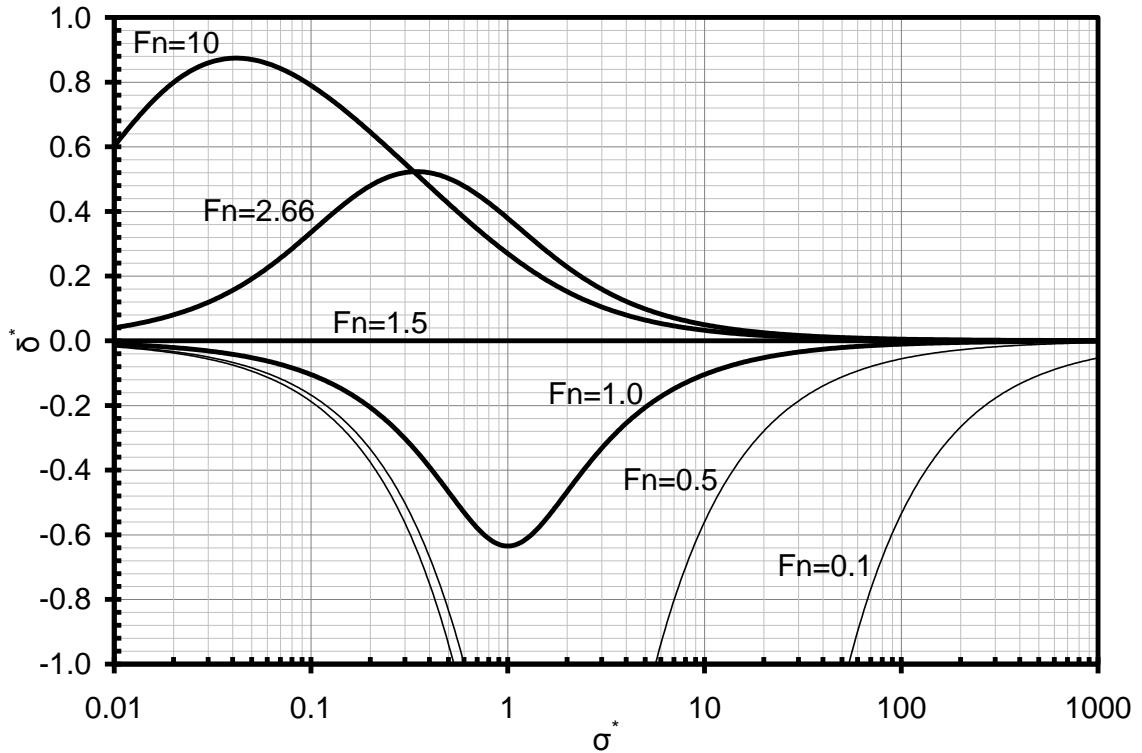
Figure 3.3 - Close up of Figure 3.2

Waves with very low Froude numbers will attenuate significantly. Amplifying waves with high Froude numbers will have a much lower absolute δ^* value than attenuating waves with low Froude numbers. The minimum point along the Fn = 0.1 line is about -15, while flow with a Froude number of 10 reaches a maximum of only about 0.87. This shows that wave attenuation is a much more prevalent phenomenon and is of a significantly higher magnitude than amplification. However, wave amplification does still occur, and is large enough that it should be taken into account in design.

It can be seen in Figure 3.3 that the dimensionless attenuation factor for all waves will approach zero when the wave number is either very large or very small. This means that waves that are quite long or quite short will have little amplitude change as they propagate. By comparing Figure 3.1 and Figure 3.3, it would appear that the celerity and attenuation/amplification of waves are interrelated. The absolute value of δ^* is highest at wave numbers corresponding to changes in the dimensionless celerity. When the dimensionless celerity is constant at high or low wave numbers, the attenuation factor will be small. As noted in previous studies (Ponce and Simons 1977), the peak of the δ^* curve will occur at the same wave number as the inflection point of the dimensionless celerity curve.

As the Froude number increases, the wave number of the peak attenuation/amplification decreases. This means that waves with high Froude numbers will amplify more when the waves are longer. Short waves at high Froude numbers will have little or no amplification. The wave number that corresponds to the peak attenuation/amplification (and thus also the inflection point of the dimensionless celerity curve) is shown in Figure 3.4 as a function of Froude number. This graph is equivalent to tracing a line through the peaks of all the different Froude number curves in Figure 3.3. This line will asymptotically approach zero as the Froude number increases. On the other end of the

spectrum, as the Froude number decreases, the peak attenuation will asymptotically approach positive infinity. There is not any evidence of a threshold at a Froude number of 1.5, or at any other value. Interestingly, the peak attenuation for critical flow (Froude number equal to one) will occur at a wave number of 1.
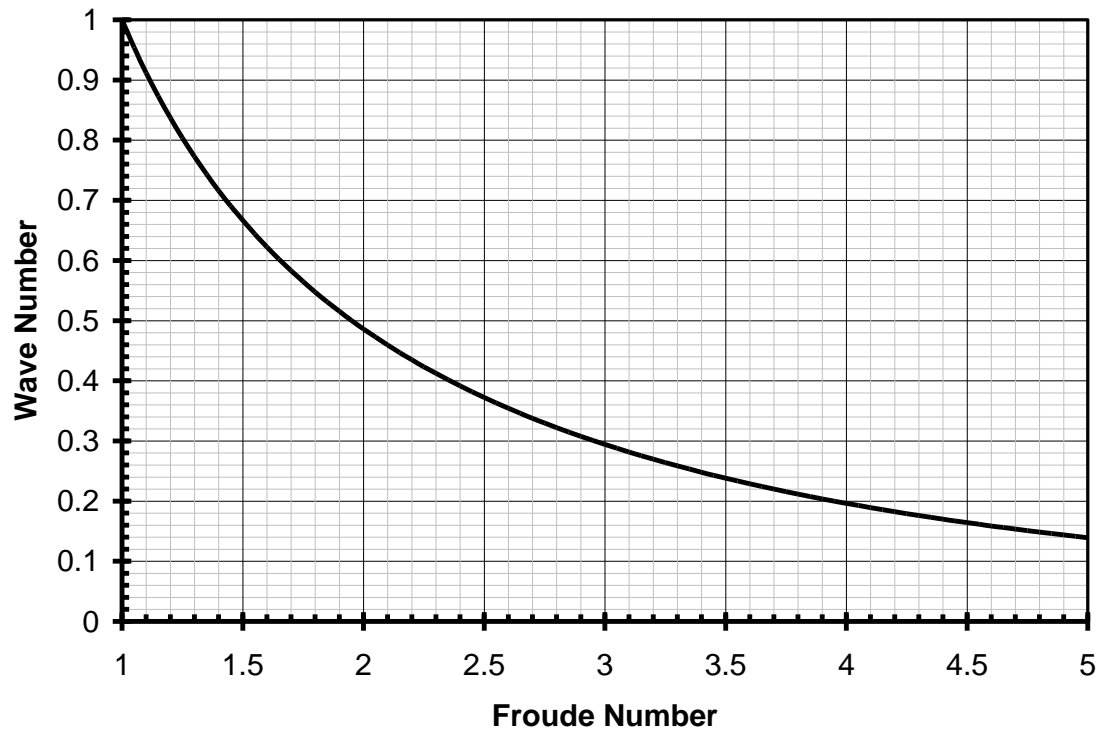
Figure 3.4 - Location of peak attenuation factor

3.2 Normalized length amplification factor

It should be noted that δ^* is a logarithmic decrement/increment. This means that it is an indication of the amplitude adjustment that will occur as the wave travels over a length of one wavelength. This is an important piece of information. The

actual amount of amplification or attenuation that a wave will experience within a channel is not dependent solely on the dimensionless attenuation factor. The wavelength of the disturbance also plays a role. A wave with a large amplification factor that also has a very long wavelength may amplify less in an absolute sense than a wave with the same amplification factor but a shorter wavelength, as shown in Figure 3.5. Thus the need for a new parameter is indicated. A dimensionless parameter that is a measure of the amplitude difference over a certain length would be a useful addition to the methods of Ponce and Simons (1977), and Tsai (2005).
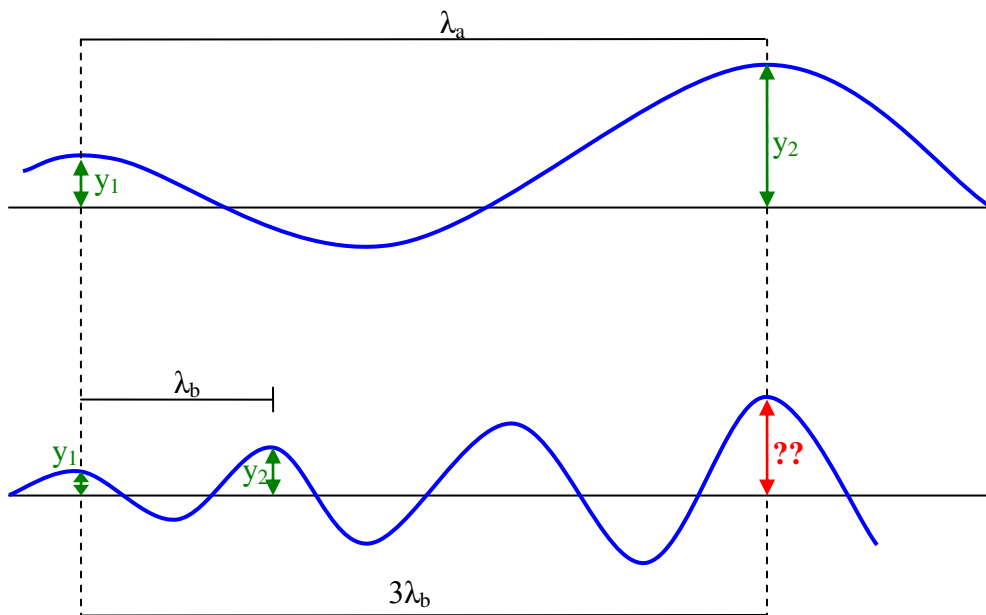
Figure 3.5 - Amplification over one wavelength for different sized waves

The definition of δ^* is

$$\delta^* = \ln\left[\frac{y^*_{t+\tau}}{y^*_t}\right]$$ (3.1)

Where:

y^*_t = depth at time t

$y^*_{t+\tau}$ = depth at time $t + \tau$, where τ is one period

The dimensionless depth at a time after one period has gone by, $y^*_{t+\tau}$, can be found using

$$y^*_{t+\tau} = e^{\delta^*}y^*_t$$ (3.2)

It follows from this that the dimensionless depth after two periods will be

$$y^*_{t+2\tau} = e^{\delta^*}y^*_{t+\tau}$$ (3.3)

Equations   (3.2) and   (3.3) can be combined to give

$$y^*_{t+2\tau} = e^{\delta^*}e^{\delta^*}y^*_t = e^{2\delta^*}y^*_t$$ (3.4)

Or more generally

$$y^*_{t+n\tau} = e^{n\delta^*}y^*_t$$ (3.5)

Where:

n = number of periods that have passed since time t

Counting the number of periods that have passed during a fixed time is analogous to counting the number of wavelengths that occur within a fixed distance. Thus Equation (3.5) will be the same if n is thought to be the number of wavelengths over a certain distance. The wave number σ^* can be thought of as a measure of the number of wavelengths a wave will have within a certain channel distance. In this case, the distance is $2\pi L_0$. This distance is therefore a function of normal depth and bed slope. It will vary when either of these parameters varies, but for the same discharge in the same channel, $2\pi L_0$ will be a constant regardless of wavelength. This gives the expression

$$y^*_2 = e^{\sigma^* \delta^*} y^*_1 \tag{3.6}$$

Where:

y^*_1 = dimensionless depth at point 1

y^*_2 = dimensionless depth at a point $2\pi L_0$ downstream of point 1

If Equation (3.6) is converted back into logarithmic form it can be expressed as

$$\sigma^* \delta^* = \ln\left(\frac{y^*_2}{y^*_1}\right) \tag{3.7}$$

The parameter $\sigma^* \delta^*$ is thus the measure of the total attenuation/amplification over a normalized length of $2\pi L_0$. This parameter, $\sigma^* \delta^*$, will be defined as $\delta`$, the normalized length attenuation factor. A plot of $\delta`$ is shown in Figure 3.6. A close up of the supercritical region is shown in Figure 3.7. This chart shows some

significant results. Figure 3.7 shows that short waves will have more attenuation or amplification than long waves over the same length. As is obvious from Equation (2.51), very long waves will have very small wave numbers, and so the normalized length attenuation factor will necessarily be close to zero. In Figure 3.3, the attenuation factor will increase for a time and then approach zero as the wave number gets large. In Figure 3.7, the normalized length attenuation factor will increase or decrease and then reach a constant non-zero value at high wave numbers. This indicates that the increasing wave numbers exactly balance out the decreasing attenuation factor.
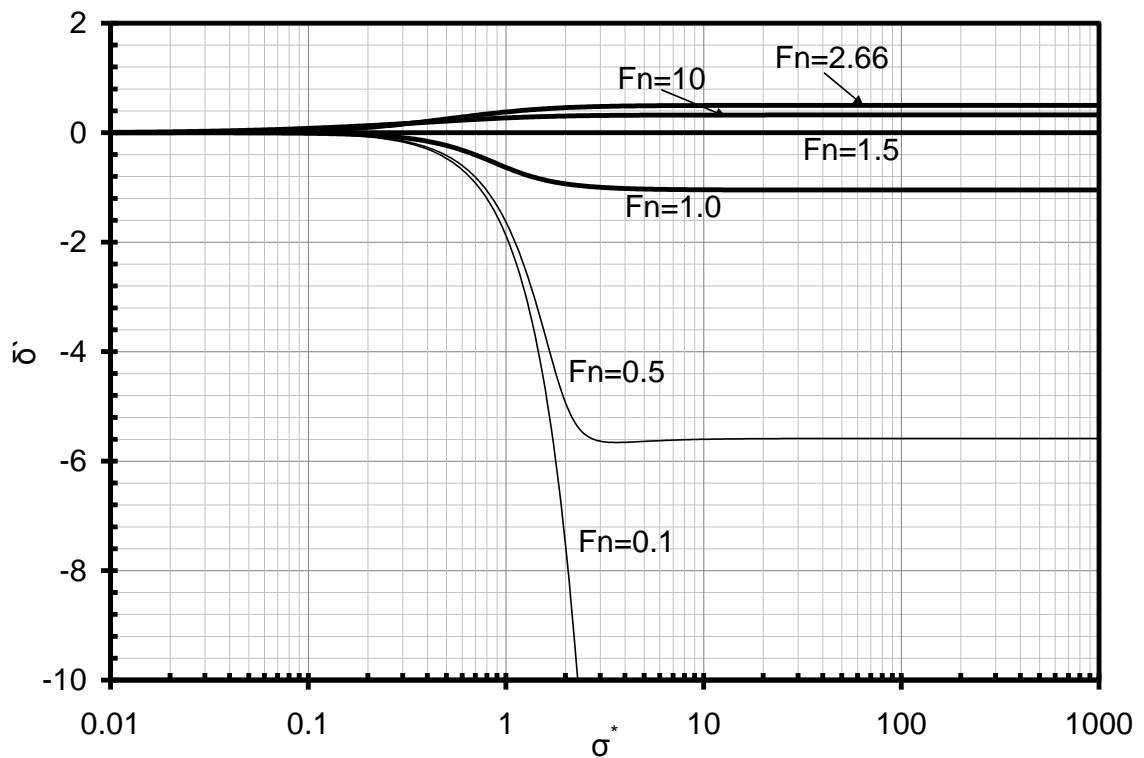
Figure 3.6 - Normalized length attenuation factor for different Froude numbers
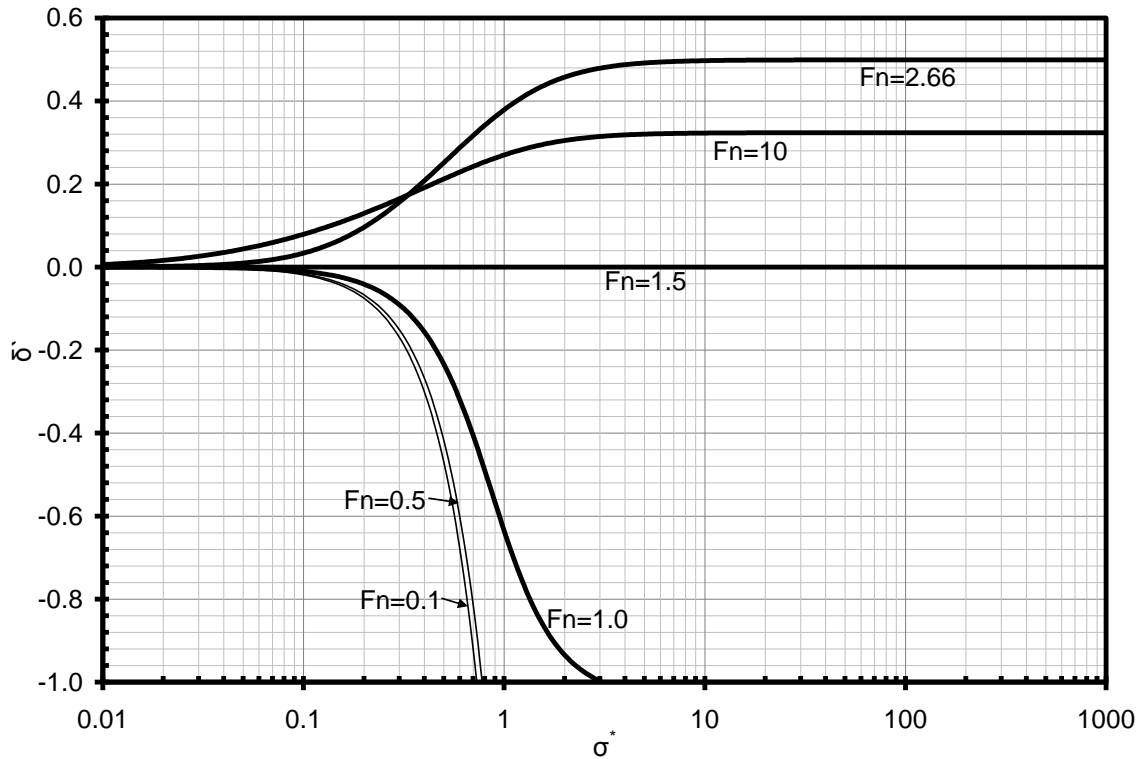
Figure 3.7 - Close-up of normalized length attenuation factor

Also interesting to note in Figure 3.7 is that the curve with the highest amplification is the *Fn* = 2.66 line. From Figure 3.3, it would appear that the maximum amplification increases with Froude number, but when the normalized length factor is used, higher Froude numbers do not necessarily mean higher amplification. Short waves will have maximum normalized length amplification at moderate Froude numbers around 3.

Figure 3.8 shows a plot of fixed-length attenuation factor as a function of the Froude number. This plot was done for a variety of wave numbers. As expected from Figure 3.7, the wave number with the highest amplification factor is the

largest wave number. Wave numbers above 10 are essentially the same as the curve for 10. This curve has a maximum amplification at $Fn = 3.44$. The fixed-length amplification factor at this point has a value of 0.53.
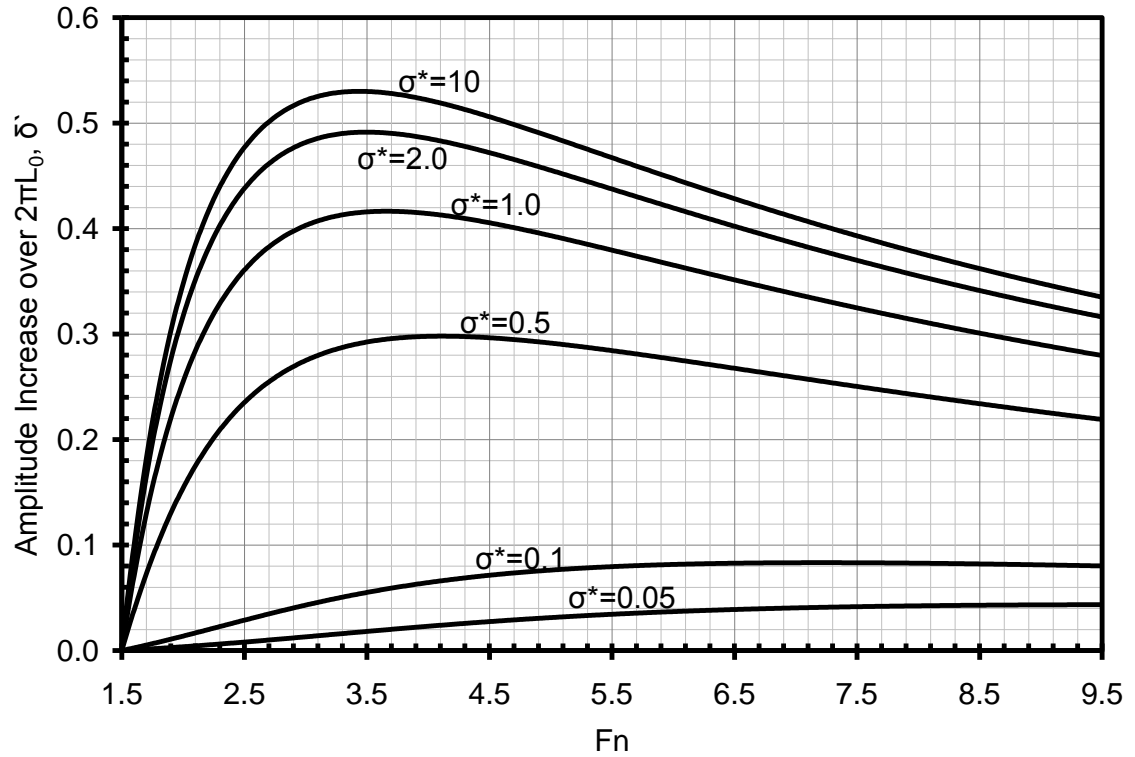
Figure 3.8 - Normalized length amplification versus Froude number

Chapter 4: Site Description

The City of Las Vegas, Nevada is situated in the southern tip of Nevada, within the Mojave Desert. The City lies in a basin (the Las Vegas Valley) surrounded by mountain ranges such as the Spring Mountains on the west side of the Valley (see Figure 4.1). The Valley drains surface runoff into the Las Vegas Wash, which drains to Lake Las Vegas and Lake Mead on the Colorado River. The Las Vegas Wash conveys flow from several sources, including urban runoff, reclaimed water and storm water (LVWCC 2007). During most of the year, the main source of water in the Wash is from water that has passed through the sewer and treatment system of the City and also Clark County. However, there are occasional rainfall events that can significantly increase the discharge passing through the Wash. Mid to late summer is considered the monsoon season, with afternoon thunderstorms not uncommon during this period. The Las Vegas Valley is considered an arid region, with an average yearly precipitation of 4.5 inches.
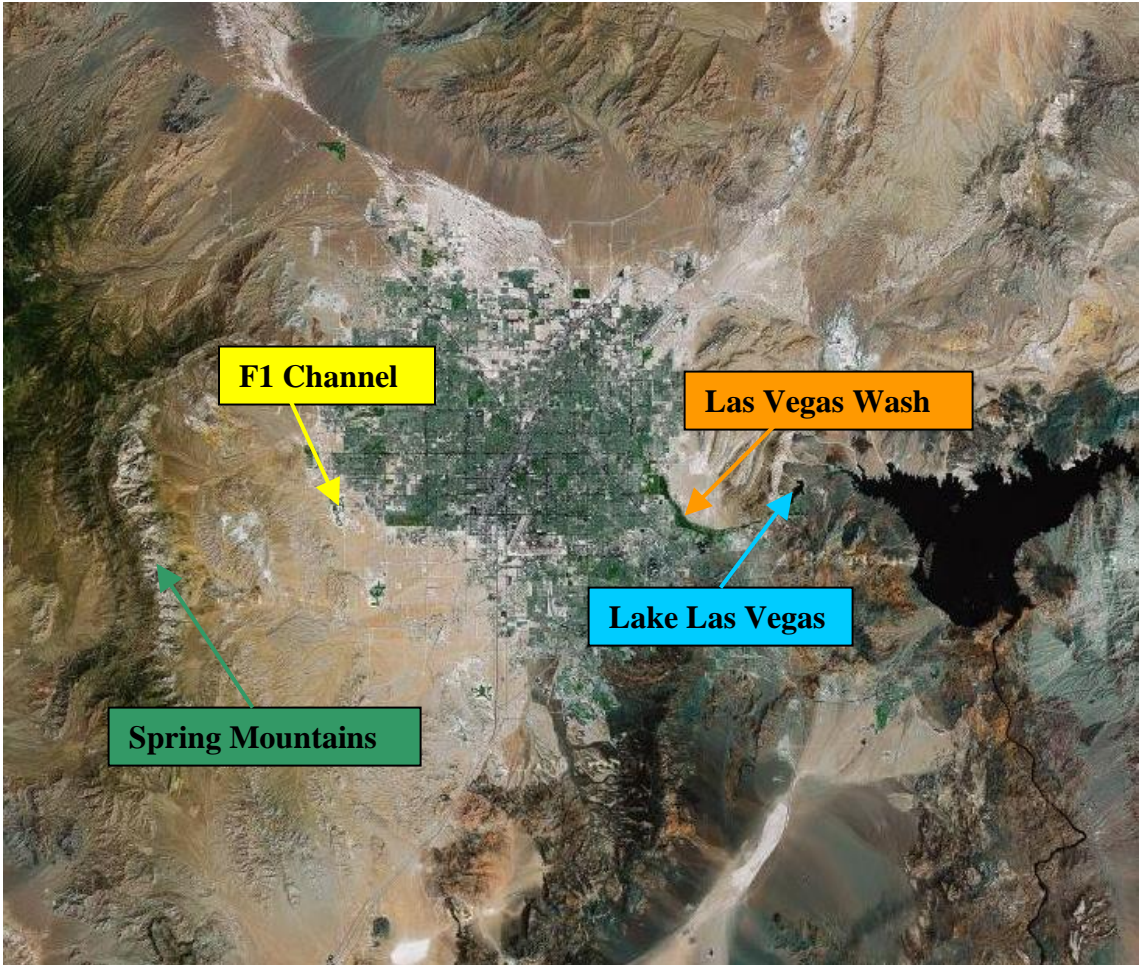
Figure 4.1 - Aerial photo of the Las Vegas Valley (from Google™ Maps)

The current City was incorporated in 1911, and has seen extensive population growth since then. Hoover Dam was constructed on the Colorado River in the 1930s, creating what is now Lake Mead. The dam and associated reservoir created job opportunities in the area, as well as providing a vital source of consistent water. The gaming industry is an important component of the City, with many large and expensive casinos and resorts having been built throughout the Valley. There is also extensive tourism in Las Vegas, with millions of people

visiting every year. Currently, almost 2 million people live within the Las Vegas Valley.

This large infusion of people into the Valley has caused widespread construction and development. This development has created a large amount of impervious surface in the Valley, and greatly increased the peak runoff created by rainfall events. The Las Vegas Valley has experienced severe flooding on a number of occasions, most recently in 1999 and 2003. See Figure 1.1 for example of the 1999 flooding. This flooding causes hazards to the residents of the Valley, and can result in expensive property damage as well. Because of the Valley's tendency toward short high-intensity storms and the rapid growth in the area, storm drainage development is important.

A network of both closed-conduit and open channel storm drainage pathways has been constructed within the Valley. This network is designed to help storm runoff pass through the City and County safely and exit into the Las Vegas Wash, and from there Lake Las Vegas and Lake Mead. Because of the potentially large discharge amounts that the storm system is designed for, as well as the natural topography of the Valley, many of the open channels that exist throughout the Valley have steep slopes of up to 3.5% (Duan and Chen 2003). These channels are typically constructed out of reinforced concrete, with either a

rectangular or trapezoidal cross sectional geometry. Average bottom width for these drainage channels is around 4 meters. Design flow depths can range from 1 to 3 meters.

4.1 Site-Specific Results

The channel that will be specifically investigated in this study is the F-1 channel. This channel is located on the west side of the Valley, as shown in Figure 4.2. Figure 4.3 shows a close up of the conjunction of the F-1 channel and F-2 channel (circled area in Figure 4.2).

Figure 4.2 - Overhead view of F-1 Channel (from Google™ Earth)

Figure 4.3 - F-1 and F-2 conjunction (from Google™ Earth)

The channel has properties typical of those found elsewhere in the City and County. The cross-sectional geometry is rectangular, with a bottom width of 4 m. The channel slopes downward at 2.5%, and is approximately 5 km long. The wall height in the channel is 3 m. The material making up the lining of the channel is standard concrete, and so the value of Manning's n can be assumed to be constant in space at 0.014. The F-1 channel is designed to pass a discharge corresponding to a 100 year storm. This design discharge is 93.4 m^3/s. See Figure 4.4 for a cross-sectional diagram of the F-1 channel. There is a slight slope towards the center of the channel; this slope will be ignored in the analysis.
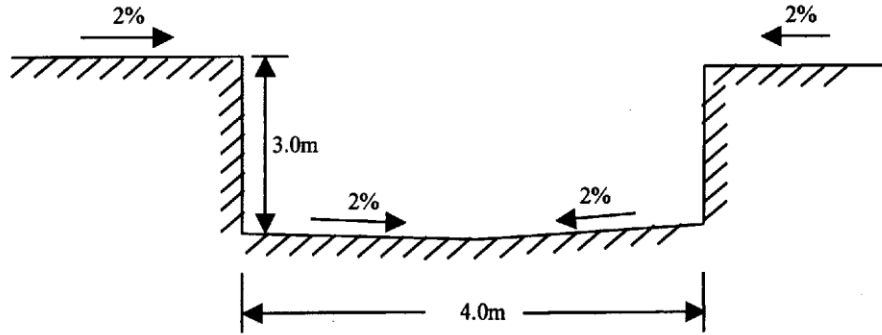
Figure 4.4 - F-1 Channel cross-section (from Duan and Chen, 2003)

The flow in this channel can be modeled, and the wave characteristics can be calculated. A calculation example to illustrate the procedure is shown below.

1) A discharge is chosen for the calculation. For this example, a discharge of 60 m^3/s was used.

2) Using Manning's equation the normal depth of flow can be determined. An initial depth is guessed, and then the area and wetted perimeter are calculated using the cross-section geometry shown in Figure 4.4. The initial guess for depth will be 2 m.

$$a = yW$$
$$= 2 \cdot 4$$
$$= 8m^2$$

$$P = W + 2y$$
$$= 4 + 2 \cdot 2$$
$$= 8m$$

Where:

        a = cross-section area

        W = channel width

        P = wetted perimeter

3) The hydraulic radius can be found using

$$R = \frac{a}{P}$$
$$= \frac{8}{8}$$
$$= 1m$$

4) Next, Manning's equation is used to find the flow rate corresponding to the assumed depth.

$$Q = \frac{1}{n} R^{\frac{2}{3}} a S^{\frac{1}{2}}$$
$$= \frac{1}{0.014} (1)^{\frac{2}{3}} (8) (0.025)^{\frac{1}{2}}$$
$$= 90.4 \, m^3/s$$

5) Using an iterative procedure, the depth can be altered until the assumed depth results in a flow rate equal to the desired rate of 60 m³/s. This depth is 1.48 m. The area for this case is 5.92 m² and the hydraulic radius is 0.85 m.

6) The normal velocity can be found using

$$u_n = \frac{Q}{a_n}$$
$$= \frac{60}{5.92}$$
$$= 10.14 \, m/s$$

Where:

a_n = normal flow area

7) The Froude number is then calculated as

$$Fn = \frac{u_n}{\sqrt{gy_n}}$$
$$= \frac{10.14}{\sqrt{9.81 \cdot 1.48}}$$
$$= 2.66$$

8) At this point, a wavelength must be chosen. This example will use 500 m. From this, the dimensionless wave number can be found using

$$\sigma^* = \frac{2\pi y_n}{S_0 \lambda}$$
$$= \frac{2 \cdot \pi \cdot 1.48}{0.025 \cdot 500}$$
$$= 0.744$$

9) With a Froude number and wave number, the dimensionless celerity and attenuation factor can be found using the method outlined in Chapter 3.

The base flow will be assumed to be uniform in this study. If the discharge is varied for a constant wavelength, a curve can be developed. By doing this for an array of wavelengths, a family of curves can be developed. A plot of these curves showing dimensionless celerity versus discharge is shown in Figure 4.5.
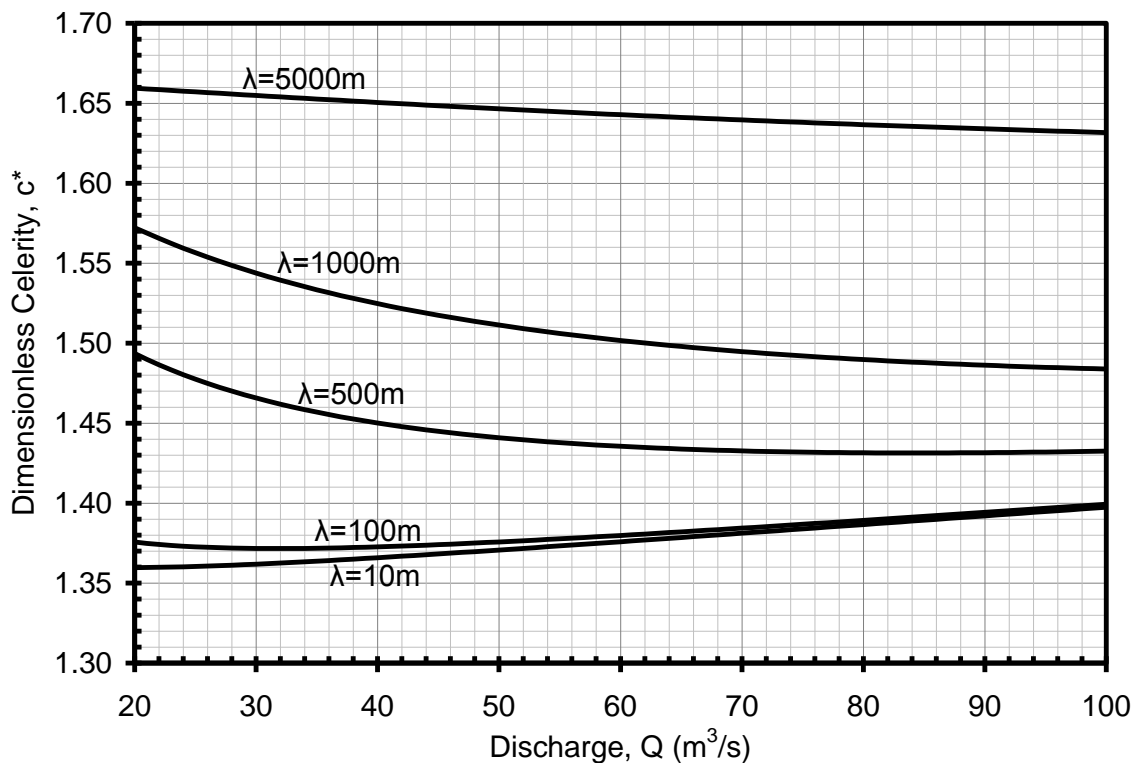
Figure 4.5 - Dimensionless celerity in F-1 channel

This plot shows that dimensionless wave celerity does not vary greatly with discharge. It can be found when examining the values used to create Figure 4.5 that the Froude number does not vary significantly over the range of discharges used. Depth and velocity will both increase with increasing discharge, and these increases will partially balance each other out, causing the Froude number to

remain close to constant. The range of Froude numbers found for discharges

ranging from 20 to 100 m^3/s is 2.52 - 2.78, with an average of 2.66. Thus the

properties of waves in the F-1 channel will exhibit similar behavior to the *Fn* =

2.66 lines in the theoretical results.

The range of wavelengths used in Figure 4.5 was 10 m through 5,000 m. Below

this range, the celerity will approach a constant independent of wavelength, and

because the channel is only 5,000 m long any waves longer than this would not

be possible. It can be observed that waves of short length tend to propagate

slower than longer waves. Also, waves around 100 m or less in length will have

increasing dimensionless celerity with increasing discharge, while medium to

long waves (500-5,000 m) will decrease dimensionless celerity with discharge.

The dimensionless celerity ranges from about 1.35 to 1.67 for the wavelengths

examined. This range is not particularly large. However, the actual propagation

speed of a wave depends not only on dimensionless celerity, but also the base

flow velocity in the channel. Multiplying the results in Figure 4.5 by the base flow

velocity gives Figure 4.6.
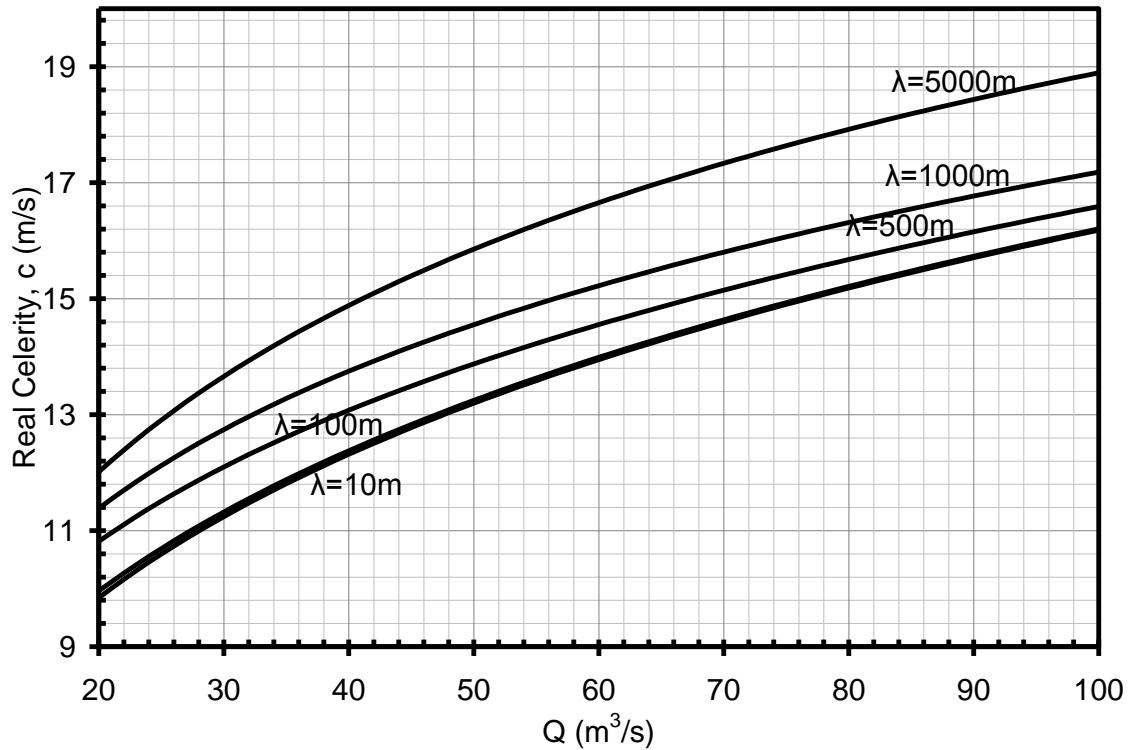
Figure 4.6 - Dimensional celerity in F-1 channel

This plot shows that the actual wave speed will increase monotonically with discharge in this channel. This is related to the fact that base flow velocity will increase with discharge. The difference in celerity between different wavelengths is seen to be small. The celerity ranges from approximately 10 to 12 m/s at a discharge of 20 m^3/s. The range expands slightly as the discharge increases, with the celerity spanning 16-19 m/s at 100 m^3/s. At the design discharge of 93.4 m^3/s an average length wave can travel at upwards of 16 m/s. This is a high speed, and indicates that the concrete lining the channel needs to be resistant to degradation from the force of the water. However, the waves will not be able to reach these speeds immediately. It will take time for them to accelerate up to a

constant velocity. An example of how to calculate the acceleration time and distance is shown below.

1) The velocity at any time t is given by $u = a_c t$ where in this case the acceleration a_c is equivalent to gravitational acceleration multiplied by the bed slope of the channel.

2) The highest velocity plotted in Figure 4.6 is 19.2 m/s. The time needed to achieve this velocity is found using

$$t = \frac{u}{gS_0}$$
$$= \frac{19.2}{9.81 \cdot 0.025}$$
$$= 78s$$

3) This time can then be expressed as a distance down the channel using

$$x = \frac{1}{2} gS_0 t^2$$
$$= 0.5 \cdot 9.81 \cdot 0.025 \cdot 78^2$$
$$= 752m$$

4) This result indicates that it will take a maximum of 752 meters for waves to reach terminal velocity in the F-1 channel. As the channel is 5 km long, it

can be seen that the waves will reach terminal velocity well before the end of the channel.

Figure 4.7 shows a plot of the dimensionless attenuation factor for F-1 channel. This graph does not have a clear and obvious trend such as that shown by dimensional celerity in Figure 4.6. With a more detailed examination however, trends can still be found. The attenuation factor is positive for all wavelengths, as would be expected considering the Froude number. For very short and very long waves, the amplification will be small. The maximum amplification occurs at medium wavelengths. Shorter waves will have maximum amplification at a low discharge, while long waves increase in amplification as discharge increases.
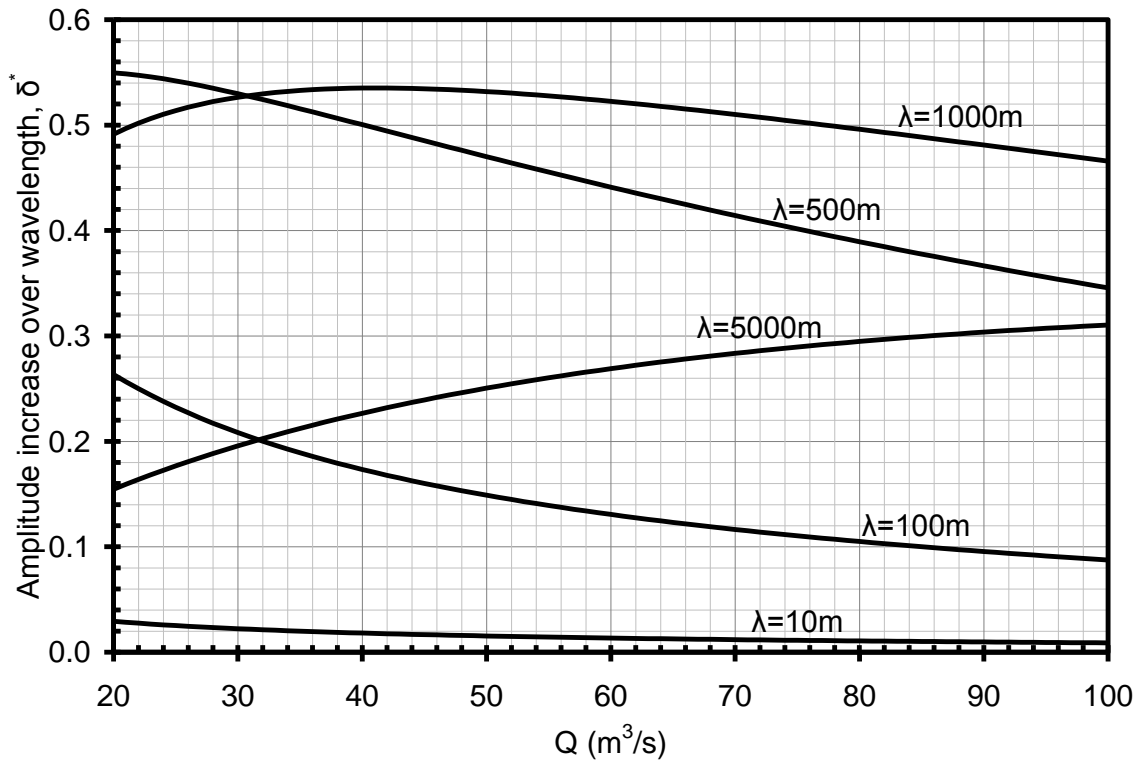
Figure 4.7 - Attenuation per wavelength for F-1 channel

As noted in the theoretical results, the dimensionless attenuation factor δ^* is a logarithmic decrement function. The value of δ^* is an indicator of the amplitude change over one wavelength (or in other words, during one wave period). This value is a good measure of the relative attenuation/amplification of waves of the same length with different Froude numbers. However, the usefulness of the δ^* parameter is limited when comparing waves with similar Froude numbers and differing lengths. As seen in Figure 4.7, short waves will typically have very low values for δ^*, while waves with medium lengths have larger values. However, a wave with a length of 10 m will cycle through many more periods in a given length than a wave of 1000 m. This is a good area for implementation of the

normalized length attenuation factor derived in the theoretical results as Equation
(3.7)

.   Figure 4.8 shows a plot of this normalized length factor as a function of
discharge for different wavelengths.   Also shown in is the same plot with a
different y-axis.   This axis shows the percent increase in wavelength that the
waves will have over each fixed length. From Equation (3.7), it can be seen that
the increase from one point to a second point a length $2\pi L_0$ away is

$$\frac{y^*_2}{y^*_1} = e^{\sigma^* \delta^*}$$

(4.1)
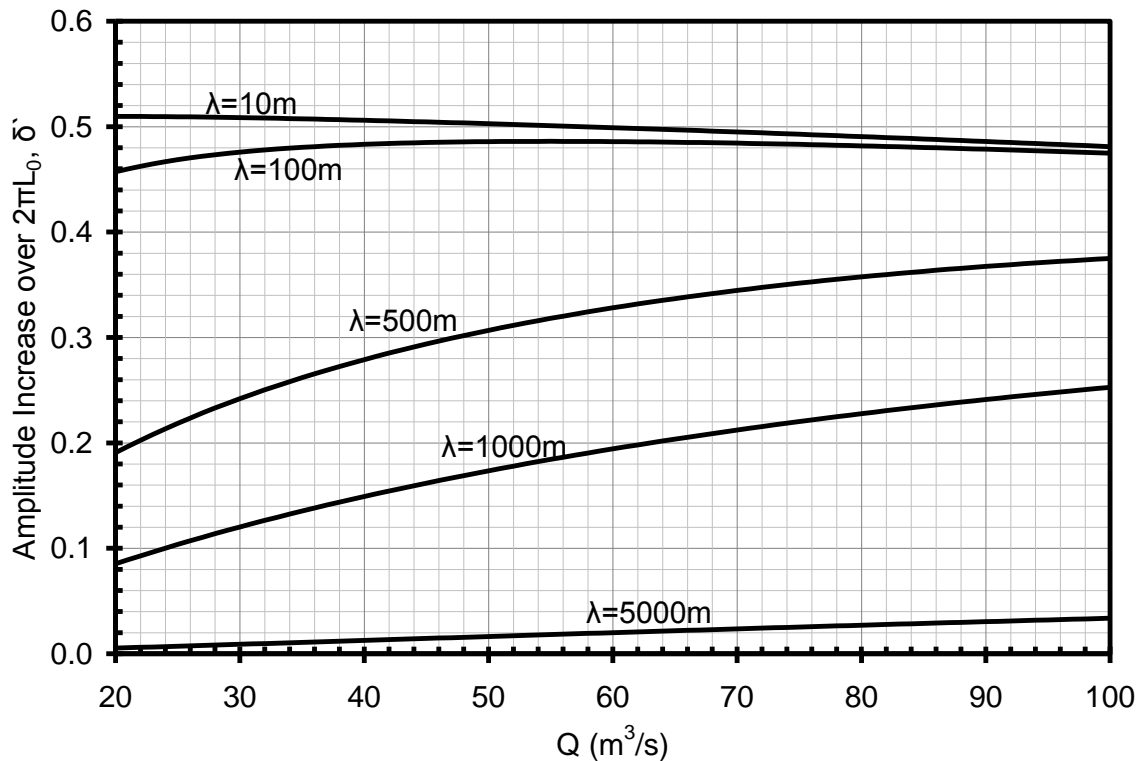
Figure 4.8 - Normalized length amplification for F-1 channel
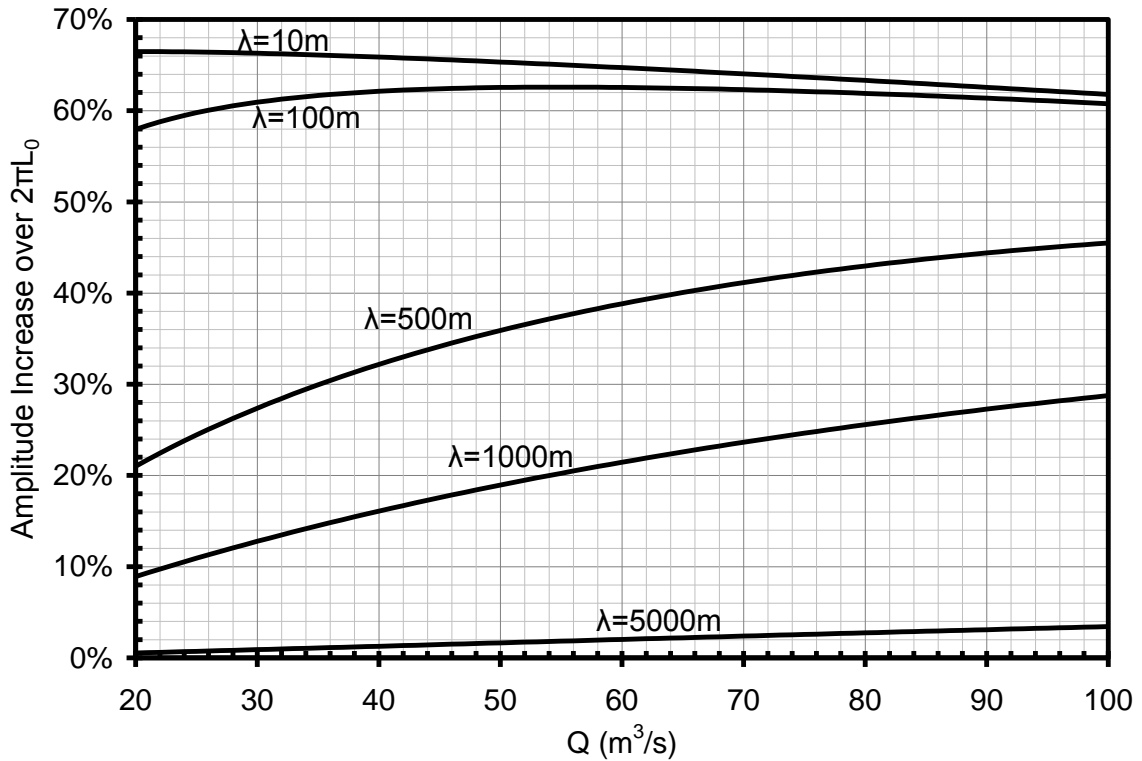
Figure 4.9 - Amplitude increase over a normalized length for F-1 channel

Figure 4.8 shows that short waves will actually amplify more over the same distance than long waves. The amplification for very long waves is close to zero. Short waves around 10 m long will have an amplification factor of about 0.5, or an increase in amplitude of 66%. Medium length waves will have increasing normalized length amplification factors with increasing discharge. The value for short waves will decrease slightly as discharge increases. Figure 4.8 signifies that reducing the length of a wave is counter-productive towards the goal of reducing amplification.

It can readily be seen from the description of the parameter L_0 in Figure 2.2 that this value will change as the normal depth or slope changes. This means that the length used in the parameter $\delta`$ is only fixed when the flow rate is fixed. For different flow rates, the distance will be different. Various values of L_0 are shown in Table 4.1 along with the value of $2\pi L_0$. It can be seen that the length L_0 will increase as the discharge increases. This result is shown graphically in Figure 4.10.

Table 4.1 - Normalized lengths at various flow rates

Q	y_n	L_0	$2\pi L_0$
m³/s	m	m	m
20	0.69	28	174
30	0.91	36	228
40	1.11	44	279
50	1.30	52	326
60	1.48	59	372
70	1.66	66	416
80	1.83	73	459
90	1.99	80	501
100	2.16	86	543
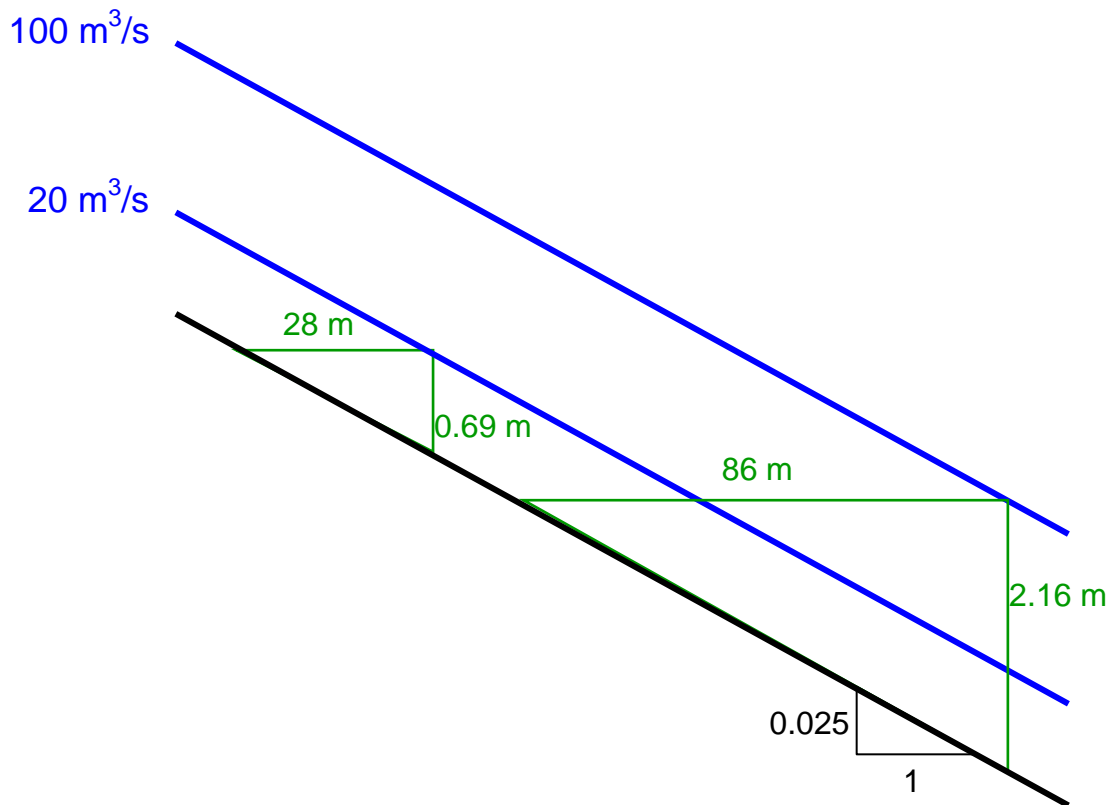
Figure 4.10 - Change in L_0 with discharge

With this in mind, the amplification over a truly fixed channel length can be found. A brief example of how to calculate this fixed length amplification is included below.

1) The length used must be chosen. This example will use 543 m, as this is the largest value of $2\pi L_0$ in Table 4.1.

2) A wavelength must be chosen, in this case 100 m. The number of waves within the overall length of 543 m is then 543/100 = 5.43.

3) By multiplying the original δ^* value by this number, the amplification factor over 543 m can be found. Note that this value is similar to δ` but will only be equal to it if $2\pi L_0$ is the same as 543 m.

4) Assuming a discharge of 50 m^3/s, the value of δ^* will be 0.149. This makes the 543 m amplification factor equal to $5.43 \cdot 0.149 = 0.808$.

5) If an actual wave height is desired, an initial height must be chosen, in this case 0.5 m. Then the final wave height after 543 m will be $e^{0.808} \cdot 0.5 = 1.12m$.

The amplification factor over 543 m was calculated for a variety of wavelengths, and the results are shown in Figure 4.11. Waves longer than 543 m would not make sense in this plot, so the lines for λ = 1000 m and λ = 5000 m are shown with dotted lines. As expected, short waves amplify the most. An interesting result from this analysis is that waves will have a higher amplification factor at lower flow rates. When looking at the normalized length amplification factor, δ`, the 10 m long waves had a higher amplification at lower discharge, but it is much more pronounced in this graph.
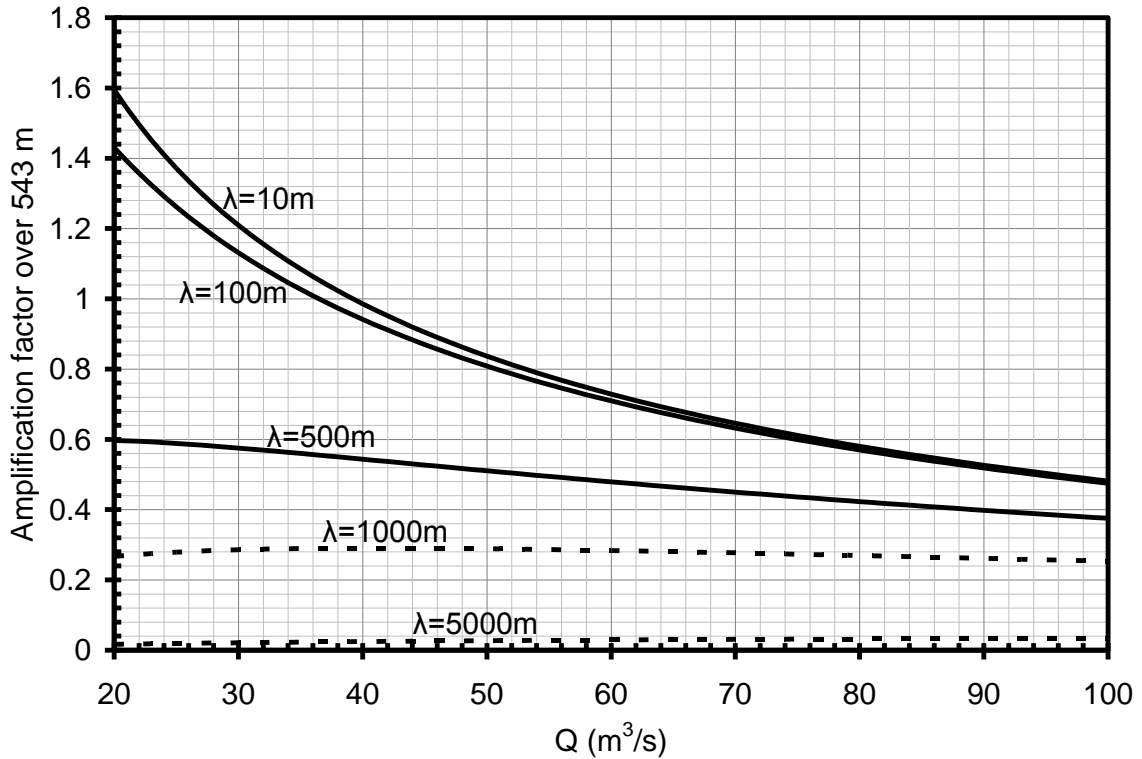
Figure 4.11 - Amplification over 543 m in F1 channel

By assuming that waves start at an initial amplitude of 0.5 m, the final amplitude

can be found as described above. These results are shown in Figure 4.12. The

linear method used in this thesis does not have a built in limit to the size of

waves. However, it is obvious from physical reality and common sense that

wave amplification will have an upper limit. One physical parameter that will limit

the growth of waves is the total water depth. When the wave amplitude is equal

to the depth of flow in the channel, the trough of the wave will be at the same

elevation as the channel bed, and the wave will obviously not be able to grow

past the bed. It should be stressed that this is not necessarily the actual limit to

amplification as wave breaking and other phenomena may lower the limit. The

line where the amplitude is equal to the normal depth is shown in Figure 4.12. Above this line, amplitudes will not be physically realistic, and so are shown with a dashed line. This graph shows that after only half a kilometer, a short wave can grow from 0.5 m to 1.2 m. Even a relatively long wave of 500 m will almost double in height to 0.9 m.
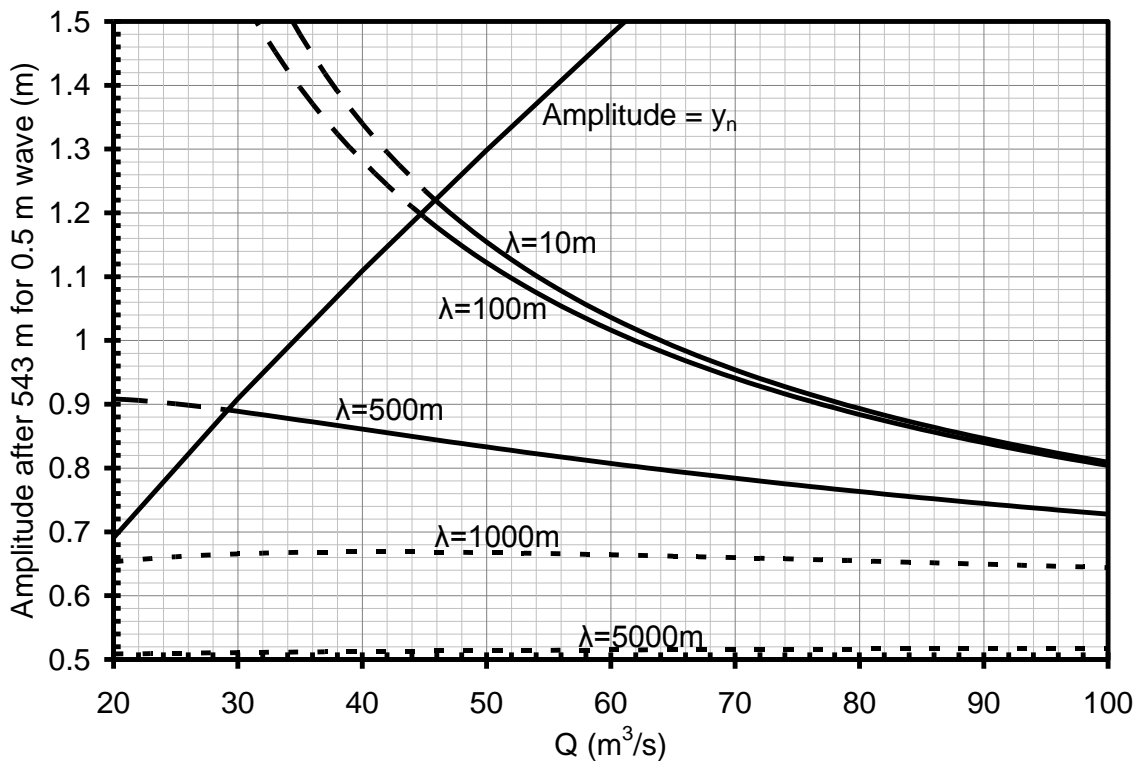
Figure 4.12 - Actual amplitude of waves initially 0.5 m high over a channel length of 543 m.

For a given flow rate, wave amplitude as a function of length can be calculated. Figure 4.13 shows wave heights for a discharge of 100 m^3/s up to a channel distance of 543 m. The lines show a slight upward curve, due to the fact that the growth is modeled as an exponential function. It would also be possible to plot

the wave heights over the entire 5 km channel length, but because of the lack of

an upper amplification limit, the amplitudes soon reach ridiculous magnitudes.
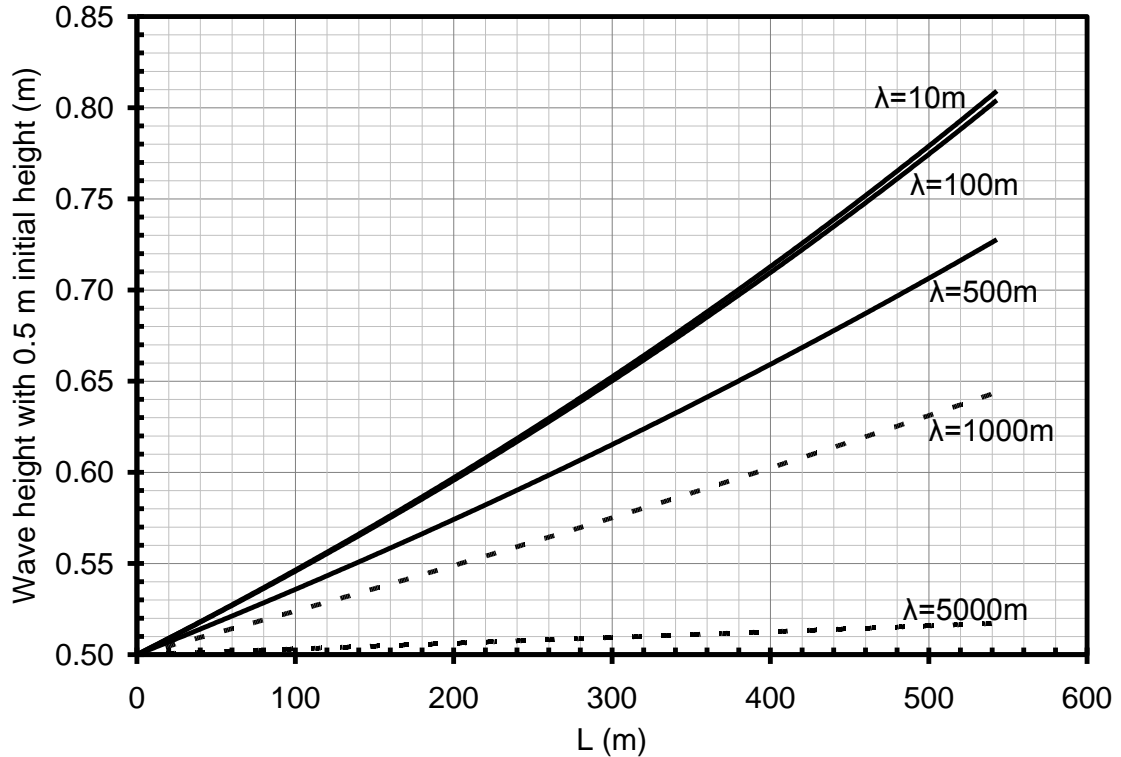
Figure 4.13 - Amplitude as a function of distance for waves with an initial height of 0.5 m and a discharge of 100 m³/s

4.2 Applicability of Results

The results presented in this study have a limited range of applicability. There

were a number of assumptions made during the derivation of the celerity and

attenuation factor equations that must be satisfied to properly use those

equations. Also, the assumption was made that Manning's equation is a good

representation of the flow dynamics for the underlying base flow. Manning's

equation is based on the assumption that friction between the bed and the fluid

will determine the flow properties at that location in the channel. In certain situations, frictional resistance may not be the prime component of the overall flow resistance.   Steeply rising waves can "break" and collapse back on themselves. This breaking action would create local energy loss that would not be factored into the equations used.

Gradually-varied flow is a key assumption in the Saint-Venant equations, (2.1) and (2.2). Rapidly changing water surfaces cannot be described by these equations. Very short waves with finite amplitude can be considered a type of rapidly-varied flow. This leads to the idea that very short waves will not be adequately described by the equations used in this study. As a rough line of demarcation, waves with amplitudes greater than one-tenth of their wavelength can be considered too short. Thus, when referring to Figure 4.8 and other figures the $\lambda = 10$ m line should not be applied to a real system if the wave amplitudes are greater than 1 m.

Another key assumption in the derivation of the celerity and attenuation factor equations used in this study is that the waves are infinitesimal linear perturbations.   This first-order approximation makes the use of analytical solutions possible. However, this assumption also limits the results. The celerity and attenuation factor developed are strictly only valid for infinitesimal waves.

However, it has been noted in past studies (Menendez 1993) that first-order approximations can give reasonable results for finite waves if the amplitudes are not too large. This suggests a further limit to the results presented in this study. Using the above criteria of having the amplitude be one-tenth of the wavelength would allow 100 m high waves to be studied if the wavelength is 1000 m. However, these waves would not fit into the linear wave assumption and would therefore not be valid.

It should also be noted that the use of the first-order approximation makes it difficult to determine exact wave heights that will be present in the channel. The amplification of a wave can be found relative to its wavelength or over a fixed distance, but this amplification is always relative to the initial amplitude of the wave. A wave that is assumed to start as 0.1 mm high will have a different calculated amplitude at the end of a reach than a wave that is assumed to start as 1.0 mm high.

Another factor that must be taken into consideration is that the equations used will predict endless amplification as a wave travels downstream. In reality, the wave amplification will be limited. Eventually the wave will reach a point where the amplitude is too high to be sustained and the wave will no longer grow larger.

4.3 Design Applications

As stated earlier, the construction of storm drainage channels has a high cost associated with it. It is desirable to minimize this cost through the minimization of freeboard. Additionally, danger to property and life increases when water flows out above the walls of a channel. Thus reducing the amplification of supercritical waves is a sought-after result.

There are several ways to accomplish this reduction. As noted earlier, waves will attenuate if the Froude number is less than 1.5. Therefore if the flow in the channel was slowed down far enough, the flow would be at a level where waves do not amplify. A second option is to increase the wavelength of the disturbance. As revealed in Figure 4.8, short waves will have a higher amplification over a fixed length than long waves. A third option for reducing wave amplification is to reduce the length over which waves can amplify uninterrupted. The following section will explore these options and give recommendations for the design of F-1 channel and other similar storm drainage channels in Las Vegas.

The first remediation option for F-1 channel is to reduce the Froude number below 1.5. The Froude number is a function of both the flow velocity and hydraulic radius. Decreasing velocity, increasing hydraulic radius or a combination of these two will reduce the Froude number. According to

Manning's equation, velocity is dependant on channel roughness, hydraulic radius, and slope. This indicates that increasing the hydraulic radius is not an effective way to reduce Froude number. Increasing the hydraulic radius will decrease Froude number, but will increase velocity, which will then act to increase the Froude number again. The better option is to reduce the velocity. This can be done either by increasing channel roughness or decreasing slope. The roughness of flat concrete is about 0.014. At the design discharge of 93.4 m^3/s, a Froude number of 1.5 requires a Manning's n value of 0.023, *ceteris paribus*. This is a quite reasonable value to achieve. Using Limerinos' equation for grain roughness, a grain diameter to reach this roughness value can be estimated. According to HEC (2002), Limerinos' equation is a good predictor of roughness values when surface roughness is the only major component, as is true in the case of F-1 channel. Limerinos' equation is

$$ n = \frac{0.0926 R^{\frac{1}{6}}}{1.16 + 2.0 \log\left(\dfrac{R}{d_s}\right)} \qquad (4.2) $$

Where:

d_s = representative grain size, in feet

R = hydraulic radius, in feet

Carefully converting between English and SI units using Equation (4.2) shows that the necessary grain size for F-1 channel to have a roughness of 0.023 is

15.3 mm. This corresponds to coarse gravel in typical classification systems (Julien 1995). Therefore, one good remediation option would be to embed particles of this size or larger in the concrete that the drainage channels are made of. A similar option would be to form the concrete into a knobbed surface rather than embed gravel particles. This would be a relatively simple and cheap solution. However, increasing the roughness to this level would increase the normal depth in the channel to 3.01 m from 2.05 m with the current roughness. The F-1 channel as currently constructed is only 3 m deep.

The next option is to decrease the bed slope in the channel. To attain a Froude number of 1.5, a slope of 0.01, or 1.0% is required. This is a significant reduction from the existing slope of 2.5%. The most feasible method of reducing the slope to this level is to alter the longitudinal profile of the channel into a stair-step configuration. This would reduce the slope in most areas, while drastically increasing the slope over very small reaches. This method would have the added benefit of breaking the flow up into smaller units that would be hydraulically disconnected from each other. This would prevent extended lengths of flow where waves could develop and grow. Normal depth at this slope is 2.92 m. Figure 4.14 shows an example of a sharp drop-off that could be used as part of a stair-step system. Ohtsu, Yasuda and Takahashi (2004) analyzed

flow in steep stepped channels and provided design guidelines for this type of channel.

Figure 4.14 - Steep drop in a storm drainage channel (from AMAFCA)

To avoid the need to build the channel deeper, the first two given options could be ignored in place of a third option. This option would be to place periodic baffles within the channel. These baffles would break up the flow and stop wave amplification. The spacing of the baffles would need to be set so that waves would not amplify over the desired height in between two baffles. The channel would then be able to be the same depth as it currently is, except in the vicinity of

the baffles. The baffles would create a backwater effect locally, increasing the depth.

Another potential route of remediation would be to increase the length of a wave. This would be difficult to do, and even more difficult to guarantee that no short waves would ever form in the channel. This method is not recommended.

A final option is to not alter the channel at all. The graphs presented in the results section of this report can be used to predict the maximum height of a wave given a certain propagation distance along the channel. As long as sufficient freeboard is constructed to contain this amplified wave, there should not be a problem. Preexisting channel features such as bends and junctions can be utilized as methods to break up wave development periodically. If this course is chosen, further investigation should be done into the effects of bends and flow confluences on wave parameters.

In summary, the potential alternatives for reduction of wave amplification in F-1 Channel are

- Increase the roughness of the bed to 0.023 by embedding coarse gravel into the concrete surface.
- Reduce the slope of the channel to 1%.

- Construct baffles to break up the development length of the waves.

- Construct sufficient freeboard to contain the waves.

Chapter 5: Conclusions

This thesis examined and analyzed wave propagation in order to satisfy the four key objectives listed in Chapter 1. The results for each of these objectives are as follows:

1. The theoretical behavior of waves propagating along a supercritical base flow was examined. The linear stability method of Ponce and Simons (1977) and Tsai (2005) was used along with Manning's equation for resistance to flow. The celerity and relative attenuation factor were calculated for a wide variety of base flows and waves. The results were comparable to previous studies done using different assumptions (such as the Chezy resistance formula instead of Manning's). Emphasis was placed on the supercritical regime when analyzing the results. As shown in previous studies, a Froude number of 1.5 is the threshold for small linear waves when using Manning's Equation. Flow with lower Froude numbers will have a celerity above that of a kinematic wave, and will attenuate for all wave numbers. Froude numbers higher than 1.5 will

amplify as they propagate, and will travel slower than a corresponding kinematic wave.

2. During the theoretical analysis, areas of potential improvement to past studies were looked for. One significant area that was identified was in the definition of the attenuation factor used in the linear stability analysis. The standard attenuation factor used first by Ponce and Simons (1977) and later by several other investigators represents the amplitude change of a wave over one wavelength. This makes it difficult to compare the attenuation or amplification characteristics of waves of differing lengths. A new parameter was defined that signifies the amplitude change over a fixed length, irrespective of wavelength. The fixed length that was chosen was $2\pi L_0$, the downstream distance required for a drop in bed elevation equal to the normal flow depth times 2π, because this choice gave a simple relationship for the new fixed-length attenuation factor using previously defined parameters. This factor was defined as the relative attenuation factor multiplied by the dimensionless wave number. New results were found for this new parameter, and compared to previous studies. It was discovered that short waves will amplify more than long waves over a set distance, and that increasing Froude number will not

always increase amplification. The maximum amplification was found to occur at Froude numbers equal to 3.44 for very short waves.

3. The theoretical ideas explored in the first part of the study were applied to a storm drainage channel in Las Vegas, Nevada. This channel is known as the F-1 channel and is located in the western part of the Valley. The flow through F-1 channel will be supercritical at most discharges. For flow rates between 20 and 100 m^3/s, the Froude number will be around 2.66. Thus, waves that form within the F-1 channel will amplify as they propagate downstream. The celerity and relative amplification of a small wave imposed on the base flow within the channel were found at a range of discharges and wavelengths. It was found that the celerity of a wave will vary between 10 and 19 m/s, depending on the flow rate and wavelength. The relative amplification factor will range from zero to about 0.5. The new parameter for normalized length amplification will also have a maximum near 0.5 (corresponding to an amplitude increase of ~65%), but will decrease significantly with increasing wavelength. Because the normalized length will vary with discharge, the amplification factor over a fixed length was also found. This factor can be as high as 1.6 for short waves. By assuming an initial wave height of 0.5 m, the height after 543

m at the maximum discharge will be up to 0.8 m. At lower discharges, this amplitude will be higher; up to 1.2 m for short waves.

4. Options for revising the design guidelines for supercritical channels were presented. Several different methods of reducing wave amplification were examined, and recommendations were made. The results from this investigation indicated that waves will attenuate as long as the Froude number is less than 1.5. Reducing the slope through a stair-step profile to 1.0% would reduce the Froude number sufficiently that amplification would not be a worry. Alternately, increasing the Manning's roughness value to n = 0.023 would also lower the Froude number adequately. This roughness would require a grain size of 15.3 mm according to Limerinos' equation. Both of these options would increase the flow depth beyond what the current channel can contain. Installing periodic baffles was recommended as a way to break up the growth of waves. By reducing the available development length for waves, the amplitude amplification could be limited to a safe value.

References

AMAFCA Flood Photos,
http://www.amafca.org/AMAFCA%20Flood%20Photos.htm (Accessed
February 25, 2007).

Burg, C. O. E., Huddleston, D. H., Berger, R. C. (2001). "Efficient Robust Design
Tool for Open-Channel Flow." *J. Hydr. Engrg*, ASCE, 127(1), 62-70.

Causon, D. M., Mingham, C. G., Ingram D. M. (1999). "Advances in Calculation
Methods for Supercritical Flow in Spillway Channels." *J. Hydr. Engrg*,
ASCE, 125(10), 1039-1050.

Chamani, M. R., Beirami, M. K. (2002). "Flow Characteristics at Drops." *J. Hydr.
Engrg*, ASCE, 128(8), 788-791.

Chung, W. H., Aldama, A. A., and Smith, J. A. (1993). "On the effects of
downstream boundary conditions on diffusive flood routing." *Adv. Water
Resour.*, 19, 259-275.

Chung, W. H., Kang, Y. L. (2006). "Classifying river waves by the Saint Venant
equations decoupled in the Laplacian frequency domain." *J. Hydr. Engrg.*,
ASCE, 132(7), 666-680.

Clark County Regional Flood Control District (CCRFCD). (1999). "Hydrologic
Criteria and Drainage Design Manual." Las Vegas, NV.

Duan, J. G., Chen, D. (2003). "Hydraulic characteristics of supercritical flow in
flood control channels in the Las Vegas Valley." Draft Report, *Desert
Research Institute*.

Einhellig, R. F., Pugh, C. A. (2001). "Physical Model Study of the San Sevaine
Side-Weir Diversion." *Proc., World Water and Environmental Resources
Congress 2001*, ASCE, Orlando Fl., 470.

Ferrick, M. G. (1985). "Analysis of river wave types." *Water Resour. Res.*, 21(2),
209-220.

Ferrick, M. G. (2005). "Simple wave and monoclinal wave models: River flow
surge applications and implications." *Water Resour. Res.*, 41, W11402,
doi:10.1029/2004WR003923.

Ferrick, M. G., and Goodman, N. J. (1998). "Analysis of linear and monoclinal river wave solutions." *J. Hydr. Engrg.*, ASCE, 124(7), 728-741.

Field, W. G., Lambert, M. F., Williams, B. J. (1998). "Energy and momentum in one dimensional open channel flow." *J. Hydraul. Res.*, 36(1), 29-42.

Gargano, R., Hager, W. H. (2002). "Supercritical Flow across Sewer Manholes." *J. Hydr. Engrg.*, ASCE, 128(11), 1014-1017.

Ghodsian, M. (2003). "Supercritical flow over a rectangular side weir." *Canadian Journal of Civil Engineering*, 30(3), 596-600.

Giudice, G. D., Gisonni, C., Hager, W. H. (2000). "Supercritical Flow in Bend Manhole." *J. Irrig. and Drain. Engrg.*, 126(1), 48-56.

Giudice, G. D., Hager, W. H. (2001). "Supercritical Flow in 45° Junction Manhole." *J. Irrig. and Drain. Engrg.*, 127(2), 100-108.

Graber, S. D. (2006). "Asymmetric Flow in Symmetric Supercritical Expansions." *J. Hydr. Engrg.*, ASCE, 132(2), 207-213.

Graf, W. H. (1998). *Fluvial Hydraulics*. Wiley, Chichester, West Sussex, England.

Hicks, F. E., Steffler, P. M., Yasmin, N. (1997). "One-Dimensional Dam-Break Solutions for Variable Width Channels." *J. Hydr. Engrg.*, ASCE, 123(5), 464-468.

Hydraulic Engineering Center (HEC). (2002). *HEC-RAS, River Analysis System, User's Manual*. US Army Corps of Engineers, Davis, CA.

Julien, P. Y. (1995). *Erosion and sedimentation*, Cambridge University Press, Cambridge, U.K.

Julien, P. Y. (2002). *River Mechanics*, Cambridge University Press, Cambridge, U.K.

Julien, P. Y., Hartley, D. M. (1986). "Formation of roll waves in laminar sheet flow." *J. Hydraul. Res.*, 24(1), 5-17.

Kruger, S., Rutschmann, P. (2001). "Discussion of 'Advances in Calculation Methods for Supercritical Flow in Spillway Channels' by Causon, Mingham, and Ingram." *J. Hydr. Engrg.*, ASCE, 127(4), 328-330.

Kruger, S., Rutschmann, P. (2006). "Modeling 3D Supercritical Flow with Extended Shallow-Water Approach." *J. Hydr. Engrg.*, ASCE, 132(9), 916-926.

Lai, C; Baltzer, R. A., Schaffranek, R. W. (2002). "Conservation-form equations of unsteady open-channel flow." *J. Hydraul. Res.*, 40(5), 567-578.

Las Vegas Wash Coordination Committee (LVWCC), http://www.lvwash.org/index.html (Accessed February 9, 2007).

Lin, C., Huang, W. Y., Suen, H. F., Hsieh, S. C. (2002). "Study on the Characteristics of Velocity Field of Free Overfallls over a Vertical Drop." *Proc., Hydr. Meas. and Exp. Meth. Conf.*, EWRI, Reston, Va., 116.

Lyn, D. A., Altinakar, M. (2002). "St. Venant–Exner Equations for Near-Critical and Transcritical Flows." *J. Hydr. Engrg.*, ASCE, 128(6), 579-587.

Martino, F. D., Gisonni, C., Hager, W. H. (2002). "Drop in Combined Sewer Manhole for Supercritical Flow." *J. Irrig. and Drain. Engrg.*, ASCE, 128(6), 397-400.

Mays, L. W. (2005). *Water Resources Engineering*, Wiley, Hoboken, NJ.

Mingham, C. G., Causon, D. M. (1998). "High-Resolution Finite-Volume Method for Shallow Water Flows." *J. Hydr. Engrg.*, ASCE, 124(6), 605-614.

Mishra, S. K., and Seth, S. M. (1996). "Use of hysteresis for defining the nature of flood wave propagation in natural channels." *Hydrol. Sci. J.*, 4(2), 153-170.

Miyamoto, H., Kanda, T. (2002). "Simultaneous Image Measurements of Velocity Field and Water-Surface Wave in Open-Channel Flows." *Proc., Hydr. Meas. and Exp. Meth. Conf.*, EWRI, Reston, Va., 87.

Mizamura, K. (1995). "Free-Surface Profile of Open-Channel Flow with Wavy Boundary." *J. Hydr. Engrg.*, ASCE, 121(7), 533-539.

Mizamura, K. (2005). "Discharge Ratio of Side Outflow to Supercritical Channel Flow." *J. Hydr. Engrg.*, ASCE, 131(9), 821-824.

Mizamura, K., Yamasaka, M., Adachi, J. (2003). "Side Outflow from Supercritical Channel Flow." *J. Hydr. Engrg.*, ASCE, 129(10), 769-776.

Molls, T., Zhao, G. (2000). "Depth-Averaged Simulation of Supercritical Flow in Channel with Wavy Sidewall." *J. Hydr. Engrg.*, ASCE, 126(6), 437-445.

Moussa, R., and Bocquillon, C. (1996). "Criteria for the choice of flood-routing methods in natural channels." *J. Hydrol.*, 186, 1-30.

Odai, S. N., Kubo, N., Onizuka, K., Osato, K. (2006). "Analytical solution of the burgers equation for simulating translatory waves in conveyance channels." *J. Hydr. Engrg., ASCE* 132(2), 194-199.

Ohtsu, I., Yasuda, Y., Takahashi, M. (2004). "Flow Characteristics of Skimming Flows in Stepped Channels." *J. Hydr. Engrg., ASCE* 130(9), 860-869.

Oliveto, G., Biggiero, V., Hager, W. H. (1997). "Bottom Outlet for Sewers." *J. Irrig. and Drain. Engrg.*, ASCE, 123(4), 246-252.

Onizuka, K., Odai, S. N. (1998). "Burgers' equation model for unsteady flow in open channels." *J. Hydr. Engrg.*, ASCE 124(5), 509-512.

Perumal, M., Shrestha, K. B., Chaube, U. C. (2004). "Reproduction of hysteresis in rating curves." *J. Hydr. Engrg.*, ASCE 130(9), 870-878.

Ponce, V. M., Simons, D. B. (1977). "Shallow wave propagation in open channel flow." *J. Hydraul. Div., Am. Soc. Civ. Eng.*, 103(12), 1461–1476.

Ponce, V. M., Rao, Y. R. S., Mansury, N. M. (1999). "Time of opening of irrigation canal gates." *J. Hydr. Engrg.*, ASCE 125(9), 979-980.

Ponce, V. M., Taher-shamsi, A., Shetty, A. V. (2003). "Dam-breach flood wave propagation using dimensionless parameters." *J. Hydr. Engrg., ASCE*, 129(10), 777-782.

Reinauer, R., Hager, W. H. (1998). "Supercritical Flow in Chute Contraction." *J. Hydr. Engrg., ASCE* 124(1), 55-64.

Ridolfi, L., Porporato, A., Revelli, R. (2006). "Green's function of the linearized de Saint-Venant equations." *J. Eng. Mech.*, ASCE, 132(2), 125-132.

Schwanenberg, D., Harms, M. (2004). "Discontinuous Galerkin Finite-Element Method for Transcritical Two-Dimensional Shallow Water Flows." *J. Hydr. Engrg., ASCE*, 130(5), 412-421.

Singh, V. P., Li, J. Z., and Wang, G-T. (1998). "Flood peak attenuation and forecast." *J. Hydro. Engrg.*, ASCE, 3(1), 20-25.

Tsai, C. W. (2003). "Applicability of kinematic, noninertia, and quasi-steady dynamic wave models to unsteady flow routing." *J. Hydr. Engrg., ASCE*, 129(8), 613-627.

Tsai, C. W. (2005). "Flood routing in mild-sloped rivers - wave characteristics and downstream backwater effect." *J. Hydrol.*, 308(1-4), 151-167.

Tsai, C. W.-S., Yen, B. C. (2001). "Linear analysis of shallow water wave propagation in open channels." *J. Eng. Mech., ASCE*, 127(5), 459-472.

Tsai, C. W., Yen, B. C. (2004). "Shallow water wave propagation in convectively accelerating open-channel flow induced by the tailwater effect." *J. Eng. Mech.*, ASCE, 130(3), 320-336.

Unami, K., Kawachi, T., Babar, M. M., Itagaki, H. (1999). "Two-Dimensional Numerical Model of Spillway Flow." *J. Hydr. Engrg., ASCE*, 125(4), 369-375.

Valiani, A., Caleffi, V. (2005). "Brief Analysis of Shallow Water Equations Suitability to Numerically Simulate Supercritical Flow in Sharp Bends." *J. Hydr. Engrg., ASCE*, 131(10), 912-916.

Wu, C., Huang, G. F., Zheng, Y. H . (1999). "Theoretical solution of dam-break shock wave." *J. Hydr. Engrg., ASCE*, 125(11), 1210-1215.

Yen, B. C., and Tsai, C. W.-S. (2001). "Nonintertia wave vs. diffusion wave in flood routing." *J. Hydrol.*, 244(1/2), 97-104.

Ying, X., Khan, A. A., Wang, S. S. Y. (2004). "Upwind Conservative Scheme for the Saint Venant Equations." *J. Hydr. Engrg.*, ASCE, 130(10), 977-987.

Zoppou, C., Roberts, S. (2003). "Explicit Schemes for Dam-Break Simulations." *J. Hydr. Engrg.*, ASCE, 129(1), 11-34.

Appendix A – Data used in graphs

Table A1 – Dimensionless celerity vs. wave number (Figure 3.1)

$F_n=$	0.1	0.3	0.5	0.7	1.0	1.5	2.0	2.66	4.0	10
σ^*	c^*									
0.01	1.67	1.67	1.67	1.67	1.67	1.67	1.67	1.67	1.66	1.58
0.01	1.67	1.67	1.67	1.67	1.67	1.67	1.67	1.67	1.66	1.57
0.01	1.67	1.67	1.67	1.67	1.67	1.67	1.67	1.67	1.66	1.55
0.01	1.67	1.67	1.67	1.67	1.67	1.67	1.67	1.67	1.66	1.54
0.02	1.67	1.67	1.67	1.67	1.67	1.67	1.67	1.67	1.66	1.52
0.02	1.67	1.67	1.67	1.67	1.67	1.67	1.67	1.67	1.66	1.51
0.02	1.67	1.67	1.67	1.67	1.67	1.67	1.67	1.66	1.66	1.49
0.02	1.67	1.67	1.67	1.67	1.67	1.67	1.67	1.66	1.65	1.47
0.02	1.67	1.67	1.67	1.67	1.67	1.67	1.67	1.66	1.65	1.45
0.03	1.67	1.67	1.67	1.67	1.67	1.67	1.67	1.66	1.64	1.43
0.03	1.67	1.67	1.67	1.67	1.67	1.67	1.67	1.66	1.64	1.42
0.03	1.67	1.67	1.67	1.67	1.67	1.67	1.67	1.66	1.63	1.40
0.04	1.67	1.67	1.67	1.67	1.67	1.67	1.67	1.66	1.63	1.38
0.04	1.67	1.67	1.67	1.67	1.67	1.67	1.66	1.66	1.62	1.36
0.05	1.67	1.67	1.67	1.67	1.67	1.67	1.66	1.66	1.61	1.35
0.05	1.67	1.67	1.67	1.67	1.67	1.67	1.66	1.65	1.60	1.33
0.06	1.67	1.67	1.67	1.67	1.67	1.67	1.66	1.65	1.59	1.32
0.07	1.67	1.67	1.67	1.67	1.67	1.67	1.66	1.65	1.58	1.30
0.08	1.67	1.67	1.67	1.67	1.67	1.67	1.66	1.64	1.56	1.29
0.09	1.67	1.67	1.67	1.67	1.67	1.67	1.66	1.64	1.55	1.27
0.10	1.67	1.67	1.67	1.67	1.67	1.67	1.66	1.63	1.54	1.26
0.11	1.67	1.67	1.67	1.67	1.67	1.67	1.66	1.62	1.52	1.25
0.12	1.67	1.67	1.67	1.67	1.67	1.67	1.65	1.61	1.50	1.24
0.14	1.67	1.67	1.67	1.67	1.67	1.67	1.65	1.60	1.49	1.23
0.15	1.67	1.67	1.67	1.67	1.67	1.67	1.65	1.59	1.47	1.21
0.17	1.67	1.67	1.67	1.67	1.67	1.67	1.64	1.58	1.46	1.20
0.19	1.67	1.67	1.67	1.67	1.67	1.67	1.64	1.57	1.44	1.20
0.22	1.67	1.67	1.67	1.67	1.68	1.67	1.63	1.56	1.43	1.19
0.25	1.67	1.67	1.67	1.67	1.68	1.67	1.63	1.55	1.41	1.18
0.28	1.67	1.67	1.67	1.68	1.68	1.67	1.62	1.54	1.40	1.17
0.31	1.67	1.67	1.67	1.68	1.68	1.67	1.61	1.52	1.38	1.16
0.35	1.67	1.67	1.68	1.68	1.69	1.67	1.60	1.51	1.37	1.16
0.39	1.67	1.67	1.68	1.69	1.69	1.67	1.60	1.50	1.36	1.15
0.44	1.67	1.67	1.68	1.69	1.70	1.67	1.59	1.48	1.34	1.14
0.49	1.67	1.67	1.69	1.70	1.71	1.67	1.58	1.47	1.33	1.14

0.55	1.67	1.68	1.69	1.71	1.72	1.67	1.57	1.46	1.32	1.13
0.62	1.67	1.68	1.70	1.72	1.73	1.67	1.56	1.45	1.31	1.13
0.69	1.67	1.68	1.70	1.73	1.75	1.67	1.55	1.44	1.31	1.13
0.78	1.67	1.68	1.72	1.75	1.77	1.67	1.55	1.43	1.30	1.12
0.87	1.67	1.69	1.73	1.78	1.79	1.67	1.54	1.42	1.29	1.12
0.98	1.67	1.70	1.75	1.81	1.81	1.67	1.53	1.42	1.28	1.12
1.10	1.67	1.70	1.77	1.85	1.84	1.67	1.53	1.41	1.28	1.11
1.23	1.67	1.71	1.81	1.90	1.86	1.67	1.52	1.40	1.27	1.11
1.38	1.67	1.73	1.85	1.96	1.88	1.67	1.52	1.40	1.27	1.11
1.55	1.67	1.75	1.92	2.02	1.90	1.67	1.52	1.40	1.27	1.11
1.74	1.68	1.77	2.01	2.09	1.92	1.67	1.51	1.39	1.26	1.11
1.95	1.68	1.81	2.13	2.15	1.93	1.67	1.51	1.39	1.26	1.11
2.19	1.68	1.86	2.26	2.20	1.95	1.67	1.51	1.39	1.26	1.10
2.45	1.69	1.94	2.40	2.24	1.96	1.67	1.51	1.38	1.26	1.10
2.75	1.69	2.07	2.52	2.28	1.96	1.67	1.51	1.38	1.26	1.10
3.09	1.70	2.29	2.62	2.31	1.97	1.67	1.50	1.38	1.25	1.10
3.47	1.71	2.61	2.70	2.33	1.98	1.67	1.50	1.38	1.25	1.10
3.89	1.72	2.97	2.76	2.35	1.98	1.67	1.50	1.38	1.25	1.10
4.37	1.74	3.28	2.81	2.37	1.99	1.67	1.50	1.38	1.25	1.10
4.90	1.76	3.52	2.85	2.38	1.99	1.67	1.50	1.38	1.25	1.10
5.50	1.80	3.70	2.88	2.39	1.99	1.67	1.50	1.38	1.25	1.10
6.17	1.84	3.84	2.91	2.40	1.99	1.67	1.50	1.38	1.25	1.10
6.92	1.92	3.94	2.93	2.40	1.99	1.67	1.50	1.38	1.25	1.10
7.76	2.05	4.03	2.94	2.41	2.00	1.67	1.50	1.38	1.25	1.10
8.71	2.32	4.09	2.95	2.41	2.00	1.67	1.50	1.38	1.25	1.10
9.77	3.20	4.14	2.96	2.42	2.00	1.67	1.50	1.38	1.25	1.10
10.96	5.33	4.18	2.97	2.42	2.00	1.67	1.50	1.38	1.25	1.10
12.30	6.90	4.21	2.98	2.42	2.00	1.67	1.50	1.38	1.25	1.10
13.80	7.93	4.24	2.98	2.42	2.00	1.67	1.50	1.38	1.25	1.10
15.49	8.66	4.26	2.99	2.42	2.00	1.67	1.50	1.38	1.25	1.10
17.38	9.19	4.27	2.99	2.42	2.00	1.67	1.50	1.38	1.25	1.10
19.50	9.59	4.29	2.99	2.43	2.00	1.67	1.50	1.38	1.25	1.10
21.88	9.90	4.30	2.99	2.43	2.00	1.67	1.50	1.38	1.25	1.10
24.55	10.14	4.30	2.99	2.43	2.00	1.67	1.50	1.38	1.25	1.10
27.54	10.32	4.31	3.00	2.43	2.00	1.67	1.50	1.38	1.25	1.10
30.90	10.46	4.31	3.00	2.43	2.00	1.67	1.50	1.38	1.25	1.10
34.67	10.58	4.32	3.00	2.43	2.00	1.67	1.50	1.38	1.25	1.10
38.90	10.67	4.32	3.00	2.43	2.00	1.67	1.50	1.38	1.25	1.10
43.65	10.74	4.32	3.00	2.43	2.00	1.67	1.50	1.38	1.25	1.10
48.98	10.79	4.33	3.00	2.43	2.00	1.67	1.50	1.38	1.25	1.10
54.95	10.83	4.33	3.00	2.43	2.00	1.67	1.50	1.38	1.25	1.10
61.66	10.87	4.33	3.00	2.43	2.00	1.67	1.50	1.38	1.25	1.10
69.18	10.90	4.33	3.00	2.43	2.00	1.67	1.50	1.38	1.25	1.10
77.62	10.92	4.33	3.00	2.43	2.00	1.67	1.50	1.38	1.25	1.10
87.10	10.93	4.33	3.00	2.43	2.00	1.67	1.50	1.38	1.25	1.10
97.72	10.95	4.33	3.00	2.43	2.00	1.67	1.50	1.38	1.25	1.10
109.65	10.96	4.33	3.00	2.43	2.00	1.67	1.50	1.38	1.25	1.10
123.03	10.97	4.33	3.00	2.43	2.00	1.67	1.50	1.38	1.25	1.10

138.04	10.97	4.33	3.00	2.43	2.00	1.67	1.50	1.38	1.25	1.10
154.88	10.98	4.33	3.00	2.43	2.00	1.67	1.50	1.38	1.25	1.10
173.78	10.98	4.33	3.00	2.43	2.00	1.67	1.50	1.38	1.25	1.10
194.98	10.99	4.33	3.00	2.43	2.00	1.67	1.50	1.38	1.25	1.10
218.78	10.99	4.33	3.00	2.43	2.00	1.67	1.50	1.38	1.25	1.10
245.47	10.99	4.33	3.00	2.43	2.00	1.67	1.50	1.38	1.25	1.10
275.42	10.99	4.33	3.00	2.43	2.00	1.67	1.50	1.38	1.25	1.10
309.03	10.99	4.33	3.00	2.43	2.00	1.67	1.50	1.38	1.25	1.10
346.74	11.00	4.33	3.00	2.43	2.00	1.67	1.50	1.38	1.25	1.10
389.05	11.00	4.33	3.00	2.43	2.00	1.67	1.50	1.38	1.25	1.10
436.52	11.00	4.33	3.00	2.43	2.00	1.67	1.50	1.38	1.25	1.10
489.78	11.00	4.33	3.00	2.43	2.00	1.67	1.50	1.38	1.25	1.10
549.54	11.00	4.33	3.00	2.43	2.00	1.67	1.50	1.38	1.25	1.10
616.60	11.00	4.33	3.00	2.43	2.00	1.67	1.50	1.38	1.25	1.10
691.83	11.00	4.33	3.00	2.43	2.00	1.67	1.50	1.38	1.25	1.10
776.25	11.00	4.33	3.00	2.43	2.00	1.67	1.50	1.38	1.25	1.10
870.96	11.00	4.33	3.00	2.43	2.00	1.67	1.50	1.38	1.25	1.10
977.24	11.00	4.33	3.00	2.43	2.00	1.67	1.50	1.38	1.25	1.10

Table A2 – Attenuation factor vs. wave number (Figure 3.2)

$F_n=$	0.1	0.3	0.5	0.7	1.0	1.5	2.0	2.66	4.0	10
σ^*					δ^*					
0.01	-0.02	-0.02	-0.02	-0.01	-0.01	0.00	0.01	0.04	0.11	0.60
0.01	-0.02	-0.02	-0.02	-0.02	-0.01	0.00	0.02	0.04	0.12	0.63
0.01	-0.02	-0.02	-0.02	-0.02	-0.01	0.00	0.02	0.05	0.14	0.67
0.01	-0.03	-0.02	-0.02	-0.02	-0.01	0.00	0.02	0.06	0.16	0.70
0.02	-0.03	-0.03	-0.03	-0.02	-0.02	0.00	0.02	0.06	0.17	0.74
0.02	-0.03	-0.03	-0.03	-0.03	-0.02	0.00	0.03	0.07	0.19	0.77
0.02	-0.04	-0.04	-0.03	-0.03	-0.02	0.00	0.03	0.08	0.22	0.79
0.02	-0.04	-0.04	-0.04	-0.03	-0.02	0.00	0.03	0.09	0.24	0.82
0.02	-0.05	-0.04	-0.04	-0.04	-0.03	0.00	0.04	0.10	0.26	0.84
0.03	-0.05	-0.05	-0.05	-0.04	-0.03	0.00	0.04	0.11	0.29	0.85
0.03	-0.06	-0.06	-0.05	-0.05	-0.03	0.00	0.04	0.12	0.32	0.86
0.03	-0.07	-0.06	-0.06	-0.05	-0.04	0.00	0.05	0.14	0.35	0.87
0.04	-0.07	-0.07	-0.07	-0.06	-0.04	0.00	0.06	0.15	0.39	0.87
0.04	-0.08	-0.08	-0.07	-0.06	-0.05	0.00	0.06	0.17	0.42	0.87
0.05	-0.09	-0.09	-0.08	-0.07	-0.05	0.00	0.07	0.19	0.45	0.87
0.05	-0.10	-0.10	-0.09	-0.08	-0.06	0.00	0.08	0.21	0.49	0.86
0.06	-0.12	-0.11	-0.10	-0.09	-0.06	0.00	0.09	0.23	0.52	0.86
0.07	-0.13	-0.13	-0.12	-0.10	-0.07	0.00	0.10	0.25	0.55	0.84
0.08	-0.15	-0.14	-0.13	-0.11	-0.08	0.00	0.11	0.28	0.59	0.83
0.09	-0.16	-0.16	-0.15	-0.13	-0.09	0.00	0.12	0.30	0.61	0.81
0.10	-0.18	-0.18	-0.16	-0.14	-0.10	0.00	0.13	0.33	0.64	0.79
0.11	-0.21	-0.20	-0.18	-0.16	-0.11	0.00	0.15	0.36	0.66	0.77
0.12	-0.23	-0.22	-0.21	-0.18	-0.13	0.00	0.16	0.38	0.68	0.75
0.14	-0.26	-0.25	-0.23	-0.20	-0.14	0.00	0.18	0.41	0.70	0.73

0.15	-0.29	-0.28	-0.26	-0.23	-0.16	0.00	0.20	0.43	0.71	0.70
0.17	-0.33	-0.31	-0.29	-0.26	-0.18	0.00	0.21	0.46	0.71	0.68
0.19	-0.37	-0.35	-0.33	-0.29	-0.20	0.00	0.23	0.48	0.71	0.65
0.22	-0.41	-0.40	-0.37	-0.32	-0.22	0.00	0.24	0.49	0.71	0.62
0.25	-0.46	-0.44	-0.41	-0.36	-0.25	0.00	0.26	0.51	0.71	0.60
0.28	-0.52	-0.50	-0.46	-0.40	-0.28	0.00	0.27	0.52	0.70	0.57
0.31	-0.58	-0.56	-0.52	-0.45	-0.31	0.00	0.29	0.52	0.68	0.54
0.35	-0.65	-0.63	-0.58	-0.51	-0.34	0.00	0.30	0.52	0.67	0.51
0.39	-0.73	-0.70	-0.65	-0.57	-0.38	0.00	0.30	0.52	0.65	0.48
0.44	-0.82	-0.79	-0.73	-0.63	-0.42	0.00	0.31	0.51	0.63	0.46
0.49	-0.92	-0.89	-0.82	-0.71	-0.46	0.00	0.31	0.50	0.60	0.43
0.55	-1.03	-0.99	-0.92	-0.79	-0.50	0.00	0.31	0.49	0.57	0.40
0.62	-1.16	-1.12	-1.03	-0.87	-0.54	0.00	0.30	0.47	0.54	0.37
0.69	-1.30	-1.25	-1.15	-0.97	-0.58	0.00	0.29	0.45	0.51	0.35
0.78	-1.46	-1.40	-1.28	-1.07	-0.61	0.00	0.28	0.43	0.48	0.32
0.87	-1.63	-1.58	-1.43	-1.17	-0.63	0.00	0.27	0.41	0.45	0.30
0.98	-1.83	-1.77	-1.60	-1.27	-0.63	0.00	0.26	0.38	0.42	0.27
1.10	-2.06	-1.98	-1.77	-1.35	-0.63	0.00	0.24	0.36	0.39	0.25
1.23	-2.31	-2.23	-1.96	-1.41	-0.61	0.00	0.23	0.33	0.36	0.23
1.38	-2.59	-2.49	-2.15	-1.44	-0.59	0.00	0.21	0.31	0.33	0.21
1.55	-2.91	-2.80	-2.32	-1.42	-0.55	0.00	0.19	0.28	0.30	0.19
1.74	-3.27	-3.13	-2.44	-1.37	-0.52	0.00	0.18	0.26	0.27	0.17
1.95	-3.67	-3.49	-2.47	-1.28	-0.48	0.00	0.16	0.23	0.25	0.16
2.19	-4.11	-3.88	-2.40	-1.18	-0.44	0.00	0.15	0.21	0.22	0.14
2.45	-4.62	-4.28	-2.23	-1.08	-0.40	0.00	0.13	0.19	0.20	0.13
2.75	-5.18	-4.62	-2.03	-0.98	-0.36	0.00	0.12	0.17	0.18	0.11
3.09	-5.82	-4.76	-1.83	-0.88	-0.32	0.00	0.11	0.16	0.16	0.10
3.47	-6.54	-4.52	-1.63	-0.79	-0.29	0.00	0.10	0.14	0.15	0.09
3.89	-7.34	-4.00	-1.45	-0.71	-0.26	0.00	0.09	0.13	0.13	0.08
4.37	-8.25	-3.45	-1.29	-0.64	-0.23	0.00	0.08	0.11	0.12	0.07
4.90	-9.26	-2.98	-1.15	-0.57	-0.21	0.00	0.07	0.10	0.11	0.07
5.50	-10.40	-2.59	-1.02	-0.51	-0.19	0.00	0.06	0.09	0.09	0.06
6.17	-11.65	-2.26	-0.91	-0.45	-0.17	0.00	0.06	0.08	0.08	0.05
6.92	-13.02	-1.98	-0.81	-0.40	-0.15	0.00	0.05	0.07	0.08	0.05
7.76	-14.39	-1.74	-0.72	-0.36	-0.13	0.00	0.04	0.06	0.07	0.04
8.71	-15.40	-1.54	-0.64	-0.32	-0.12	0.00	0.04	0.06	0.06	0.04
9.77	-14.00	-1.36	-0.57	-0.29	-0.11	0.00	0.04	0.05	0.05	0.03
10.96	-9.09	-1.20	-0.51	-0.26	-0.10	0.00	0.03	0.05	0.05	0.03
12.30	-6.57	-1.07	-0.45	-0.23	-0.08	0.00	0.03	0.04	0.04	0.03
13.80	-5.19	-0.95	-0.41	-0.20	-0.08	0.00	0.03	0.04	0.04	0.02
15.49	-4.28	-0.84	-0.36	-0.18	-0.07	0.00	0.02	0.03	0.03	0.02
17.38	-3.61	-0.75	-0.32	-0.16	-0.06	0.00	0.02	0.03	0.03	0.02
19.50	-3.10	-0.67	-0.29	-0.14	-0.05	0.00	0.02	0.03	0.03	0.02
21.88	-2.68	-0.59	-0.26	-0.13	-0.05	0.00	0.02	0.02	0.02	0.01
24.55	-2.34	-0.53	-0.23	-0.11	-0.04	0.00	0.01	0.02	0.02	0.01
27.54	-2.05	-0.47	-0.20	-0.10	-0.04	0.00	0.01	0.02	0.02	0.01
30.90	-1.81	-0.42	-0.18	-0.09	-0.03	0.00	0.01	0.02	0.02	0.01
34.67	-1.59	-0.37	-0.16	-0.08	-0.03	0.00	0.01	0.01	0.02	0.01

38.90	-1.41	-0.33	-0.14	-0.07	-0.03	0.00	0.01	0.01	0.01	0.01
43.65	-1.25	-0.30	-0.13	-0.06	-0.02	0.00	0.01	0.01	0.01	0.01
48.98	-1.11	-0.26	-0.11	-0.06	-0.02	0.00	0.01	0.01	0.01	0.01
54.95	-0.98	-0.23	-0.10	-0.05	-0.02	0.00	0.01	0.01	0.01	0.01
61.66	-0.87	-0.21	-0.09	-0.05	-0.02	0.00	0.01	0.01	0.01	0.01
69.18	-0.78	-0.19	-0.08	-0.04	-0.02	0.00	0.01	0.01	0.01	0.00
77.62	-0.69	-0.17	-0.07	-0.04	-0.01	0.00	0.00	0.01	0.01	0.00
87.10	-0.62	-0.15	-0.06	-0.03	-0.01	0.00	0.00	0.01	0.01	0.00
97.72	-0.55	-0.13	-0.06	-0.03	-0.01	0.00	0.00	0.01	0.01	0.00
109.65	-0.49	-0.12	-0.05	-0.03	-0.01	0.00	0.00	0.00	0.00	0.00
123.03	-0.43	-0.10	-0.05	-0.02	-0.01	0.00	0.00	0.00	0.00	0.00
138.04	-0.39	-0.09	-0.04	-0.02	-0.01	0.00	0.00	0.00	0.00	0.00
154.88	-0.34	-0.08	-0.04	-0.02	-0.01	0.00	0.00	0.00	0.00	0.00
173.78	-0.31	-0.07	-0.03	-0.02	-0.01	0.00	0.00	0.00	0.00	0.00
194.98	-0.27	-0.07	-0.03	-0.01	-0.01	0.00	0.00	0.00	0.00	0.00
218.78	-0.24	-0.06	-0.03	-0.01	0.00	0.00	0.00	0.00	0.00	0.00
245.47	-0.22	-0.05	-0.02	-0.01	0.00	0.00	0.00	0.00	0.00	0.00
275.42	-0.19	-0.05	-0.02	-0.01	0.00	0.00	0.00	0.00	0.00	0.00
309.03	-0.17	-0.04	-0.02	-0.01	0.00	0.00	0.00	0.00	0.00	0.00
346.74	-0.15	-0.04	-0.02	-0.01	0.00	0.00	0.00	0.00	0.00	0.00
389.05	-0.14	-0.03	-0.01	-0.01	0.00	0.00	0.00	0.00	0.00	0.00
436.52	-0.12	-0.03	-0.01	-0.01	0.00	0.00	0.00	0.00	0.00	0.00
489.78	-0.11	-0.03	-0.01	-0.01	0.00	0.00	0.00	0.00	0.00	0.00
549.54	-0.10	-0.02	-0.01	-0.01	0.00	0.00	0.00	0.00	0.00	0.00
616.60	-0.09	-0.02	-0.01	0.00	0.00	0.00	0.00	0.00	0.00	0.00
691.83	-0.08	-0.02	-0.01	0.00	0.00	0.00	0.00	0.00	0.00	0.00
776.25	-0.07	-0.02	-0.01	0.00	0.00	0.00	0.00	0.00	0.00	0.00
870.96	-0.06	-0.01	-0.01	0.00	0.00	0.00	0.00	0.00	0.00	0.00
977.24	-0.05	-0.01	-0.01	0.00	0.00	0.00	0.00	0.00	0.00	0.00

Table A3 – Normalized length amplification factor vs. wave number (Figure 3.6)

$F_n=$	0.1	0.3	0.5	0.7	1.0	1.5	2.0	2.66	4.0	10
σ^*	$\delta`$									
0.01	0.00	0.00	0.00	0.00	0.00	0.00	0.00	0.00	0.00	0.01
0.01	0.00	0.00	0.00	0.00	0.00	0.00	0.00	0.00	0.00	0.01
0.01	0.00	0.00	0.00	0.00	0.00	0.00	0.00	0.00	0.00	0.01
0.01	0.00	0.00	0.00	0.00	0.00	0.00	0.00	0.00	0.00	0.01
0.02	0.00	0.00	0.00	0.00	0.00	0.00	0.00	0.00	0.00	0.01
0.02	0.00	0.00	0.00	0.00	0.00	0.00	0.00	0.00	0.00	0.01
0.02	0.00	0.00	0.00	0.00	0.00	0.00	0.00	0.00	0.00	0.02
0.02	0.00	0.00	0.00	0.00	0.00	0.00	0.00	0.00	0.01	0.02
0.02	0.00	0.00	0.00	0.00	0.00	0.00	0.00	0.00	0.01	0.02
0.03	0.00	0.00	0.00	0.00	0.00	0.00	0.00	0.00	0.01	0.02
0.03	0.00	0.00	0.00	0.00	0.00	0.00	0.00	0.00	0.01	0.03
0.03	0.00	0.00	0.00	0.00	0.00	0.00	0.00	0.00	0.01	0.03
0.04	0.00	0.00	0.00	0.00	0.00	0.00	0.00	0.01	0.02	0.03

0.04	0.00	0.00	0.00	0.00	0.00	0.00	0.00	0.01	0.02	0.04
0.05	0.00	0.00	0.00	0.00	0.00	0.00	0.00	0.01	0.02	0.04
0.05	-0.01	-0.01	-0.01	0.00	0.00	0.00	0.00	0.01	0.03	0.05
0.06	-0.01	-0.01	-0.01	-0.01	0.00	0.00	0.01	0.01	0.03	0.05
0.07	-0.01	-0.01	-0.01	-0.01	-0.01	0.00	0.01	0.02	0.04	0.06
0.08	-0.01	-0.01	-0.01	-0.01	-0.01	0.00	0.01	0.02	0.05	0.06
0.09	-0.01	-0.01	-0.01	-0.01	-0.01	0.00	0.01	0.03	0.05	0.07
0.10	-0.02	-0.02	-0.02	-0.01	-0.01	0.00	0.01	0.03	0.06	0.08
0.11	-0.02	-0.02	-0.02	-0.02	-0.01	0.00	0.02	0.04	0.07	0.08
0.12	-0.03	-0.03	-0.03	-0.02	-0.02	0.00	0.02	0.05	0.08	0.09
0.14	-0.04	-0.03	-0.03	-0.03	-0.02	0.00	0.02	0.06	0.10	0.10
0.15	-0.05	-0.04	-0.04	-0.04	-0.02	0.00	0.03	0.07	0.11	0.11
0.17	-0.06	-0.05	-0.05	-0.04	-0.03	0.00	0.04	0.08	0.12	0.12
0.19	-0.07	-0.07	-0.06	-0.06	-0.04	0.00	0.04	0.09	0.14	0.13
0.22	-0.09	-0.09	-0.08	-0.07	-0.05	0.00	0.05	0.11	0.16	0.14
0.25	-0.11	-0.11	-0.10	-0.09	-0.06	0.00	0.06	0.12	0.17	0.15
0.28	-0.14	-0.14	-0.13	-0.11	-0.08	0.00	0.08	0.14	0.19	0.16
0.31	-0.18	-0.17	-0.16	-0.14	-0.10	0.00	0.09	0.16	0.21	0.17
0.35	-0.23	-0.22	-0.20	-0.18	-0.12	0.00	0.10	0.18	0.23	0.18
0.39	-0.28	-0.27	-0.25	-0.22	-0.15	0.00	0.12	0.20	0.25	0.19
0.44	-0.36	-0.34	-0.32	-0.28	-0.18	0.00	0.13	0.22	0.27	0.20
0.49	-0.45	-0.43	-0.40	-0.35	-0.23	0.00	0.15	0.25	0.29	0.21
0.55	-0.57	-0.55	-0.50	-0.43	-0.28	0.00	0.17	0.27	0.32	0.22
0.62	-0.71	-0.69	-0.63	-0.54	-0.33	0.00	0.19	0.29	0.34	0.23
0.69	-0.90	-0.87	-0.79	-0.67	-0.40	0.00	0.20	0.31	0.36	0.24
0.78	-1.13	-1.09	-1.00	-0.83	-0.47	0.00	0.22	0.34	0.38	0.25
0.87	-1.42	-1.37	-1.25	-1.02	-0.54	0.00	0.24	0.36	0.39	0.26
0.98	-1.79	-1.73	-1.56	-1.24	-0.62	0.00	0.25	0.38	0.41	0.27
1.10	-2.26	-2.18	-1.95	-1.48	-0.69	0.00	0.27	0.39	0.43	0.28
1.23	-2.84	-2.74	-2.41	-1.74	-0.76	0.00	0.28	0.41	0.44	0.28
1.38	-3.58	-3.44	-2.97	-1.99	-0.81	0.00	0.29	0.42	0.45	0.29
1.55	-4.51	-4.33	-3.59	-2.20	-0.86	0.00	0.30	0.44	0.47	0.30
1.74	-5.67	-5.44	-4.24	-2.38	-0.90	0.00	0.31	0.45	0.48	0.30
1.95	-7.15	-6.81	-4.82	-2.50	-0.93	0.00	0.32	0.46	0.48	0.30
2.19	-9.00	-8.50	-5.24	-2.59	-0.95	0.00	0.32	0.46	0.49	0.31
2.45	-11.34	-10.50	-5.48	-2.65	-0.97	0.00	0.33	0.47	0.50	0.31
2.75	-14.28	-12.72	-5.60	-2.70	-0.99	0.00	0.33	0.48	0.50	0.31
3.09	-17.99	-14.71	-5.64	-2.73	-1.00	0.00	0.33	0.48	0.51	0.32
3.47	-22.67	-15.67	-5.66	-2.75	-1.01	0.00	0.34	0.48	0.51	0.32
3.89	-28.57	-15.55	-5.66	-2.76	-1.02	0.00	0.34	0.49	0.51	0.32
4.37	-36.00	-15.07	-5.65	-2.78	-1.02	0.00	0.34	0.49	0.51	0.32
4.90	-45.36	-14.60	-5.64	-2.79	-1.03	0.00	0.34	0.49	0.52	0.32
5.50	-57.13	-14.22	-5.63	-2.79	-1.03	0.00	0.34	0.49	0.52	0.32
6.17	-71.86	-13.92	-5.62	-2.80	-1.04	0.00	0.35	0.49	0.52	0.32
6.92	-90.05	-13.69	-5.62	-2.80	-1.04	0.00	0.35	0.50	0.52	0.32
7.76	-111.73	-13.52	-5.61	-2.80	-1.04	0.00	0.35	0.50	0.52	0.32
8.71	-134.09	-13.38	-5.61	-2.81	-1.04	0.00	0.35	0.50	0.52	0.32
9.77	-136.77	-13.28	-5.60	-2.81	-1.04	0.00	0.35	0.50	0.52	0.32

10.96	-99.66	-13.19	-5.60	-2.81	-1.04	0.00	0.35	0.50	0.52	0.32
12.30	-80.80	-13.13	-5.60	-2.81	-1.04	0.00	0.35	0.50	0.52	0.32
13.80	-71.62	-13.08	-5.59	-2.81	-1.04	0.00	0.35	0.50	0.52	0.32
15.49	-66.26	-13.04	-5.59	-2.81	-1.05	0.00	0.35	0.50	0.52	0.32
17.38	-62.79	-13.01	-5.59	-2.81	-1.05	0.00	0.35	0.50	0.52	0.32
19.50	-60.41	-12.98	-5.59	-2.81	-1.05	0.00	0.35	0.50	0.52	0.32
21.88	-58.71	-12.96	-5.59	-2.81	-1.05	0.00	0.35	0.50	0.52	0.32
24.55	-57.46	-12.95	-5.59	-2.81	-1.05	0.00	0.35	0.50	0.52	0.32
27.54	-56.52	-12.94	-5.59	-2.82	-1.05	0.00	0.35	0.50	0.52	0.32
30.90	-55.81	-12.93	-5.59	-2.82	-1.05	0.00	0.35	0.50	0.52	0.32
34.67	-55.27	-12.92	-5.59	-2.82	-1.05	0.00	0.35	0.50	0.52	0.32
38.90	-54.85	-12.91	-5.59	-2.82	-1.05	0.00	0.35	0.50	0.52	0.32
43.65	-54.52	-12.91	-5.59	-2.82	-1.05	0.00	0.35	0.50	0.52	0.32
48.98	-54.26	-12.90	-5.59	-2.82	-1.05	0.00	0.35	0.50	0.52	0.32
54.95	-54.06	-12.90	-5.59	-2.82	-1.05	0.00	0.35	0.50	0.52	0.32
61.66	-53.91	-12.90	-5.59	-2.82	-1.05	0.00	0.35	0.50	0.52	0.32
69.18	-53.78	-12.90	-5.59	-2.82	-1.05	0.00	0.35	0.50	0.52	0.32
77.62	-53.68	-12.89	-5.59	-2.82	-1.05	0.00	0.35	0.50	0.52	0.32
87.10	-53.61	-12.89	-5.59	-2.82	-1.05	0.00	0.35	0.50	0.52	0.32
97.72	-53.55	-12.89	-5.59	-2.82	-1.05	0.00	0.35	0.50	0.52	0.32
109.65	-53.50	-12.89	-5.59	-2.82	-1.05	0.00	0.35	0.50	0.52	0.32
123.03	-53.46	-12.89	-5.59	-2.82	-1.05	0.00	0.35	0.50	0.52	0.32
138.04	-53.43	-12.89	-5.59	-2.82	-1.05	0.00	0.35	0.50	0.52	0.32
154.88	-53.40	-12.89	-5.59	-2.82	-1.05	0.00	0.35	0.50	0.52	0.32
173.78	-53.39	-12.89	-5.59	-2.82	-1.05	0.00	0.35	0.50	0.52	0.32
194.98	-53.37	-12.89	-5.59	-2.82	-1.05	0.00	0.35	0.50	0.52	0.32
218.78	-53.36	-12.89	-5.59	-2.82	-1.05	0.00	0.35	0.50	0.52	0.32
245.47	-53.35	-12.89	-5.59	-2.82	-1.05	0.00	0.35	0.50	0.52	0.32
275.42	-53.34	-12.89	-5.59	-2.82	-1.05	0.00	0.35	0.50	0.52	0.32
309.03	-53.34	-12.89	-5.59	-2.82	-1.05	0.00	0.35	0.50	0.52	0.32
346.74	-53.33	-12.89	-5.59	-2.82	-1.05	0.00	0.35	0.50	0.52	0.32
389.05	-53.33	-12.89	-5.59	-2.82	-1.05	0.00	0.35	0.50	0.52	0.32
436.52	-53.32	-12.89	-5.59	-2.82	-1.05	0.00	0.35	0.50	0.52	0.32
489.78	-53.32	-12.89	-5.59	-2.82	-1.05	0.00	0.35	0.50	0.52	0.32
549.54	-53.32	-12.89	-5.59	-2.82	-1.05	0.00	0.35	0.50	0.52	0.32
616.60	-53.32	-12.89	-5.59	-2.82	-1.05	0.00	0.35	0.50	0.52	0.32
691.83	-53.32	-12.89	-5.59	-2.82	-1.05	0.00	0.35	0.50	0.52	0.32
776.25	-53.32	-12.89	-5.59	-2.82	-1.05	0.00	0.35	0.50	0.52	0.32
870.96	-53.31	-12.89	-5.59	-2.82	-1.05	0.00	0.35	0.50	0.52	0.32
977.24	-53.31	-12.89	-5.59	-2.82	-1.05	0.00	0.35	0.50	0.52	0.32

Table A4 – Normalized length amplification factor vs. Froude number (Figure 3.8)

$\sigma^* =$	0.01	0.05	0.1	0.5	1.0	2.0	10	100	1000	10000
F_n					δ`					
1.5	0.00	0.00	0.00	0.00	0.00	0.00	0.00	0.00	0.00	0.00
1.54	0.00	0.00	0.00	0.02	0.03	0.04	0.04	0.04	0.04	0.04

1.59	0.00	0.00	0.00	0.03	0.06	0.08	0.09	0.09	0.09	0.09
1.64	0.00	0.00	0.00	0.05	0.10	0.12	0.13	0.14	0.14	0.14
1.69	0.00	0.00	0.00	0.07	0.12	0.16	0.17	0.18	0.18	0.18
1.74	0.00	0.00	0.01	0.09	0.15	0.19	0.21	0.21	0.21	0.21
1.79	0.00	0.00	0.01	0.10	0.17	0.22	0.24	0.24	0.24	0.24
1.84	0.00	0.00	0.01	0.11	0.20	0.25	0.27	0.27	0.27	0.27
1.89	0.00	0.00	0.01	0.13	0.22	0.27	0.30	0.30	0.30	0.30
1.94	0.00	0.00	0.01	0.14	0.23	0.29	0.32	0.32	0.32	0.32
1.99	0.00	0.00	0.01	0.15	0.25	0.31	0.34	0.34	0.34	0.34
2.04	0.00	0.00	0.01	0.16	0.27	0.33	0.36	0.36	0.36	0.36
2.09	0.00	0.00	0.02	0.17	0.28	0.35	0.38	0.38	0.38	0.38
2.14	0.00	0.00	0.02	0.18	0.29	0.36	0.40	0.40	0.40	0.40
2.19	0.00	0.01	0.02	0.19	0.31	0.38	0.41	0.41	0.41	0.41
2.24	0.00	0.01	0.02	0.20	0.32	0.39	0.43	0.43	0.43	0.43
2.29	0.00	0.01	0.02	0.21	0.33	0.40	0.44	0.44	0.44	0.44
2.34	0.00	0.01	0.02	0.21	0.34	0.41	0.45	0.45	0.45	0.45
2.39	0.00	0.01	0.03	0.22	0.34	0.42	0.46	0.46	0.46	0.46
2.44	0.00	0.01	0.03	0.23	0.35	0.43	0.47	0.47	0.47	0.47
2.49	0.00	0.01	0.03	0.23	0.36	0.44	0.48	0.48	0.48	0.48
2.54	0.00	0.01	0.03	0.24	0.37	0.44	0.48	0.48	0.48	0.48
2.59	0.00	0.01	0.03	0.24	0.37	0.45	0.49	0.49	0.49	0.49
2.64	0.00	0.01	0.03	0.25	0.38	0.46	0.49	0.50	0.50	0.50
2.69	0.00	0.01	0.03	0.25	0.38	0.46	0.50	0.50	0.50	0.50
2.74	0.00	0.01	0.04	0.26	0.39	0.47	0.50	0.51	0.51	0.51
2.79	0.00	0.01	0.04	0.26	0.39	0.47	0.51	0.51	0.51	0.51
2.84	0.00	0.01	0.04	0.27	0.39	0.47	0.51	0.51	0.51	0.51
2.89	0.00	0.01	0.04	0.27	0.40	0.48	0.52	0.52	0.52	0.52
2.94	0.00	0.01	0.04	0.27	0.40	0.48	0.52	0.52	0.52	0.52
2.99	0.00	0.01	0.04	0.27	0.40	0.48	0.52	0.52	0.52	0.52
3.04	0.00	0.01	0.04	0.28	0.40	0.48	0.52	0.53	0.53	0.53
3.09	0.00	0.01	0.05	0.28	0.41	0.49	0.53	0.53	0.53	0.53
3.14	0.00	0.01	0.05	0.28	0.41	0.49	0.53	0.53	0.53	0.53
3.19	0.00	0.01	0.05	0.28	0.41	0.49	0.53	0.53	0.53	0.53
3.24	0.00	0.02	0.05	0.29	0.41	0.49	0.53	0.53	0.53	0.53
3.29	0.00	0.02	0.05	0.29	0.41	0.49	0.53	0.53	0.53	0.53
3.34	0.00	0.02	0.05	0.29	0.41	0.49	0.53	0.53	0.53	0.53
3.39	0.00	0.02	0.05	0.29	0.41	0.49	0.53	0.53	0.53	0.53
3.44	0.00	0.02	0.05	0.29	0.42	0.49	0.53	0.53	0.53	0.53
3.49	0.00	0.02	0.05	0.29	0.42	0.49	0.53	0.53	0.53	0.53
3.54	0.00	0.02	0.06	0.29	0.42	0.49	0.53	0.53	0.53	0.53
3.59	0.00	0.02	0.06	0.29	0.42	0.49	0.53	0.53	0.53	0.53
3.64	0.00	0.02	0.06	0.29	0.42	0.49	0.53	0.53	0.53	0.53
3.69	0.00	0.02	0.06	0.30	0.42	0.49	0.53	0.53	0.53	0.53
3.74	0.00	0.02	0.06	0.30	0.42	0.49	0.53	0.53	0.53	0.53
3.79	0.00	0.02	0.06	0.30	0.42	0.49	0.53	0.53	0.53	0.53
3.84	0.00	0.02	0.06	0.30	0.42	0.49	0.53	0.53	0.53	0.53
3.89	0.00	0.02	0.06	0.30	0.42	0.49	0.52	0.53	0.53	0.53
3.94	0.00	0.02	0.06	0.30	0.41	0.49	0.52	0.53	0.53	0.53

3.99	0.00	0.02	0.06	0.30	0.41	0.49	0.52	0.52	0.52	0.52
4.04	0.00	0.02	0.07	0.30	0.41	0.48	0.52	0.52	0.52	0.52
4.09	0.00	0.02	0.07	0.30	0.41	0.48	0.52	0.52	0.52	0.52
4.14	0.00	0.02	0.07	0.30	0.41	0.48	0.52	0.52	0.52	0.52
4.19	0.00	0.02	0.07	0.30	0.41	0.48	0.52	0.52	0.52	0.52
4.24	0.00	0.03	0.07	0.30	0.41	0.48	0.51	0.52	0.52	0.52
4.29	0.00	0.03	0.07	0.30	0.41	0.48	0.51	0.51	0.51	0.51
4.34	0.00	0.03	0.07	0.30	0.41	0.48	0.51	0.51	0.51	0.51
4.39	0.00	0.03	0.07	0.30	0.41	0.48	0.51	0.51	0.51	0.51
4.44	0.00	0.03	0.07	0.30	0.41	0.47	0.51	0.51	0.51	0.51
4.49	0.00	0.03	0.07	0.30	0.41	0.47	0.51	0.51	0.51	0.51
4.54	0.00	0.03	0.07	0.30	0.40	0.47	0.50	0.51	0.51	0.51
4.59	0.00	0.03	0.07	0.30	0.40	0.47	0.50	0.50	0.50	0.50
4.64	0.00	0.03	0.07	0.30	0.40	0.47	0.50	0.50	0.50	0.50
4.69	0.00	0.03	0.07	0.29	0.40	0.47	0.50	0.50	0.50	0.50
4.74	0.00	0.03	0.07	0.29	0.40	0.46	0.50	0.50	0.50	0.50
4.79	0.00	0.03	0.07	0.29	0.40	0.46	0.50	0.50	0.50	0.50
4.84	0.00	0.03	0.07	0.29	0.40	0.46	0.49	0.49	0.49	0.49
4.89	0.00	0.03	0.08	0.29	0.40	0.46	0.49	0.49	0.49	0.49
4.94	0.00	0.03	0.08	0.29	0.39	0.46	0.49	0.49	0.49	0.49
4.99	0.00	0.03	0.08	0.29	0.39	0.46	0.49	0.49	0.49	0.49
5.04	0.00	0.03	0.08	0.29	0.39	0.45	0.49	0.49	0.49	0.49
5.09	0.00	0.03	0.08	0.29	0.39	0.45	0.48	0.49	0.49	0.49
5.14	0.00	0.03	0.08	0.29	0.39	0.45	0.48	0.48	0.48	0.48
5.19	0.00	0.03	0.08	0.29	0.39	0.45	0.48	0.48	0.48	0.48
5.24	0.00	0.03	0.08	0.29	0.39	0.45	0.48	0.48	0.48	0.48
5.29	0.00	0.03	0.08	0.29	0.39	0.45	0.48	0.48	0.48	0.48
5.34	0.00	0.03	0.08	0.29	0.38	0.44	0.47	0.48	0.48	0.48
5.39	0.00	0.03	0.08	0.29	0.38	0.44	0.47	0.47	0.47	0.47
5.44	0.00	0.03	0.08	0.29	0.38	0.44	0.47	0.47	0.47	0.47
5.49	0.00	0.03	0.08	0.28	0.38	0.44	0.47	0.47	0.47	0.47
5.54	0.00	0.03	0.08	0.28	0.38	0.44	0.47	0.47	0.47	0.47
5.59	0.00	0.03	0.08	0.28	0.38	0.43	0.46	0.47	0.47	0.47
5.64	0.00	0.04	0.08	0.28	0.38	0.43	0.46	0.46	0.46	0.46
5.69	0.00	0.04	0.08	0.28	0.37	0.43	0.46	0.46	0.46	0.46
5.74	0.00	0.04	0.08	0.28	0.37	0.43	0.46	0.46	0.46	0.46
5.79	0.00	0.04	0.08	0.28	0.37	0.43	0.46	0.46	0.46	0.46
5.84	0.00	0.04	0.08	0.28	0.37	0.43	0.45	0.46	0.46	0.46
5.89	0.00	0.04	0.08	0.28	0.37	0.42	0.45	0.45	0.45	0.45
5.94	0.00	0.04	0.08	0.28	0.37	0.42	0.45	0.45	0.45	0.45
5.99	0.00	0.04	0.08	0.28	0.37	0.42	0.45	0.45	0.45	0.45
6.04	0.00	0.04	0.08	0.28	0.36	0.42	0.45	0.45	0.45	0.45
6.09	0.00	0.04	0.08	0.27	0.36	0.42	0.44	0.45	0.45	0.45
6.14	0.00	0.04	0.08	0.27	0.36	0.41	0.44	0.44	0.44	0.44
6.19	0.00	0.04	0.08	0.27	0.36	0.41	0.44	0.44	0.44	0.44
6.24	0.00	0.04	0.08	0.27	0.36	0.41	0.44	0.44	0.44	0.44
6.29	0.00	0.04	0.08	0.27	0.36	0.41	0.44	0.44	0.44	0.44
6.34	0.00	0.04	0.08	0.27	0.36	0.41	0.43	0.44	0.44	0.44

6.39	0.00	0.04	0.08	0.27	0.35	0.41	0.43	0.43	0.43	0.43
6.44	0.00	0.04	0.08	0.27	0.35	0.40	0.43	0.43	0.43	0.43
6.49	0.00	0.04	0.08	0.27	0.35	0.40	0.43	0.43	0.43	0.43
6.54	0.00	0.04	0.08	0.27	0.35	0.40	0.43	0.43	0.43	0.43
6.59	0.00	0.04	0.08	0.27	0.35	0.40	0.42	0.43	0.43	0.43
6.64	0.00	0.04	0.08	0.27	0.35	0.40	0.42	0.42	0.42	0.42
6.69	0.00	0.04	0.08	0.26	0.35	0.40	0.42	0.42	0.42	0.42
6.74	0.00	0.04	0.08	0.26	0.34	0.39	0.42	0.42	0.42	0.42
6.79	0.00	0.04	0.08	0.26	0.34	0.39	0.42	0.42	0.42	0.42
6.84	0.00	0.04	0.08	0.26	0.34	0.39	0.42	0.42	0.42	0.42
6.89	0.00	0.04	0.08	0.26	0.34	0.39	0.41	0.42	0.42	0.42
6.94	0.00	0.04	0.08	0.26	0.34	0.39	0.41	0.41	0.41	0.41
6.99	0.00	0.04	0.08	0.26	0.34	0.39	0.41	0.41	0.41	0.41
7.04	0.00	0.04	0.08	0.26	0.34	0.38	0.41	0.41	0.41	0.41
7.09	0.00	0.04	0.08	0.26	0.34	0.38	0.41	0.41	0.41	0.41
7.14	0.00	0.04	0.08	0.26	0.33	0.38	0.41	0.41	0.41	0.41
7.19	0.00	0.04	0.08	0.26	0.33	0.38	0.40	0.40	0.40	0.40
7.24	0.00	0.04	0.08	0.25	0.33	0.38	0.40	0.40	0.40	0.40
7.29	0.00	0.04	0.08	0.25	0.33	0.38	0.40	0.40	0.40	0.40
7.34	0.00	0.04	0.08	0.25	0.33	0.37	0.40	0.40	0.40	0.40
7.39	0.00	0.04	0.08	0.25	0.33	0.37	0.40	0.40	0.40	0.40
7.44	0.00	0.04	0.08	0.25	0.33	0.37	0.40	0.40	0.40	0.40
7.49	0.00	0.04	0.08	0.25	0.33	0.37	0.39	0.39	0.39	0.39
7.54	0.00	0.04	0.08	0.25	0.32	0.37	0.39	0.39	0.39	0.39
7.59	0.00	0.04	0.08	0.25	0.32	0.37	0.39	0.39	0.39	0.39
7.64	0.00	0.04	0.08	0.25	0.32	0.37	0.39	0.39	0.39	0.39
7.69	0.00	0.04	0.08	0.25	0.32	0.36	0.39	0.39	0.39	0.39
7.74	0.00	0.04	0.08	0.25	0.32	0.36	0.39	0.39	0.39	0.39
7.79	0.00	0.04	0.08	0.25	0.32	0.36	0.38	0.38	0.38	0.38
7.84	0.00	0.04	0.08	0.24	0.32	0.36	0.38	0.38	0.38	0.38
7.89	0.00	0.04	0.08	0.24	0.32	0.36	0.38	0.38	0.38	0.38
7.94	0.00	0.04	0.08	0.24	0.31	0.36	0.38	0.38	0.38	0.38
7.99	0.00	0.04	0.08	0.24	0.31	0.36	0.38	0.38	0.38	0.38
8.04	0.00	0.04	0.08	0.24	0.31	0.35	0.38	0.38	0.38	0.38
8.09	0.00	0.04	0.08	0.24	0.31	0.35	0.37	0.38	0.38	0.38
8.14	0.00	0.04	0.08	0.24	0.31	0.35	0.37	0.37	0.37	0.37
8.19	0.00	0.04	0.08	0.24	0.31	0.35	0.37	0.37	0.37	0.37
8.24	0.00	0.04	0.08	0.24	0.31	0.35	0.37	0.37	0.37	0.37
8.29	0.00	0.04	0.08	0.24	0.31	0.35	0.37	0.37	0.37	0.37
8.34	0.00	0.04	0.08	0.24	0.30	0.35	0.37	0.37	0.37	0.37
8.39	0.00	0.04	0.08	0.24	0.30	0.34	0.37	0.37	0.37	0.37
8.44	0.00	0.04	0.08	0.23	0.30	0.34	0.36	0.36	0.36	0.36
8.49	0.00	0.04	0.08	0.23	0.30	0.34	0.36	0.36	0.36	0.36
8.54	0.00	0.04	0.08	0.23	0.30	0.34	0.36	0.36	0.36	0.36
8.59	0.00	0.04	0.08	0.23	0.30	0.34	0.36	0.36	0.36	0.36
8.64	0.00	0.04	0.08	0.23	0.30	0.34	0.36	0.36	0.36	0.36
8.69	0.01	0.04	0.08	0.23	0.30	0.34	0.36	0.36	0.36	0.36
8.74	0.01	0.04	0.08	0.23	0.30	0.33	0.36	0.36	0.36	0.36

8.79	0.01	0.04	0.08	0.23	0.29	0.33	0.35	0.35	0.35	0.35
8.84	0.01	0.04	0.08	0.23	0.29	0.33	0.35	0.35	0.35	0.35
8.89	0.01	0.04	0.08	0.23	0.29	0.33	0.35	0.35	0.35	0.35
8.94	0.01	0.04	0.08	0.23	0.29	0.33	0.35	0.35	0.35	0.35
8.99	0.01	0.04	0.08	0.23	0.29	0.33	0.35	0.35	0.35	0.35
9.04	0.01	0.04	0.08	0.23	0.29	0.33	0.35	0.35	0.35	0.35
9.09	0.01	0.04	0.08	0.22	0.29	0.33	0.35	0.35	0.35	0.35
9.14	0.01	0.04	0.08	0.22	0.29	0.32	0.34	0.35	0.35	0.35
9.19	0.01	0.04	0.08	0.22	0.29	0.32	0.34	0.34	0.34	0.34
9.24	0.01	0.04	0.08	0.22	0.28	0.32	0.34	0.34	0.34	0.34
9.29	0.01	0.04	0.08	0.22	0.28	0.32	0.34	0.34	0.34	0.34
9.34	0.01	0.04	0.08	0.22	0.28	0.32	0.34	0.34	0.34	0.34
9.39	0.01	0.04	0.08	0.22	0.28	0.32	0.34	0.34	0.34	0.34
9.44	0.01	0.04	0.08	0.22	0.28	0.32	0.34	0.34	0.34	0.34
9.49	0.01	0.04	0.08	0.22	0.28	0.32	0.34	0.34	0.34	0.34
9.54	0.01	0.04	0.08	0.22	0.28	0.32	0.33	0.33	0.33	0.33
9.59	0.01	0.04	0.08	0.22	0.28	0.31	0.33	0.33	0.33	0.33
9.64	0.01	0.04	0.08	0.22	0.28	0.31	0.33	0.33	0.33	0.33
9.69	0.01	0.04	0.08	0.22	0.28	0.31	0.33	0.33	0.33	0.33
9.74	0.01	0.04	0.08	0.22	0.27	0.31	0.33	0.33	0.33	0.33
9.79	0.01	0.04	0.08	0.21	0.27	0.31	0.33	0.33	0.33	0.33
9.84	0.01	0.04	0.08	0.21	0.27	0.31	0.33	0.33	0.33	0.33
9.89	0.01	0.04	0.08	0.21	0.27	0.31	0.33	0.33	0.33	0.33
9.94	0.01	0.04	0.08	0.21	0.27	0.31	0.32	0.33	0.33	0.33
9.99	0.01	0.04	0.08	0.21	0.27	0.31	0.32	0.32	0.32	0.32

Table A5 – Dimensionless celerity vs. discharge (Figure 4.5)

λ= (m)	1	10	100	500	1000	5000	10000
Q_0 (cms)				c^*			
20	1.359	1.360	1.376	1.494	1.572	1.659	1.665
21	1.360	1.360	1.375	1.490	1.569	1.659	1.665
22	1.360	1.360	1.374	1.486	1.566	1.659	1.665
23	1.360	1.360	1.374	1.483	1.562	1.658	1.664
24	1.360	1.360	1.373	1.480	1.559	1.658	1.664
25	1.360	1.360	1.373	1.478	1.557	1.657	1.664
26	1.360	1.361	1.372	1.475	1.554	1.657	1.664
27	1.361	1.361	1.372	1.472	1.551	1.656	1.664
28	1.361	1.361	1.372	1.470	1.549	1.656	1.664
29	1.361	1.361	1.372	1.468	1.546	1.655	1.664
30	1.362	1.362	1.372	1.466	1.544	1.655	1.664
31	1.362	1.362	1.372	1.464	1.542	1.654	1.663
32	1.362	1.363	1.372	1.462	1.539	1.654	1.663
33	1.363	1.363	1.372	1.460	1.537	1.654	1.663
34	1.363	1.363	1.372	1.458	1.535	1.653	1.663

35	1.364	1.364	1.372	1.457	1.533	1.653	1.663
36	1.364	1.364	1.372	1.455	1.532	1.652	1.663
37	1.364	1.365	1.372	1.454	1.530	1.652	1.663
38	1.365	1.365	1.372	1.453	1.528	1.651	1.663
39	1.365	1.365	1.372	1.451	1.526	1.651	1.662
40	1.366	1.366	1.373	1.450	1.525	1.651	1.662
41	1.366	1.366	1.373	1.449	1.523	1.650	1.662
42	1.367	1.367	1.373	1.448	1.522	1.650	1.662
43	1.367	1.367	1.373	1.447	1.520	1.649	1.662
44	1.368	1.368	1.374	1.446	1.519	1.649	1.662
45	1.368	1.368	1.374	1.445	1.517	1.648	1.662
46	1.369	1.369	1.374	1.444	1.516	1.648	1.662
47	1.369	1.369	1.375	1.443	1.515	1.648	1.661
48	1.370	1.370	1.375	1.442	1.514	1.647	1.661
49	1.370	1.370	1.375	1.442	1.512	1.647	1.661
50	1.371	1.371	1.376	1.441	1.511	1.647	1.661
51	1.371	1.371	1.376	1.440	1.510	1.646	1.661
52	1.372	1.372	1.376	1.440	1.509	1.646	1.661
53	1.372	1.372	1.377	1.439	1.508	1.645	1.661
54	1.373	1.373	1.377	1.438	1.507	1.645	1.661
55	1.373	1.373	1.378	1.438	1.506	1.645	1.661
56	1.374	1.374	1.378	1.437	1.505	1.644	1.660
57	1.374	1.374	1.378	1.437	1.504	1.644	1.660
58	1.375	1.375	1.379	1.436	1.503	1.644	1.660
59	1.375	1.375	1.379	1.436	1.503	1.643	1.660
60	1.376	1.376	1.380	1.436	1.502	1.643	1.660
61	1.376	1.376	1.380	1.435	1.501	1.643	1.660
62	1.377	1.377	1.381	1.435	1.500	1.642	1.660
63	1.377	1.377	1.381	1.434	1.499	1.642	1.660
64	1.378	1.378	1.382	1.434	1.499	1.642	1.660
65	1.378	1.379	1.382	1.434	1.498	1.641	1.659
66	1.379	1.379	1.382	1.434	1.497	1.641	1.659
67	1.380	1.380	1.383	1.433	1.497	1.641	1.659
68	1.380	1.380	1.383	1.433	1.496	1.640	1.659
69	1.381	1.381	1.384	1.433	1.495	1.640	1.659
70	1.381	1.381	1.384	1.433	1.495	1.640	1.659
71	1.382	1.382	1.385	1.432	1.494	1.639	1.659
72	1.382	1.382	1.385	1.432	1.494	1.639	1.659
73	1.383	1.383	1.386	1.432	1.493	1.639	1.659
74	1.383	1.383	1.386	1.432	1.493	1.638	1.659
75	1.384	1.384	1.387	1.432	1.492	1.638	1.658
76	1.384	1.384	1.387	1.432	1.492	1.638	1.658
77	1.385	1.385	1.388	1.432	1.491	1.637	1.658
78	1.385	1.386	1.388	1.432	1.491	1.637	1.658

79	1.386	1.386	1.389	1.432	1.490	1.637	1.658
80	1.387	1.387	1.389	1.431	1.490	1.637	1.658
81	1.387	1.387	1.390	1.431	1.489	1.636	1.658
82	1.388	1.388	1.390	1.431	1.489	1.636	1.658
83	1.388	1.388	1.391	1.431	1.489	1.636	1.658
84	1.389	1.389	1.391	1.431	1.488	1.636	1.658
85	1.389	1.389	1.392	1.431	1.488	1.635	1.657
86	1.390	1.390	1.392	1.431	1.487	1.635	1.657
87	1.390	1.390	1.393	1.431	1.487	1.635	1.657
88	1.391	1.391	1.393	1.431	1.487	1.635	1.657
89	1.391	1.391	1.394	1.432	1.487	1.634	1.657
90	1.392	1.392	1.394	1.432	1.486	1.634	1.657
91	1.393	1.393	1.395	1.432	1.486	1.634	1.657
92	1.393	1.393	1.395	1.432	1.486	1.634	1.657
93	1.394	1.394	1.396	1.432	1.485	1.633	1.657
94	1.394	1.394	1.396	1.432	1.485	1.633	1.657
95	1.395	1.395	1.397	1.432	1.485	1.633	1.657
96	1.395	1.395	1.397	1.432	1.485	1.633	1.657
97	1.396	1.396	1.398	1.432	1.484	1.632	1.656
98	1.396	1.396	1.398	1.432	1.484	1.632	1.656
99	1.397	1.397	1.399	1.432	1.484	1.632	1.656
100	1.397	1.397	1.399	1.433	1.484	1.632	1.656

Table A6 – Celerity vs. discharge (Figure 4.6)

λ= (m)	1	10	100	500	1000	5000	10000
Q_0 (cms)				c (m/s)			
20	9.843	9.845	9.961	10.814	11.383	12.015	12.054
21	10.004	10.005	10.116	10.963	11.543	12.207	12.249
22	10.159	10.160	10.267	11.106	11.697	12.392	12.437
23	10.309	10.310	10.413	11.245	11.844	12.569	12.618
24	10.454	10.455	10.554	11.378	11.986	12.741	12.792
25	10.594	10.595	10.691	11.508	12.123	12.907	12.961
26	10.731	10.732	10.824	11.633	12.256	13.067	13.125
27	10.863	10.864	10.953	11.754	12.383	13.222	13.283
28	10.992	10.993	11.079	11.872	12.507	13.372	13.437
29	11.117	11.118	11.202	11.987	12.627	13.518	13.586
30	11.240	11.241	11.322	12.098	12.743	13.659	13.731
31	11.359	11.360	11.438	12.207	12.856	13.797	13.872
32	11.475	11.476	11.552	12.313	12.966	13.930	14.009
33	11.588	11.589	11.663	12.416	13.073	14.060	14.142
34	11.699	11.700	11.772	12.517	13.176	14.187	14.272
35	11.807	11.808	11.878	12.615	13.278	14.310	14.399
36	11.913	11.914	11.982	12.711	13.376	14.431	14.523
37	12.017	12.018	12.084	12.805	13.473	14.548	14.643

38	12.119	12.119	12.184	12.897	13.567	14.662	14.761
39	12.218	12.219	12.282	12.987	13.659	14.774	14.877
40	12.316	12.316	12.377	13.076	13.749	14.883	14.989
41	12.411	12.412	12.471	13.162	13.837	14.990	15.099
42	12.505	12.505	12.564	13.247	13.923	15.094	15.207
43	12.597	12.597	12.654	13.330	14.007	15.196	15.313
44	12.687	12.688	12.743	13.412	14.089	15.296	15.416
45	12.776	12.777	12.831	13.493	14.170	15.394	15.517
46	12.863	12.864	12.917	13.571	14.249	15.489	15.616
47	12.949	12.949	13.001	13.649	14.327	15.583	15.714
48	13.033	13.034	13.084	13.725	14.404	15.675	15.809
49	13.116	13.116	13.166	13.800	14.478	15.765	15.903
50	13.197	13.198	13.247	13.874	14.552	15.854	15.994
51	13.278	13.278	13.326	13.946	14.624	15.941	16.084
52	13.357	13.357	13.404	14.018	14.695	16.026	16.173
53	13.434	13.435	13.480	14.088	14.765	16.109	16.260
54	13.511	13.511	13.556	14.157	14.834	16.191	16.345
55	13.586	13.587	13.631	14.226	14.901	16.272	16.429
56	13.661	13.661	13.704	14.293	14.968	16.351	16.512
57	13.734	13.734	13.777	14.359	15.033	16.429	16.593
58	13.806	13.807	13.848	14.425	15.098	16.506	16.673
59	13.877	13.878	13.918	14.489	15.161	16.581	16.751
60	13.948	13.948	13.988	14.553	15.224	16.655	16.828
61	14.017	14.017	14.056	14.616	15.285	16.728	16.904
62	14.085	14.086	14.124	14.678	15.346	16.799	16.979
63	14.153	14.153	14.191	14.739	15.406	16.870	17.053
64	14.219	14.220	14.257	14.799	15.465	16.939	17.125
65	14.285	14.285	14.322	14.859	15.523	17.007	17.197
66	14.350	14.350	14.386	14.918	15.580	17.075	17.267
67	14.414	14.414	14.450	14.976	15.637	17.141	17.336
68	14.477	14.478	14.512	15.033	15.693	17.206	17.405
69	14.540	14.540	14.574	15.090	15.748	17.270	17.472
70	14.602	14.602	14.636	15.146	15.803	17.334	17.538
71	14.663	14.663	14.696	15.202	15.856	17.396	17.604
72	14.723	14.724	14.756	15.257	15.910	17.458	17.668
73	14.783	14.783	14.815	15.311	15.962	17.519	17.732
74	14.842	14.842	14.874	15.364	16.014	17.578	17.795
75	14.900	14.901	14.932	15.418	16.065	17.637	17.856
76	14.958	14.958	14.989	15.470	16.116	17.696	17.918
77	15.015	15.016	15.045	15.522	16.166	17.753	17.978
78	15.072	15.072	15.101	15.573	16.215	17.810	18.037
79	15.128	15.128	15.157	15.624	16.264	17.866	18.096
80	15.183	15.183	15.212	15.675	16.312	17.921	18.154
81	15.238	15.238	15.266	15.725	16.360	17.975	18.211
82	15.292	15.292	15.320	15.774	16.408	18.029	18.268

83	15.345	15.346	15.373	15.823	16.454	18.082	18.324
84	15.398	15.399	15.426	15.871	16.501	18.135	18.379
85	15.451	15.451	15.478	15.919	16.547	18.187	18.433
86	15.503	15.503	15.529	15.967	16.592	18.238	18.487
87	15.554	15.555	15.580	16.014	16.637	18.288	18.540
88	15.605	15.606	15.631	16.060	16.681	18.338	18.593
89	15.656	15.656	15.681	16.106	16.725	18.388	18.645
90	15.706	15.706	15.731	16.152	16.769	18.436	18.696
91	15.755	15.756	15.780	16.198	16.812	18.485	18.747
92	15.805	15.805	15.829	16.242	16.855	18.532	18.797
93	15.853	15.853	15.877	16.287	16.897	18.579	18.846
94	15.901	15.902	15.925	16.331	16.939	18.626	18.895
95	15.949	15.949	15.973	16.375	16.980	18.672	18.944
96	15.997	15.997	16.020	16.418	17.021	18.717	18.992
97	16.043	16.044	16.066	16.461	17.062	18.762	19.039
98	16.090	16.090	16.113	16.504	17.103	18.807	19.086
99	16.136	16.136	16.158	16.546	17.143	18.851	19.132
100	16.182	16.182	16.204	16.588	17.182	18.895	19.178

Table A7 – Attenuation factor vs. discharge (Figure 4.7)

λ= (m)	1	10	100	500	1000	5000	10000
Q_0 (cms)				δ^*			
20	0.003	0.029	0.263	0.550	0.491	0.155	0.079
21	0.003	0.028	0.256	0.549	0.497	0.159	0.082
22	0.003	0.028	0.250	0.547	0.502	0.164	0.084
23	0.003	0.027	0.244	0.546	0.506	0.168	0.087
24	0.003	0.026	0.238	0.544	0.510	0.173	0.089
25	0.003	0.025	0.232	0.542	0.514	0.177	0.091
26	0.002	0.025	0.227	0.540	0.517	0.181	0.093
27	0.002	0.024	0.222	0.537	0.520	0.185	0.096
28	0.002	0.023	0.217	0.535	0.522	0.188	0.098
29	0.002	0.023	0.213	0.532	0.525	0.192	0.100
30	0.002	0.022	0.208	0.530	0.526	0.196	0.102
31	0.002	0.022	0.204	0.527	0.528	0.199	0.104
32	0.002	0.021	0.200	0.524	0.530	0.203	0.106
33	0.002	0.021	0.196	0.521	0.531	0.206	0.108
34	0.002	0.020	0.193	0.518	0.532	0.209	0.109
35	0.002	0.020	0.189	0.516	0.533	0.212	0.111
36	0.002	0.020	0.186	0.513	0.534	0.215	0.113
37	0.002	0.019	0.182	0.510	0.534	0.218	0.115
38	0.002	0.019	0.179	0.507	0.535	0.221	0.116
39	0.002	0.018	0.176	0.503	0.535	0.224	0.118
40	0.002	0.018	0.173	0.500	0.535	0.227	0.120

41	0.002	0.018	0.171	0.497	0.535	0.229	0.121
42	0.002	0.018	0.168	0.494	0.535	0.232	0.123
43	0.002	0.017	0.165	0.491	0.535	0.234	0.124
44	0.002	0.017	0.163	0.488	0.535	0.237	0.126
45	0.002	0.017	0.160	0.485	0.534	0.239	0.127
46	0.002	0.016	0.158	0.482	0.534	0.242	0.129
47	0.002	0.016	0.155	0.479	0.534	0.244	0.130
48	0.002	0.016	0.153	0.476	0.533	0.246	0.131
49	0.002	0.016	0.151	0.473	0.532	0.248	0.133
50	0.002	0.015	0.149	0.470	0.532	0.250	0.134
51	0.002	0.015	0.147	0.467	0.531	0.253	0.135
52	0.001	0.015	0.145	0.464	0.530	0.255	0.137
53	0.001	0.015	0.143	0.461	0.530	0.256	0.138
54	0.001	0.015	0.141	0.458	0.529	0.258	0.139
55	0.001	0.014	0.139	0.455	0.528	0.260	0.140
56	0.001	0.014	0.137	0.453	0.527	0.262	0.141
57	0.001	0.014	0.136	0.450	0.526	0.264	0.143
58	0.001	0.014	0.134	0.447	0.525	0.266	0.144
59	0.001	0.014	0.132	0.444	0.524	0.267	0.145
60	0.001	0.013	0.131	0.441	0.523	0.269	0.146
61	0.001	0.013	0.129	0.438	0.521	0.271	0.147
62	0.001	0.013	0.128	0.436	0.520	0.272	0.148
63	0.001	0.013	0.126	0.433	0.519	0.274	0.149
64	0.001	0.013	0.125	0.430	0.518	0.275	0.150
65	0.001	0.013	0.123	0.427	0.517	0.277	0.151
66	0.001	0.012	0.122	0.425	0.515	0.278	0.152
67	0.001	0.012	0.120	0.422	0.514	0.279	0.153
68	0.001	0.012	0.119	0.419	0.513	0.281	0.154
69	0.001	0.012	0.118	0.417	0.511	0.282	0.155
70	0.001	0.012	0.116	0.414	0.510	0.283	0.156
71	0.001	0.012	0.115	0.412	0.509	0.285	0.157
72	0.001	0.012	0.114	0.409	0.507	0.286	0.157
73	0.001	0.012	0.113	0.407	0.506	0.287	0.158
74	0.001	0.011	0.112	0.404	0.505	0.288	0.159
75	0.001	0.011	0.110	0.402	0.503	0.289	0.160
76	0.001	0.011	0.109	0.399	0.502	0.291	0.161
77	0.001	0.011	0.108	0.397	0.500	0.292	0.162
78	0.001	0.011	0.107	0.394	0.499	0.293	0.162
79	0.001	0.011	0.106	0.392	0.497	0.294	0.163
80	0.001	0.011	0.105	0.389	0.496	0.295	0.164
81	0.001	0.011	0.104	0.387	0.495	0.296	0.165
82	0.001	0.010	0.103	0.385	0.493	0.297	0.165
83	0.001	0.010	0.102	0.382	0.492	0.298	0.166
84	0.001	0.010	0.101	0.380	0.490	0.299	0.167
85	0.001	0.010	0.100	0.378	0.489	0.299	0.167

86	0.001	0.010	0.099	0.375	0.487	0.300	0.168
87	0.001	0.010	0.098	0.373	0.486	0.301	0.169
88	0.001	0.010	0.097	0.371	0.484	0.302	0.169
89	0.001	0.010	0.096	0.369	0.483	0.303	0.170
90	0.001	0.010	0.095	0.367	0.481	0.304	0.171
91	0.001	0.010	0.095	0.364	0.480	0.304	0.171
92	0.001	0.010	0.094	0.362	0.478	0.305	0.172
93	0.001	0.009	0.093	0.360	0.477	0.306	0.172
94	0.001	0.009	0.092	0.358	0.475	0.307	0.173
95	0.001	0.009	0.091	0.356	0.473	0.307	0.174
96	0.001	0.009	0.091	0.354	0.472	0.308	0.174
97	0.001	0.009	0.090	0.352	0.470	0.308	0.175
98	0.001	0.009	0.089	0.350	0.469	0.309	0.175
99	0.001	0.009	0.088	0.348	0.467	0.310	0.176
100	0.001	0.009	0.088	0.346	0.466	0.310	0.176

Table A8 – Normalized amplification factor vs. discharge (Figure 4.8)

λ= (m)	1	10	100	500	1000	5000	10000
Q_0 (cms)	δ`						
20	0.510	0.510	0.457	0.191	0.085	0.005	0.001
21	0.510	0.510	0.460	0.197	0.089	0.006	0.001
22	0.510	0.510	0.462	0.203	0.093	0.006	0.002
23	0.510	0.510	0.465	0.208	0.097	0.006	0.002
24	0.510	0.510	0.467	0.213	0.100	0.007	0.002
25	0.510	0.509	0.469	0.219	0.104	0.007	0.002
26	0.510	0.509	0.470	0.224	0.107	0.007	0.002
27	0.510	0.509	0.472	0.228	0.110	0.008	0.002
28	0.509	0.509	0.473	0.233	0.114	0.008	0.002
29	0.509	0.509	0.475	0.238	0.117	0.009	0.002
30	0.509	0.509	0.476	0.242	0.120	0.009	0.002
31	0.509	0.508	0.477	0.246	0.123	0.009	0.002
32	0.509	0.508	0.478	0.250	0.126	0.010	0.003
33	0.508	0.508	0.479	0.254	0.129	0.010	0.003
34	0.508	0.508	0.480	0.258	0.132	0.010	0.003
35	0.508	0.507	0.480	0.262	0.135	0.011	0.003
36	0.507	0.507	0.481	0.265	0.138	0.011	0.003
37	0.507	0.507	0.482	0.269	0.141	0.012	0.003
38	0.507	0.507	0.482	0.272	0.144	0.012	0.003
39	0.507	0.506	0.483	0.276	0.146	0.012	0.003
40	0.506	0.506	0.483	0.279	0.149	0.013	0.003
41	0.506	0.506	0.484	0.282	0.152	0.013	0.003
42	0.506	0.505	0.484	0.285	0.154	0.013	0.004
43	0.505	0.505	0.484	0.288	0.157	0.014	0.004

44	0.505	0.505	0.485	0.291	0.159	0.014	0.004
45	0.505	0.504	0.485	0.294	0.162	0.014	0.004
46	0.504	0.504	0.485	0.297	0.164	0.015	0.004
47	0.504	0.504	0.485	0.299	0.167	0.015	0.004
48	0.504	0.503	0.486	0.302	0.169	0.016	0.004
49	0.503	0.503	0.486	0.304	0.171	0.016	0.004
50	0.503	0.503	0.486	0.307	0.174	0.016	0.004
51	0.503	0.502	0.486	0.309	0.176	0.017	0.004
52	0.502	0.502	0.486	0.311	0.178	0.017	0.005
53	0.502	0.502	0.486	0.314	0.180	0.017	0.005
54	0.502	0.501	0.486	0.316	0.182	0.018	0.005
55	0.501	0.501	0.486	0.318	0.184	0.018	0.005
56	0.501	0.501	0.486	0.320	0.186	0.019	0.005
57	0.500	0.500	0.486	0.322	0.188	0.019	0.005
58	0.500	0.500	0.486	0.324	0.190	0.019	0.005
59	0.500	0.499	0.486	0.326	0.192	0.020	0.005
60	0.499	0.499	0.486	0.328	0.194	0.020	0.005
61	0.499	0.499	0.486	0.330	0.196	0.020	0.006
62	0.498	0.498	0.486	0.332	0.198	0.021	0.006
63	0.498	0.498	0.485	0.334	0.200	0.021	0.006
64	0.498	0.497	0.485	0.335	0.202	0.021	0.006
65	0.497	0.497	0.485	0.337	0.204	0.022	0.006
66	0.497	0.497	0.485	0.339	0.205	0.022	0.006
67	0.496	0.496	0.485	0.340	0.207	0.023	0.006
68	0.496	0.496	0.485	0.342	0.209	0.023	0.006
69	0.495	0.495	0.485	0.343	0.211	0.023	0.006
70	0.495	0.495	0.484	0.345	0.212	0.024	0.006
71	0.495	0.495	0.484	0.346	0.214	0.024	0.007
72	0.494	0.494	0.484	0.347	0.215	0.024	0.007
73	0.494	0.494	0.484	0.349	0.217	0.025	0.007
74	0.493	0.493	0.483	0.350	0.219	0.025	0.007
75	0.493	0.493	0.483	0.351	0.220	0.025	0.007
76	0.492	0.492	0.483	0.353	0.222	0.026	0.007
77	0.492	0.492	0.483	0.354	0.223	0.026	0.007
78	0.492	0.491	0.482	0.355	0.225	0.026	0.007
79	0.491	0.491	0.482	0.356	0.226	0.027	0.007
80	0.491	0.491	0.482	0.357	0.228	0.027	0.008
81	0.490	0.490	0.482	0.359	0.229	0.027	0.008
82	0.490	0.490	0.481	0.360	0.231	0.028	0.008
83	0.489	0.489	0.481	0.361	0.232	0.028	0.008
84	0.489	0.489	0.481	0.362	0.233	0.028	0.008
85	0.488	0.488	0.480	0.363	0.235	0.029	0.008
86	0.488	0.488	0.480	0.364	0.236	0.029	0.008
87	0.487	0.487	0.480	0.365	0.237	0.029	0.008
88	0.487	0.487	0.479	0.366	0.239	0.030	0.008
89	0.486	0.486	0.479	0.367	0.240	0.030	0.008
90	0.486	0.486	0.479	0.367	0.241	0.030	0.009

91	0.486	0.485	0.478	0.368	0.242	0.031	0.009
92	0.485	0.485	0.478	0.369	0.244	0.031	0.009
93	0.485	0.484	0.477	0.370	0.245	0.031	0.009
94	0.484	0.484	0.477	0.371	0.246	0.032	0.009
95	0.484	0.484	0.477	0.371	0.247	0.032	0.009
96	0.483	0.483	0.476	0.372	0.248	0.032	0.009
97	0.483	0.483	0.476	0.373	0.249	0.033	0.009
98	0.482	0.482	0.476	0.374	0.251	0.033	0.009
99	0.482	0.482	0.475	0.374	0.252	0.033	0.009
100	0.481	0.481	0.475	0.375	0.253	0.034	0.010

Table A9 – Amplitude increase in percent vs. discharge (Figure 4.9)

λ= (m)	1	10	100	500	1000	5000	10000
Q_0 (cms)	% Increase over $2\pi L_0$						
20	66.6%	66.5%	58.0%	21.0%	8.9%	0.54%	0.14%
21	66.6%	66.5%	58.4%	21.7%	9.3%	0.57%	0.15%
22	66.6%	66.5%	58.8%	22.4%	9.7%	0.61%	0.16%
23	66.6%	66.5%	59.2%	23.1%	10.1%	0.64%	0.17%
24	66.5%	66.5%	59.5%	23.8%	10.5%	0.68%	0.17%
25	66.5%	66.4%	59.8%	24.4%	10.9%	0.72%	0.18%
26	66.5%	66.4%	60.1%	25.1%	11.3%	0.75%	0.19%
27	66.5%	66.4%	60.3%	25.7%	11.7%	0.79%	0.20%
28	66.4%	66.4%	60.5%	26.2%	12.0%	0.82%	0.21%
29	66.4%	66.3%	60.7%	26.8%	12.4%	0.86%	0.22%
30	66.4%	66.3%	60.9%	27.4%	12.8%	0.90%	0.23%
31	66.3%	66.3%	61.1%	27.9%	13.1%	0.94%	0.24%
32	66.3%	66.2%	61.3%	28.4%	13.5%	0.97%	0.25%
33	66.2%	66.2%	61.4%	29.0%	13.8%	1.01%	0.26%
34	66.2%	66.1%	61.5%	29.4%	14.2%	1.05%	0.27%
35	66.2%	66.1%	61.7%	29.9%	14.5%	1.08%	0.28%
36	66.1%	66.1%	61.8%	30.4%	14.8%	1.12%	0.29%
37	66.1%	66.0%	61.9%	30.9%	15.1%	1.16%	0.30%
38	66.0%	66.0%	62.0%	31.3%	15.5%	1.20%	0.31%
39	66.0%	65.9%	62.1%	31.7%	15.8%	1.23%	0.32%
40	65.9%	65.9%	62.1%	32.2%	16.1%	1.27%	0.33%
41	65.9%	65.8%	62.2%	32.6%	16.4%	1.31%	0.34%
42	65.8%	65.8%	62.3%	33.0%	16.7%	1.35%	0.35%
43	65.8%	65.7%	62.3%	33.4%	17.0%	1.38%	0.37%
44	65.7%	65.7%	62.4%	33.8%	17.3%	1.42%	0.38%
45	65.7%	65.6%	62.4%	34.2%	17.6%	1.46%	0.39%
46	65.6%	65.6%	62.4%	34.5%	17.9%	1.50%	0.40%
47	65.5%	65.5%	62.5%	34.9%	18.1%	1.54%	0.41%
48	65.5%	65.4%	62.5%	35.2%	18.4%	1.57%	0.42%

49	65.4%	65.4%	62.5%	35.6%	18.7%	1.61%	0.43%
50	65.4%	65.3%	62.5%	35.9%	18.9%	1.65%	0.44%
51	65.3%	65.3%	62.6%	36.2%	19.2%	1.69%	0.45%
52	65.2%	65.2%	62.6%	36.5%	19.5%	1.72%	0.46%
53	65.2%	65.2%	62.6%	36.9%	19.7%	1.76%	0.47%
54	65.1%	65.1%	62.6%	37.2%	20.0%	1.80%	0.48%
55	65.1%	65.0%	62.6%	37.5%	20.2%	1.83%	0.49%
56	65.0%	65.0%	62.6%	37.7%	20.5%	1.87%	0.50%
57	64.9%	64.9%	62.6%	38.0%	20.7%	1.91%	0.51%
58	64.9%	64.8%	62.6%	38.3%	21.0%	1.95%	0.52%
59	64.8%	64.8%	62.6%	38.6%	21.2%	1.98%	0.53%
60	64.7%	64.7%	62.6%	38.8%	21.4%	2.02%	0.54%
61	64.7%	64.7%	62.5%	39.1%	21.7%	2.06%	0.55%
62	64.6%	64.6%	62.5%	39.3%	21.9%	2.09%	0.57%
63	64.5%	64.5%	62.5%	39.6%	22.1%	2.13%	0.58%
64	64.5%	64.5%	62.5%	39.8%	22.4%	2.17%	0.59%
65	64.4%	64.4%	62.5%	40.1%	22.6%	2.20%	0.60%
66	64.3%	64.3%	62.4%	40.3%	22.8%	2.24%	0.61%
67	64.3%	64.2%	62.4%	40.5%	23.0%	2.28%	0.62%
68	64.2%	64.2%	62.4%	40.7%	23.2%	2.31%	0.63%
69	64.1%	64.1%	62.3%	40.9%	23.4%	2.35%	0.64%
70	64.1%	64.0%	62.3%	41.1%	23.6%	2.39%	0.65%
71	64.0%	64.0%	62.3%	41.4%	23.8%	2.42%	0.66%
72	63.9%	63.9%	62.2%	41.5%	24.0%	2.46%	0.67%
73	63.8%	63.8%	62.2%	41.7%	24.2%	2.49%	0.68%
74	63.8%	63.8%	62.2%	41.9%	24.4%	2.53%	0.69%
75	63.7%	63.7%	62.1%	42.1%	24.6%	2.57%	0.70%
76	63.6%	63.6%	62.1%	42.3%	24.8%	2.60%	0.71%
77	63.6%	63.5%	62.0%	42.5%	25.0%	2.64%	0.72%
78	63.5%	63.5%	62.0%	42.6%	25.2%	2.67%	0.73%
79	63.4%	63.4%	61.9%	42.8%	25.4%	2.71%	0.74%
80	63.3%	63.3%	61.9%	43.0%	25.6%	2.74%	0.76%
81	63.3%	63.2%	61.9%	43.1%	25.8%	2.78%	0.77%
82	63.2%	63.2%	61.8%	43.3%	25.9%	2.81%	0.78%
83	63.1%	63.1%	61.8%	43.4%	26.1%	2.85%	0.79%
84	63.0%	63.0%	61.7%	43.6%	26.3%	2.88%	0.80%
85	63.0%	62.9%	61.6%	43.7%	26.4%	2.92%	0.81%
86	62.9%	62.9%	61.6%	43.9%	26.6%	2.95%	0.82%
87	62.8%	62.8%	61.5%	44.0%	26.8%	2.99%	0.83%
88	62.7%	62.7%	61.5%	44.1%	26.9%	3.02%	0.84%
89	62.7%	62.6%	61.4%	44.3%	27.1%	3.06%	0.85%
90	62.6%	62.6%	61.4%	44.4%	27.3%	3.09%	0.86%
91	62.5%	62.5%	61.3%	44.5%	27.4%	3.12%	0.87%
92	62.4%	62.4%	61.3%	44.6%	27.6%	3.16%	0.88%
93	62.3%	62.3%	61.2%	44.8%	27.7%	3.19%	0.89%
94	62.3%	62.3%	61.1%	44.9%	27.9%	3.23%	0.90%
95	62.2%	62.2%	61.1%	45.0%	28.0%	3.26%	0.91%

96	62.1%	62.1%	61.0%	45.1%	28.2%	3.29%	0.92%
97	62.0%	62.0%	61.0%	45.2%	28.3%	3.33%	0.93%
98	61.9%	61.9%	60.9%	45.3%	28.5%	3.36%	0.94%
99	61.9%	61.9%	60.8%	45.4%	28.6%	3.39%	0.95%
100	61.8%	61.8%	60.8%	45.5%	28.8%	3.43%	0.96%

Table A10 – Amplification over 543 m vs. discharge (Figure 4.11)

λ= (m)	1	10	100	500	1000	5000	10000
Q_0 (cms)	% Increase over 543m						
20	393.7%	392.7%	318.0%	81.6%	30.6%	1.69%	0.43%
21	368.9%	368.1%	302.6%	81.4%	31.0%	1.74%	0.44%
22	347.1%	346.3%	288.5%	81.2%	31.3%	1.80%	0.46%
23	327.6%	327.0%	275.7%	80.9%	31.6%	1.84%	0.47%
24	310.3%	309.7%	263.9%	80.5%	31.9%	1.89%	0.48%
25	294.6%	294.1%	253.1%	80.1%	32.2%	1.94%	0.50%
26	280.5%	280.1%	243.2%	79.7%	32.4%	1.98%	0.51%
27	267.7%	267.3%	233.9%	79.3%	32.6%	2.03%	0.52%
28	256.0%	255.6%	225.4%	78.8%	32.8%	2.07%	0.53%
29	245.3%	244.9%	217.4%	78.3%	33.0%	2.11%	0.54%
30	235.4%	235.1%	210.0%	77.8%	33.1%	2.15%	0.55%
31	226.3%	226.1%	203.0%	77.2%	33.2%	2.19%	0.56%
32	217.9%	217.7%	196.5%	76.7%	33.3%	2.22%	0.58%
33	210.1%	209.9%	190.4%	76.2%	33.4%	2.26%	0.59%
34	202.9%	202.7%	184.7%	75.6%	33.5%	2.30%	0.60%
35	196.1%	195.9%	179.3%	75.0%	33.6%	2.33%	0.61%
36	189.8%	189.6%	174.2%	74.5%	33.6%	2.37%	0.62%
37	183.9%	183.7%	169.3%	73.9%	33.7%	2.40%	0.62%
38	178.3%	178.2%	164.8%	73.3%	33.7%	2.43%	0.63%
39	173.1%	172.9%	160.5%	72.8%	33.7%	2.46%	0.64%
40	168.2%	168.0%	156.4%	72.2%	33.7%	2.49%	0.65%
41	163.5%	163.4%	152.4%	71.6%	33.7%	2.52%	0.66%
42	159.1%	159.0%	148.7%	71.1%	33.7%	2.55%	0.67%
43	154.9%	154.8%	145.2%	70.5%	33.7%	2.58%	0.68%
44	151.0%	150.9%	141.8%	69.9%	33.7%	2.61%	0.69%
45	147.2%	147.1%	138.6%	69.4%	33.7%	2.63%	0.69%
46	143.7%	143.6%	135.5%	68.8%	33.6%	2.66%	0.70%
47	140.3%	140.2%	132.6%	68.3%	33.6%	2.68%	0.71%
48	137.0%	136.9%	129.8%	67.7%	33.6%	2.71%	0.72%
49	133.9%	133.8%	127.0%	67.2%	33.5%	2.73%	0.72%
50	131.0%	130.9%	124.4%	66.6%	33.5%	2.76%	0.73%
51	128.1%	128.1%	122.0%	66.1%	33.4%	2.78%	0.74%
52	125.4%	125.4%	119.6%	65.5%	33.4%	2.80%	0.74%

53	122.8%	122.8%	117.3%	65.0%	33.3%	2.82%	0.75%
54	120.3%	120.3%	115.0%	64.5%	33.2%	2.85%	0.76%
55	117.9%	117.9%	112.9%	64.0%	33.2%	2.87%	0.76%
56	115.6%	115.6%	110.8%	63.5%	33.1%	2.89%	0.77%
57	113.4%	113.4%	108.8%	63.0%	33.0%	2.91%	0.78%
58	111.3%	111.3%	106.9%	62.5%	33.0%	2.93%	0.78%
59	109.3%	109.2%	105.1%	62.0%	32.9%	2.95%	0.79%
60	107.3%	107.2%	103.3%	61.5%	32.8%	2.96%	0.80%
61	105.4%	105.3%	101.5%	61.0%	32.7%	2.98%	0.80%
62	103.5%	103.5%	99.9%	60.5%	32.6%	3.00%	0.81%
63	101.8%	101.7%	98.2%	60.0%	32.6%	3.02%	0.81%
64	100.0%	100.0%	96.7%	59.5%	32.5%	3.03%	0.82%
65	98.4%	98.3%	95.1%	59.1%	32.4%	3.05%	0.82%
66	96.8%	96.7%	93.7%	58.6%	32.3%	3.07%	0.83%
67	95.2%	95.2%	92.2%	58.1%	32.2%	3.08%	0.83%
68	93.7%	93.7%	90.8%	57.7%	32.1%	3.10%	0.84%
69	92.2%	92.2%	89.5%	57.2%	32.0%	3.11%	0.84%
70	90.8%	90.8%	88.2%	56.8%	31.9%	3.13%	0.85%
71	89.4%	89.4%	86.9%	56.4%	31.8%	3.14%	0.85%
72	88.1%	88.1%	85.6%	55.9%	31.7%	3.15%	0.86%
73	86.8%	86.8%	84.4%	55.5%	31.6%	3.17%	0.86%
74	85.5%	85.5%	83.3%	55.1%	31.5%	3.18%	0.87%
75	84.3%	84.3%	82.1%	54.7%	31.4%	3.19%	0.87%
76	83.1%	83.1%	81.0%	54.2%	31.3%	3.21%	0.88%
77	82.0%	81.9%	79.9%	53.8%	31.2%	3.22%	0.88%
78	80.8%	80.8%	78.9%	53.4%	31.1%	3.23%	0.89%
79	79.7%	79.7%	77.8%	53.0%	31.0%	3.24%	0.89%
80	78.7%	78.7%	76.8%	52.6%	30.9%	3.25%	0.89%
81	77.6%	77.6%	75.8%	52.2%	30.8%	3.26%	0.90%
82	76.6%	76.6%	74.9%	51.9%	30.7%	3.27%	0.90%
83	75.6%	75.6%	73.9%	51.5%	30.6%	3.29%	0.91%
84	74.6%	74.6%	73.0%	51.1%	30.5%	3.30%	0.91%
85	73.7%	73.7%	72.1%	50.7%	30.4%	3.31%	0.91%
86	72.8%	72.8%	71.3%	50.3%	30.3%	3.32%	0.92%
87	71.9%	71.9%	70.4%	50.0%	30.2%	3.32%	0.92%
88	71.0%	71.0%	69.6%	49.6%	30.1%	3.33%	0.92%
89	70.1%	70.1%	68.7%	49.2%	30.0%	3.34%	0.93%
90	69.3%	69.3%	67.9%	48.9%	29.9%	3.35%	0.93%
91	68.5%	68.5%	67.2%	48.5%	29.7%	3.36%	0.93%
92	67.7%	67.7%	66.4%	48.2%	29.6%	3.37%	0.94%
93	66.9%	66.9%	65.7%	47.8%	29.5%	3.38%	0.94%
94	66.1%	66.1%	64.9%	47.5%	29.4%	3.38%	0.94%
95	65.4%	65.4%	64.2%	47.2%	29.3%	3.39%	0.95%
96	64.6%	64.6%	63.5%	46.8%	29.2%	3.40%	0.95%
97	63.9%	63.9%	62.8%	46.5%	29.1%	3.41%	0.95%
98	63.2%	63.2%	62.1%	46.2%	29.0%	3.41%	0.96%
99	62.5%	62.5%	61.5%	45.9%	28.9%	3.42%	0.96%
100	61.8%	61.8%	60.8%	45.5%	28.8%	3.43%	0.96%

Table A11 – Amplitude of an initially 0.5 m wave over 543 m vs. discharge
(Figure 4.12)

λ= (m)	1	10	100	500	1000	5000	10000
Q_0 (cms)	Amplitude after 543 m, starting at 0.5 m (m)						
20	2.469	2.464	2.090	0.908	0.653	0.508	0.502
21	2.345	2.340	2.013	0.907	0.655	0.509	0.502
22	2.235	2.232	1.943	0.906	0.657	0.509	0.502
23	2.138	2.135	1.879	0.904	0.658	0.509	0.502
24	2.051	2.049	1.820	0.903	0.660	0.509	0.502
25	1.973	1.971	1.766	0.901	0.661	0.510	0.502
26	1.903	1.900	1.716	0.899	0.662	0.510	0.503
27	1.838	1.836	1.670	0.896	0.663	0.510	0.503
28	1.780	1.778	1.627	0.894	0.664	0.510	0.503
29	1.726	1.725	1.587	0.891	0.665	0.511	0.503
30	1.677	1.676	1.550	0.889	0.665	0.511	0.503
31	1.632	1.630	1.515	0.886	0.666	0.511	0.503
32	1.590	1.588	1.483	0.884	0.667	0.511	0.503
33	1.551	1.550	1.452	0.881	0.667	0.511	0.503
34	1.514	1.513	1.423	0.878	0.667	0.511	0.503
35	1.481	1.480	1.396	0.875	0.668	0.512	0.503
36	1.449	1.448	1.371	0.872	0.668	0.512	0.503
37	1.419	1.419	1.347	0.870	0.668	0.512	0.503
38	1.392	1.391	1.324	0.867	0.668	0.512	0.503
39	1.365	1.365	1.302	0.864	0.669	0.512	0.503
40	1.341	1.340	1.282	0.861	0.669	0.512	0.503
41	1.317	1.317	1.262	0.858	0.669	0.513	0.503
42	1.295	1.295	1.244	0.855	0.669	0.513	0.503
43	1.275	1.274	1.226	0.852	0.669	0.513	0.503
44	1.255	1.254	1.209	0.850	0.668	0.513	0.503
45	1.236	1.236	1.193	0.847	0.668	0.513	0.503
46	1.218	1.218	1.178	0.844	0.668	0.513	0.504
47	1.201	1.201	1.163	0.841	0.668	0.513	0.504
48	1.185	1.185	1.149	0.839	0.668	0.514	0.504
49	1.170	1.169	1.135	0.836	0.668	0.514	0.504
50	1.155	1.154	1.122	0.833	0.667	0.514	0.504
51	1.141	1.140	1.110	0.830	0.667	0.514	0.504
52	1.127	1.127	1.098	0.828	0.667	0.514	0.504
53	1.114	1.114	1.086	0.825	0.667	0.514	0.504
54	1.102	1.101	1.075	0.822	0.666	0.514	0.504
55	1.090	1.089	1.064	0.820	0.666	0.514	0.504

56	1.078	1.078	1.054	0.817	0.666	0.514	0.504
57	1.067	1.067	1.044	0.815	0.665	0.515	0.504
58	1.057	1.056	1.035	0.812	0.665	0.515	0.504
59	1.046	1.046	1.025	0.810	0.664	0.515	0.504
60	1.036	1.036	1.016	0.807	0.664	0.515	0.504
61	1.027	1.027	1.008	0.805	0.664	0.515	0.504
62	1.018	1.017	0.999	0.802	0.663	0.515	0.504
63	1.009	1.009	0.991	0.800	0.663	0.515	0.504
64	1.000	1.000	0.983	0.798	0.662	0.515	0.504
65	0.992	0.992	0.976	0.795	0.662	0.515	0.504
66	0.984	0.984	0.968	0.793	0.661	0.515	0.504
67	0.976	0.976	0.961	0.791	0.661	0.515	0.504
68	0.969	0.968	0.954	0.788	0.661	0.515	0.504
69	0.961	0.961	0.947	0.786	0.660	0.516	0.504
70	0.954	0.954	0.941	0.784	0.660	0.516	0.504
71	0.947	0.947	0.934	0.782	0.659	0.516	0.504
72	0.941	0.940	0.928	0.780	0.659	0.516	0.504
73	0.934	0.934	0.922	0.778	0.658	0.516	0.504
74	0.928	0.928	0.916	0.775	0.658	0.516	0.504
75	0.922	0.921	0.911	0.773	0.657	0.516	0.504
76	0.916	0.916	0.905	0.771	0.657	0.516	0.504
77	0.910	0.910	0.900	0.769	0.656	0.516	0.504
78	0.904	0.904	0.894	0.767	0.656	0.516	0.504
79	0.899	0.899	0.889	0.765	0.655	0.516	0.504
80	0.893	0.893	0.884	0.763	0.655	0.516	0.504
81	0.888	0.888	0.879	0.761	0.654	0.516	0.504
82	0.883	0.883	0.874	0.759	0.654	0.516	0.505
83	0.878	0.878	0.870	0.757	0.653	0.516	0.505
84	0.873	0.873	0.865	0.755	0.652	0.516	0.505
85	0.869	0.868	0.861	0.754	0.652	0.517	0.505
86	0.864	0.864	0.856	0.752	0.651	0.517	0.505
87	0.859	0.859	0.852	0.750	0.651	0.517	0.505
88	0.855	0.855	0.848	0.748	0.650	0.517	0.505
89	0.851	0.851	0.844	0.746	0.650	0.517	0.505
90	0.847	0.846	0.840	0.744	0.649	0.517	0.505
91	0.842	0.842	0.836	0.743	0.649	0.517	0.505
92	0.838	0.838	0.832	0.741	0.648	0.517	0.505
93	0.834	0.834	0.828	0.739	0.648	0.517	0.505
94	0.831	0.831	0.825	0.738	0.647	0.517	0.505
95	0.827	0.827	0.821	0.736	0.647	0.517	0.505
96	0.823	0.823	0.818	0.734	0.646	0.517	0.505
97	0.820	0.820	0.814	0.733	0.646	0.517	0.505
98	0.816	0.816	0.811	0.731	0.645	0.517	0.505
99	0.813	0.813	0.807	0.729	0.644	0.517	0.505
100	0.809	0.809	0.804	0.728	0.644	0.517	0.505

Table A12 – Wave amplitude vs. distance (Figure 4.13)

λ= (m)	10	100	500	1000	5000
Length (m)		Amplitude of an intially 0.5 m wave			
0	0.500	0.500	0.500	0.500	0.500
10	0.504	0.504	0.503	0.502	0.500
11	0.505	0.505	0.504	0.503	0.500
12	0.505	0.505	0.504	0.503	0.500
13	0.506	0.506	0.505	0.503	0.500
14	0.506	0.506	0.505	0.503	0.500
15	0.507	0.507	0.505	0.504	0.500
16	0.507	0.507	0.506	0.504	0.500
17	0.508	0.507	0.506	0.504	0.501
18	0.508	0.508	0.506	0.504	0.501
19	0.508	0.508	0.507	0.504	0.501
20	0.509	0.509	0.507	0.505	0.501
21	0.509	0.509	0.507	0.505	0.501
22	0.510	0.510	0.508	0.505	0.501
23	0.510	0.510	0.508	0.505	0.501
24	0.511	0.511	0.508	0.506	0.501
25	0.511	0.511	0.509	0.506	0.501
26	0.512	0.512	0.509	0.506	0.501
27	0.512	0.512	0.509	0.506	0.501
28	0.513	0.512	0.510	0.507	0.501
29	0.513	0.513	0.510	0.507	0.501
30	0.513	0.513	0.510	0.507	0.501
31	0.514	0.514	0.511	0.507	0.501
32	0.514	0.514	0.511	0.508	0.501
33	0.515	0.515	0.512	0.508	0.501
34	0.515	0.515	0.512	0.508	0.501
35	0.516	0.516	0.512	0.508	0.501
36	0.516	0.516	0.513	0.508	0.501
37	0.517	0.516	0.513	0.509	0.501
38	0.517	0.517	0.513	0.509	0.501
39	0.518	0.517	0.514	0.509	0.501
40	0.518	0.518	0.514	0.509	0.501
41	0.519	0.518	0.514	0.510	0.501
42	0.519	0.519	0.515	0.510	0.501
43	0.519	0.519	0.515	0.510	0.501
44	0.520	0.520	0.515	0.510	0.501
45	0.520	0.520	0.516	0.511	0.501
46	0.521	0.521	0.516	0.511	0.501
47	0.521	0.521	0.517	0.511	0.501

48	0.522	0.521	0.517	0.511	0.501
49	0.522	0.522	0.517	0.512	0.502
50	0.523	0.522	0.518	0.512	0.502
51	0.523	0.523	0.518	0.512	0.502
52	0.524	0.523	0.518	0.512	0.502
53	0.524	0.524	0.519	0.512	0.502
54	0.525	0.524	0.519	0.513	0.502
55	0.525	0.525	0.519	0.513	0.502
56	0.525	0.525	0.520	0.513	0.502
57	0.526	0.526	0.520	0.513	0.502
58	0.526	0.526	0.520	0.514	0.502
59	0.527	0.526	0.521	0.514	0.502
60	0.527	0.527	0.521	0.514	0.502
61	0.528	0.527	0.522	0.514	0.502
62	0.528	0.528	0.522	0.515	0.502
63	0.529	0.528	0.522	0.515	0.502
64	0.529	0.529	0.523	0.515	0.502
65	0.530	0.529	0.523	0.515	0.502
66	0.530	0.530	0.523	0.516	0.502
67	0.531	0.530	0.524	0.516	0.502
68	0.531	0.531	0.524	0.516	0.502
69	0.532	0.531	0.524	0.516	0.502
70	0.532	0.532	0.525	0.517	0.502
71	0.532	0.532	0.525	0.517	0.502
72	0.533	0.533	0.526	0.517	0.502
73	0.533	0.533	0.526	0.517	0.502
74	0.534	0.533	0.526	0.518	0.502
75	0.534	0.534	0.527	0.518	0.502
76	0.535	0.534	0.527	0.518	0.502
77	0.535	0.535	0.527	0.518	0.502
78	0.536	0.535	0.528	0.519	0.502
79	0.536	0.536	0.528	0.519	0.502
80	0.537	0.536	0.528	0.519	0.502
81	0.537	0.537	0.529	0.519	0.503
82	0.538	0.537	0.529	0.519	0.503
83	0.538	0.538	0.530	0.520	0.503
84	0.539	0.538	0.530	0.520	0.503
85	0.539	0.539	0.530	0.520	0.503
86	0.540	0.539	0.531	0.520	0.503
87	0.540	0.540	0.531	0.521	0.503
88	0.541	0.540	0.531	0.521	0.503
89	0.541	0.540	0.532	0.521	0.503
90	0.542	0.541	0.532	0.521	0.503
91	0.542	0.541	0.532	0.522	0.503
92	0.542	0.542	0.533	0.522	0.503
93	0.543	0.542	0.533	0.522	0.503
94	0.543	0.543	0.534	0.522	0.503
95	0.544	0.543	0.534	0.523	0.503

96	0.544	0.544	0.534	0.523	0.503
97	0.545	0.544	0.535	0.523	0.503
98	0.545	0.545	0.535	0.523	0.503
99	0.546	0.545	0.535	0.524	0.503
100	0.546	0.546	0.536	0.524	0.503
101	0.547	0.546	0.536	0.524	0.503
102	0.547	0.547	0.537	0.524	0.503
103	0.548	0.547	0.537	0.525	0.503
104	0.548	0.548	0.537	0.525	0.503
105	0.549	0.548	0.538	0.525	0.503
106	0.549	0.549	0.538	0.525	0.503
107	0.550	0.549	0.538	0.526	0.503
108	0.550	0.550	0.539	0.526	0.503
109	0.551	0.550	0.539	0.526	0.503
110	0.551	0.551	0.539	0.526	0.503
111	0.552	0.551	0.540	0.527	0.503
112	0.552	0.551	0.540	0.527	0.503
113	0.553	0.552	0.541	0.527	0.504
114	0.553	0.552	0.541	0.527	0.504
115	0.554	0.553	0.541	0.528	0.504
116	0.554	0.553	0.542	0.528	0.504
117	0.555	0.554	0.542	0.528	0.504
118	0.555	0.554	0.542	0.528	0.504
119	0.556	0.555	0.543	0.528	0.504
120	0.556	0.555	0.543	0.529	0.504
121	0.557	0.556	0.544	0.529	0.504
122	0.557	0.556	0.544	0.529	0.504
123	0.558	0.557	0.544	0.529	0.504
124	0.558	0.557	0.545	0.530	0.504
125	0.559	0.558	0.545	0.530	0.504
126	0.559	0.558	0.545	0.530	0.504
127	0.560	0.559	0.546	0.530	0.504
128	0.560	0.559	0.546	0.531	0.504
129	0.561	0.560	0.547	0.531	0.504
130	0.561	0.560	0.547	0.531	0.504
131	0.562	0.561	0.547	0.531	0.504
132	0.562	0.561	0.548	0.532	0.504
133	0.563	0.562	0.548	0.532	0.504
134	0.563	0.562	0.549	0.532	0.504
135	0.564	0.563	0.549	0.532	0.504
136	0.564	0.563	0.549	0.533	0.504
137	0.565	0.564	0.550	0.533	0.504
138	0.565	0.564	0.550	0.533	0.504
139	0.566	0.565	0.550	0.533	0.504
140	0.566	0.565	0.551	0.534	0.504
141	0.567	0.566	0.551	0.534	0.504
142	0.567	0.566	0.552	0.534	0.504
143	0.568	0.567	0.552	0.534	0.504
144	0.568	0.567	0.552	0.535	0.504

145	0.569	0.568	0.553	0.535	0.505
146	0.569	0.568	0.553	0.535	0.505
147	0.570	0.569	0.553	0.535	0.505
148	0.570	0.569	0.554	0.536	0.505
149	0.571	0.570	0.554	0.536	0.505
150	0.571	0.570	0.555	0.536	0.505
151	0.572	0.571	0.555	0.536	0.505
152	0.572	0.571	0.555	0.537	0.505
153	0.573	0.572	0.556	0.537	0.505
154	0.573	0.572	0.556	0.537	0.505
155	0.574	0.573	0.557	0.537	0.505
156	0.574	0.573	0.557	0.538	0.505
157	0.575	0.574	0.557	0.538	0.505
158	0.575	0.574	0.558	0.538	0.505
159	0.576	0.575	0.558	0.538	0.505
160	0.576	0.575	0.558	0.539	0.505
161	0.577	0.576	0.559	0.539	0.505
162	0.577	0.576	0.559	0.539	0.505
163	0.578	0.577	0.560	0.539	0.505
164	0.578	0.577	0.560	0.540	0.505
165	0.579	0.578	0.560	0.540	0.505
166	0.579	0.578	0.561	0.540	0.505
167	0.580	0.579	0.561	0.540	0.505
168	0.580	0.579	0.562	0.541	0.505
169	0.581	0.580	0.562	0.541	0.505
170	0.581	0.580	0.562	0.541	0.505
171	0.582	0.581	0.563	0.541	0.505
172	0.582	0.581	0.563	0.542	0.505
173	0.583	0.582	0.564	0.542	0.505
174	0.583	0.582	0.564	0.542	0.505
175	0.584	0.583	0.564	0.542	0.505
176	0.584	0.583	0.565	0.543	0.505
177	0.585	0.584	0.565	0.543	0.506
178	0.585	0.584	0.565	0.543	0.506
179	0.586	0.585	0.566	0.543	0.506
180	0.587	0.585	0.566	0.544	0.506
181	0.587	0.586	0.567	0.544	0.506
182	0.588	0.586	0.567	0.544	0.506
183	0.588	0.587	0.567	0.544	0.506
184	0.589	0.587	0.568	0.545	0.506
185	0.589	0.588	0.568	0.545	0.506
186	0.590	0.588	0.569	0.545	0.506
187	0.590	0.589	0.569	0.546	0.506
188	0.591	0.589	0.569	0.546	0.506
189	0.591	0.590	0.570	0.546	0.506
190	0.592	0.590	0.570	0.546	0.506
191	0.592	0.591	0.571	0.547	0.506
192	0.593	0.591	0.571	0.547	0.506
193	0.593	0.592	0.571	0.547	0.506

194	0.594	0.593	0.572	0.547	0.506
195	0.594	0.593	0.572	0.548	0.506
196	0.595	0.594	0.573	0.548	0.506
197	0.595	0.594	0.573	0.548	0.506
198	0.596	0.595	0.573	0.548	0.506
199	0.596	0.595	0.574	0.549	0.506
200	0.597	0.596	0.574	0.549	0.506
201	0.598	0.596	0.575	0.549	0.506
202	0.598	0.597	0.575	0.549	0.506
203	0.599	0.597	0.575	0.550	0.506
204	0.599	0.598	0.576	0.550	0.506
205	0.600	0.598	0.576	0.550	0.506
206	0.600	0.599	0.577	0.550	0.506
207	0.601	0.599	0.577	0.551	0.506
208	0.601	0.600	0.577	0.551	0.506
209	0.602	0.600	0.578	0.551	0.507
210	0.602	0.601	0.578	0.551	0.507
211	0.603	0.601	0.578	0.552	0.507
212	0.603	0.602	0.579	0.552	0.507
213	0.604	0.602	0.579	0.552	0.507
214	0.604	0.603	0.580	0.552	0.507
215	0.605	0.603	0.580	0.553	0.507
216	0.606	0.604	0.580	0.553	0.507
217	0.606	0.605	0.581	0.553	0.507
218	0.607	0.605	0.581	0.553	0.507
219	0.607	0.606	0.582	0.554	0.507
220	0.608	0.606	0.582	0.554	0.507
221	0.608	0.607	0.583	0.554	0.507
222	0.609	0.607	0.583	0.554	0.507
223	0.609	0.608	0.583	0.555	0.507
224	0.610	0.608	0.584	0.555	0.507
225	0.610	0.609	0.584	0.555	0.507
226	0.611	0.609	0.585	0.556	0.507
227	0.611	0.610	0.585	0.556	0.507
228	0.612	0.610	0.585	0.556	0.507
229	0.613	0.611	0.586	0.556	0.507
230	0.613	0.611	0.586	0.557	0.507
231	0.614	0.612	0.587	0.557	0.507
232	0.614	0.613	0.587	0.557	0.507
233	0.615	0.613	0.587	0.557	0.507
234	0.615	0.614	0.588	0.558	0.507
235	0.616	0.614	0.588	0.558	0.507
236	0.616	0.615	0.589	0.558	0.507
237	0.617	0.615	0.589	0.558	0.507
238	0.617	0.616	0.589	0.559	0.507
239	0.618	0.616	0.590	0.559	0.507
240	0.619	0.617	0.590	0.559	0.508
241	0.619	0.617	0.591	0.559	0.508
242	0.620	0.618	0.591	0.560	0.508

243	0.620	0.618	0.591	0.560	0.508
244	0.621	0.619	0.592	0.560	0.508
245	0.621	0.620	0.592	0.560	0.508
246	0.622	0.620	0.593	0.561	0.508
247	0.622	0.621	0.593	0.561	0.508
248	0.623	0.621	0.593	0.561	0.508
249	0.624	0.622	0.594	0.561	0.508
250	0.624	0.622	0.594	0.562	0.508
251	0.625	0.623	0.595	0.562	0.508
252	0.625	0.623	0.595	0.562	0.508
253	0.626	0.624	0.596	0.563	0.508
254	0.626	0.624	0.596	0.563	0.508
255	0.627	0.625	0.596	0.563	0.508
256	0.627	0.626	0.597	0.563	0.508
257	0.628	0.626	0.597	0.564	0.508
258	0.629	0.627	0.598	0.564	0.508
259	0.629	0.627	0.598	0.564	0.508
260	0.630	0.628	0.598	0.564	0.508
261	0.630	0.628	0.599	0.565	0.508
262	0.631	0.629	0.599	0.565	0.508
263	0.631	0.629	0.600	0.565	0.508
264	0.632	0.630	0.600	0.565	0.508
265	0.632	0.630	0.600	0.566	0.508
266	0.633	0.631	0.601	0.566	0.508
267	0.634	0.632	0.601	0.566	0.508
268	0.634	0.632	0.602	0.566	0.508
269	0.635	0.633	0.602	0.567	0.508
270	0.635	0.633	0.603	0.567	0.508
271	0.636	0.634	0.603	0.567	0.508
272	0.636	0.634	0.603	0.568	0.509
273	0.637	0.635	0.604	0.568	0.509
274	0.637	0.635	0.604	0.568	0.509
275	0.638	0.636	0.605	0.568	0.509
276	0.639	0.637	0.605	0.569	0.509
277	0.639	0.637	0.605	0.569	0.509
278	0.640	0.638	0.606	0.569	0.509
279	0.640	0.638	0.606	0.569	0.509
280	0.641	0.639	0.607	0.570	0.509
281	0.641	0.639	0.607	0.570	0.509
282	0.642	0.640	0.608	0.570	0.509
283	0.643	0.640	0.608	0.570	0.509
284	0.643	0.641	0.608	0.571	0.509
285	0.644	0.642	0.609	0.571	0.509
286	0.644	0.642	0.609	0.571	0.509
287	0.645	0.643	0.610	0.572	0.509
288	0.645	0.643	0.610	0.572	0.509
289	0.646	0.644	0.611	0.572	0.509
290	0.647	0.644	0.611	0.572	0.509
291	0.647	0.645	0.611	0.573	0.509

292	0.648	0.646	0.612	0.573	0.509
293	0.648	0.646	0.612	0.573	0.509
294	0.649	0.647	0.613	0.573	0.509
295	0.649	0.647	0.613	0.574	0.509
296	0.650	0.648	0.613	0.574	0.509
297	0.651	0.648	0.614	0.574	0.509
298	0.651	0.649	0.614	0.574	0.509
299	0.652	0.650	0.615	0.575	0.509
300	0.652	0.650	0.615	0.575	0.509
301	0.653	0.651	0.616	0.575	0.509
302	0.654	0.651	0.616	0.576	0.509
303	0.654	0.652	0.616	0.576	0.509
304	0.655	0.652	0.617	0.576	0.510
305	0.655	0.653	0.617	0.576	0.510
306	0.656	0.654	0.618	0.577	0.510
307	0.656	0.654	0.618	0.577	0.510
308	0.657	0.655	0.619	0.577	0.510
309	0.658	0.655	0.619	0.577	0.510
310	0.658	0.656	0.619	0.578	0.510
311	0.659	0.656	0.620	0.578	0.510
312	0.659	0.657	0.620	0.578	0.510
313	0.660	0.658	0.621	0.578	0.510
314	0.660	0.658	0.621	0.579	0.510
315	0.661	0.659	0.622	0.579	0.510
316	0.662	0.659	0.622	0.579	0.510
317	0.662	0.660	0.622	0.580	0.510
318	0.663	0.660	0.623	0.580	0.510
319	0.663	0.661	0.623	0.580	0.510
320	0.664	0.662	0.624	0.580	0.510
321	0.665	0.662	0.624	0.581	0.510
322	0.665	0.663	0.625	0.581	0.510
323	0.666	0.663	0.625	0.581	0.510
324	0.666	0.664	0.625	0.581	0.510
325	0.667	0.664	0.626	0.582	0.510
326	0.668	0.665	0.626	0.582	0.510
327	0.668	0.666	0.627	0.582	0.510
328	0.669	0.666	0.627	0.583	0.510
329	0.669	0.667	0.628	0.583	0.510
330	0.670	0.667	0.628	0.583	0.510
331	0.671	0.668	0.629	0.583	0.510
332	0.671	0.669	0.629	0.584	0.510
333	0.672	0.669	0.629	0.584	0.510
334	0.672	0.670	0.630	0.584	0.510
335	0.673	0.670	0.630	0.584	0.511
336	0.674	0.671	0.631	0.585	0.511
337	0.674	0.671	0.631	0.585	0.511
338	0.675	0.672	0.632	0.585	0.511
339	0.675	0.673	0.632	0.586	0.511
340	0.676	0.673	0.632	0.586	0.511

341	0.676	0.674	0.633	0.586	0.511
342	0.677	0.674	0.633	0.586	0.511
343	0.678	0.675	0.634	0.587	0.511
344	0.678	0.676	0.634	0.587	0.511
345	0.679	0.676	0.635	0.587	0.511
346	0.680	0.677	0.635	0.587	0.511
347	0.680	0.677	0.636	0.588	0.511
348	0.681	0.678	0.636	0.588	0.511
349	0.681	0.679	0.636	0.588	0.511
350	0.682	0.679	0.637	0.589	0.511
351	0.683	0.680	0.637	0.589	0.511
352	0.683	0.680	0.638	0.589	0.511
353	0.684	0.681	0.638	0.589	0.511
354	0.684	0.682	0.639	0.590	0.511
355	0.685	0.682	0.639	0.590	0.511
356	0.686	0.683	0.639	0.590	0.511
357	0.686	0.683	0.640	0.590	0.511
358	0.687	0.684	0.640	0.591	0.511
359	0.687	0.685	0.641	0.591	0.511
360	0.688	0.685	0.641	0.591	0.511
361	0.689	0.686	0.642	0.592	0.511
362	0.689	0.686	0.642	0.592	0.511
363	0.690	0.687	0.643	0.592	0.511
364	0.690	0.688	0.643	0.592	0.511
365	0.691	0.688	0.643	0.593	0.511
366	0.692	0.689	0.644	0.593	0.511
367	0.692	0.689	0.644	0.593	0.512
368	0.693	0.690	0.645	0.593	0.512
369	0.694	0.691	0.645	0.594	0.512
370	0.694	0.691	0.646	0.594	0.512
371	0.695	0.692	0.646	0.594	0.512
372	0.695	0.692	0.647	0.595	0.512
373	0.696	0.693	0.647	0.595	0.512
374	0.697	0.694	0.647	0.595	0.512
375	0.697	0.694	0.648	0.595	0.512
376	0.698	0.695	0.648	0.596	0.512
377	0.698	0.695	0.649	0.596	0.512
378	0.699	0.696	0.649	0.596	0.512
379	0.700	0.697	0.650	0.597	0.512
380	0.700	0.697	0.650	0.597	0.512
381	0.701	0.698	0.651	0.597	0.512
382	0.702	0.698	0.651	0.597	0.512
383	0.702	0.699	0.652	0.598	0.512
384	0.703	0.700	0.652	0.598	0.512
385	0.703	0.700	0.652	0.598	0.512
386	0.704	0.701	0.653	0.598	0.512
387	0.705	0.702	0.653	0.599	0.512
388	0.705	0.702	0.654	0.599	0.512
389	0.706	0.703	0.654	0.599	0.512

390	0.707	0.703	0.655	0.600	0.512
391	0.707	0.704	0.655	0.600	0.512
392	0.708	0.705	0.656	0.600	0.512
393	0.708	0.705	0.656	0.600	0.512
394	0.709	0.706	0.656	0.601	0.512
395	0.710	0.706	0.657	0.601	0.512
396	0.710	0.707	0.657	0.601	0.512
397	0.711	0.708	0.658	0.602	0.512
398	0.712	0.708	0.658	0.602	0.513
399	0.712	0.709	0.659	0.602	0.513
400	0.713	0.710	0.659	0.602	0.513
401	0.713	0.710	0.660	0.603	0.513
402	0.714	0.711	0.660	0.603	0.513
403	0.715	0.711	0.661	0.603	0.513
404	0.715	0.712	0.661	0.604	0.513
405	0.716	0.713	0.661	0.604	0.513
406	0.717	0.713	0.662	0.604	0.513
407	0.717	0.714	0.662	0.604	0.513
408	0.718	0.715	0.663	0.605	0.513
409	0.719	0.715	0.663	0.605	0.513
410	0.719	0.716	0.664	0.605	0.513
411	0.720	0.716	0.664	0.605	0.513
412	0.720	0.717	0.665	0.606	0.513
413	0.721	0.718	0.665	0.606	0.513
414	0.722	0.718	0.666	0.606	0.513
415	0.722	0.719	0.666	0.607	0.513
416	0.723	0.720	0.667	0.607	0.513
417	0.724	0.720	0.667	0.607	0.513
418	0.724	0.721	0.667	0.607	0.513
419	0.725	0.721	0.668	0.608	0.513
420	0.726	0.722	0.668	0.608	0.513
421	0.726	0.723	0.669	0.608	0.513
422	0.727	0.723	0.669	0.609	0.513
423	0.728	0.724	0.670	0.609	0.513
424	0.728	0.725	0.670	0.609	0.513
425	0.729	0.725	0.671	0.609	0.513
426	0.729	0.726	0.671	0.610	0.513
427	0.730	0.727	0.672	0.610	0.513
428	0.731	0.727	0.672	0.610	0.513
429	0.731	0.728	0.673	0.611	0.513
430	0.732	0.728	0.673	0.611	0.514
431	0.733	0.729	0.673	0.611	0.514
432	0.733	0.730	0.674	0.611	0.514
433	0.734	0.730	0.674	0.612	0.514
434	0.735	0.731	0.675	0.612	0.514
435	0.735	0.732	0.675	0.612	0.514
436	0.736	0.732	0.676	0.613	0.514
437	0.737	0.733	0.676	0.613	0.514
438	0.737	0.734	0.677	0.613	0.514

439	0.738	0.734	0.677	0.613	0.514
440	0.739	0.735	0.678	0.614	0.514
441	0.739	0.735	0.678	0.614	0.514
442	0.740	0.736	0.679	0.614	0.514
443	0.741	0.737	0.679	0.615	0.514
444	0.741	0.737	0.680	0.615	0.514
445	0.742	0.738	0.680	0.615	0.514
446	0.742	0.739	0.681	0.615	0.514
447	0.743	0.739	0.681	0.616	0.514
448	0.744	0.740	0.681	0.616	0.514
449	0.744	0.741	0.682	0.616	0.514
450	0.745	0.741	0.682	0.617	0.514
451	0.746	0.742	0.683	0.617	0.514
452	0.746	0.743	0.683	0.617	0.514
453	0.747	0.743	0.684	0.617	0.514
454	0.748	0.744	0.684	0.618	0.514
455	0.748	0.745	0.685	0.618	0.514
456	0.749	0.745	0.685	0.618	0.514
457	0.750	0.746	0.686	0.619	0.514
458	0.750	0.746	0.686	0.619	0.514
459	0.751	0.747	0.687	0.619	0.514
460	0.752	0.748	0.687	0.619	0.514
461	0.752	0.748	0.688	0.620	0.515
462	0.753	0.749	0.688	0.620	0.515
463	0.754	0.750	0.689	0.620	0.515
464	0.754	0.750	0.689	0.621	0.515
465	0.755	0.751	0.690	0.621	0.515
466	0.756	0.752	0.690	0.621	0.515
467	0.756	0.752	0.690	0.622	0.515
468	0.757	0.753	0.691	0.622	0.515
469	0.758	0.754	0.691	0.622	0.515
470	0.758	0.754	0.692	0.622	0.515
471	0.759	0.755	0.692	0.623	0.515
472	0.760	0.756	0.693	0.623	0.515
473	0.760	0.756	0.693	0.623	0.515
474	0.761	0.757	0.694	0.624	0.515
475	0.762	0.758	0.694	0.624	0.515
476	0.763	0.758	0.695	0.624	0.515
477	0.763	0.759	0.695	0.624	0.515
478	0.764	0.760	0.696	0.625	0.515
479	0.765	0.760	0.696	0.625	0.515
480	0.765	0.761	0.697	0.625	0.515
481	0.766	0.762	0.697	0.626	0.515
482	0.767	0.762	0.698	0.626	0.515
483	0.767	0.763	0.698	0.626	0.515
484	0.768	0.764	0.699	0.626	0.515
485	0.769	0.764	0.699	0.627	0.515
486	0.769	0.765	0.700	0.627	0.515
487	0.770	0.766	0.700	0.627	0.515

488	0.771	0.766	0.701	0.628	0.515
489	0.771	0.767	0.701	0.628	0.515
490	0.772	0.768	0.702	0.628	0.515
491	0.773	0.768	0.702	0.628	0.515
492	0.773	0.769	0.702	0.629	0.516
493	0.774	0.770	0.703	0.629	0.516
494	0.775	0.770	0.703	0.629	0.516
495	0.775	0.771	0.704	0.630	0.516
496	0.776	0.772	0.704	0.630	0.516
497	0.777	0.772	0.705	0.630	0.516
498	0.778	0.773	0.705	0.631	0.516
499	0.778	0.774	0.706	0.631	0.516
500	0.779	0.774	0.706	0.631	0.516
501	0.780	0.775	0.707	0.631	0.516
502	0.780	0.776	0.707	0.632	0.516
503	0.781	0.776	0.708	0.632	0.516
504	0.782	0.777	0.708	0.632	0.516
505	0.782	0.778	0.709	0.633	0.516
506	0.783	0.779	0.709	0.633	0.516
507	0.784	0.779	0.710	0.633	0.516
508	0.784	0.780	0.710	0.633	0.516
509	0.785	0.781	0.711	0.634	0.516
510	0.786	0.781	0.711	0.634	0.516
511	0.787	0.782	0.712	0.634	0.516
512	0.787	0.783	0.712	0.635	0.516
513	0.788	0.783	0.713	0.635	0.516
514	0.789	0.784	0.713	0.635	0.516
515	0.789	0.785	0.714	0.636	0.516
516	0.790	0.785	0.714	0.636	0.516
517	0.791	0.786	0.715	0.636	0.516
518	0.791	0.787	0.715	0.636	0.516
519	0.792	0.787	0.716	0.637	0.516
520	0.793	0.788	0.716	0.637	0.516
521	0.794	0.789	0.717	0.637	0.516
522	0.794	0.789	0.717	0.638	0.516
523	0.795	0.790	0.718	0.638	0.516
524	0.796	0.791	0.718	0.638	0.517
525	0.796	0.792	0.719	0.639	0.517
526	0.797	0.792	0.719	0.639	0.517
527	0.798	0.793	0.720	0.639	0.517
528	0.798	0.794	0.720	0.639	0.517
529	0.799	0.794	0.721	0.640	0.517
530	0.800	0.795	0.721	0.640	0.517
531	0.801	0.796	0.722	0.640	0.517
532	0.801	0.796	0.722	0.641	0.517
533	0.802	0.797	0.723	0.641	0.517
534	0.803	0.798	0.723	0.641	0.517
535	0.803	0.799	0.724	0.642	0.517
536	0.804	0.799	0.724	0.642	0.517

537	0.805	0.800	0.725	0.642	0.517
538	0.806	0.801	0.725	0.642	0.517
539	0.806	0.801	0.726	0.643	0.517
540	0.807	0.802	0.726	0.643	0.517
541	0.808	0.803	0.727	0.643	0.517
542	0.808	0.803	0.727	0.644	0.517
543	0.809	0.804	0.728	0.644	0.517